A STUDY OF CONSENSUS AND COLLISION AVOIDANCE IN A PLATOON OF VEHICLES USING ADAPTIVE CRUISE CONTROL

by

AUDREY DEVIN PORTER

Presented to the Faculty of the Graduate School of

The University of Texas at Arlington in Partial Fulfillment

of the Requirements

for the Degree of

MASTER OF SCIENCE IN ELECTRICAL ENGINEERING

THE UNIVERSITY OF TEXAS AT ARLINGTON

May 2017

Acknowledgements

I would like to thank Dr. Frank Lewis for introducing me to the interesting topic of distributed control theory and for providing advice and support during the process of writing this thesis. I would likewise like to thank Dr. Yan Wan and Dr. Mike Niestroy for being members of my thesis defense committee.

I am ever grateful to my mother Dr. Barbara Birdwell and my father Mr. Donald Porter for their support and encouragement throughout my entire life. Thanks so much to mom and dad, and also to my sister Jessie Embrey and my niece and nephew Madison and Haskell for peeling me away from my computer for good times, love, and laughter.

April 13, 2017

Abstract

A STUDY OF CONSENSUS AND COLLISION AVOIDANCE IN A PLATOON OF VEHICLES USING ADAPTIVE CRUISE CONTROL

Audrey D. Porter, MS

The University of Texas at Arlington, 2017

Supervising Professor: Frank Lewis

Vehicle platooning has been the subject of much research. Transfer function analysis of intervehicle distance errors is traditionally utilized to analyze the string stability of platoons. Consensus theory has been the subject of recent study of close-loop stability of platoons. This thesis extends the cooperative control approach to platoon behavior analysis to include the leader as an internal source of information for the communication graph of a platoon. A 1-Leader Type (1LT) graph is defined and an equation is proposed for the formation consensus values of leader and follower nodes in a platoon. Simulations are performed to support the proposed equations. A method is proposed to tune controller gains to achieve collision avoidance despite string instability.

Table of Contents

List of Illustrations

List of Tables

Chapter 1:

Introduction

This chapter provides the literature review and statement of purpose for the study of consensus and collision avoidance in a platoon of vehicles using adaptive cruise control.

Section 1.1 – Literature Review

The benefits of organizing vehicles into platoons with small intervehicle distances are well known [1] [2]. Reducing intervehicle spacing in a platoon to a few meters has been shown to increase traffic flow, reduce fuel consumption, and improve highway safety [1] [3] [4] [5] [6].

Automated longitudinal control of vehicles in platoons can be done either in a centralized manner or a decentralized manner [7]. In centralized control, a roadside unit (RSU) provides speed or acceleration commands to vehicles via wireless communication. This can provide excellent controllability and optimization of traffic flow and capacity because it provides closed-loop control of traffic density profiles [8]. However, since RSUs will not be ubiquitous in infrastructure soon, this thesis will focus on the decentralized control techniques that can be utilized with existing infrastructure, commercially available vehicle technology and the soon-to-be available V2V communication. Decentralized longitudinal control means that each vehicle has its own on-board controller and determines its own acceleration using information received from neighbor(s) in the platoon.

Vehicles with Adaptive Cruise Control (ACC) are currently commercially available. ACC vehicles have onboard longitudinal controllers which modify the driver's velocity set point to maintain a desired time or spacing distance from a preceding vehicle,

if a preceding vehicle is within sensor range. ACC utilizes a distance sensor such as radar to determine the distance between the front of the ACC vehicle and the rear of the preceding vehicle [9] [10] [11], hereafter referred to as the intervehicle distance.

ACC vehicles can currently perform vehicle following at large intervehicle distances [4]. However, since ACC is intended for driver convenience and not for improvement of traffic flow, capacity, or fuel economy, a minimum 1s time headway is standard [11]. This standard exists because for time gaps less than 1s, as well as for small constant-distance gaps, it has been shown that a string of ACC vehicles (a platoon) with homogeneous linear controllers who's vehicles use only the measured distance between themselves and the immediately preceding vehicle is a string unstable platoon, regardless of the gains chosen [5] [12] [13] [14] [15]. An explanation of string unstable behavior follows.

String unstable means that disturbances such as velocity changes of the lead vehicle or a preceding vehicle cause intervehicle distance errors in follower vehicles to amplify down the string [3] [5] [12] [13] [14] [15] [16]. If the error is too large in one direction, the intervehicle distance is too large and the platoon loses "coherence" [14] thereby losing fuel economy and traffic efficiency benefits. On the other hand, if the error is too large in the opposite direction, the intervehicle distance is too small, causing collision. These errors get larger and larger between vehicles further down the platoon. This is known as string unstable behavior. String stability means that intervehicle distance errors due to disturbances attenuate down the string. In a string stable platoon, a large intervehicle distance error in the front of the platoon caused by sudden change in velocity of a preceding vehicle does not propagate down the string. Since it is highly desirable to reduce the time-gaps to less than 1s, maintain the platoon cohesion and

avoid collision, designing longitudinal controllers that ensure string stability of ACC platoons at small intervehicle distances is desirable.

Closed-loop stability is also an important topic in platooning. Closed-loop stability in the context of vehicle platoons means that all the vehicles eventually reach the same velocity [2] [17] [18]. Well-known methods of closed-loop stability analysis such Routh-Hurwitz test [11] [18] [19], consensus theory [2] [17] [18] and PDE models [7] [20] have been employed to determine if all vehicles in the platoon will converge asymptotically to the velocity state of the leader, and to design controllers to ensure convergence.

Therefore, the current primary analysis and design of longitudinal controllers in platooning vehicles consists of determining if the vehicles will reach the same velocity as well as attenuate intervehicle distance errors. In other words, it is currently considered a requirement that control system designers choose algorithms and gains such that the platoon is closed-loop stable as well as string stable.

There are several methods for string stabilizing platoons of ACC vehicles at small time gaps. See [14] [21] and the references therein. Each method surveyed is some combination of the following: increasing the number of states or relative states of the leader and other platoon members available to each vehicle; increasing the number of platoon members each vehicle gets information from; modifying the control policy (constant distance gap or constant time gap); changing the type and gains of onboard controllers [12]; and changing the number of vehicles in the platoon. The combination chosen each has varying degrees of effectiveness (in terms of string stabilization) and cost (in terms of system complexity and overhead).

Cooperative Adaptive Cruise Control (CACC) allows for wireless communication between ACC vehicles in a platoon to enhance the feedback information used by each vehicle's controllers and by changing the way the vehicles interact. With CACC, string

stability can be achieved [5] [13] [15] [22] at time-gaps of less than 1s. A thorough review of CACC is provided with references in [21]. CACC can allow for more states (position, velocity, acceleration, jerk) to be received by a follower vehicle's controller. It can also allow for each follower vehicle to receive state information from more than one platoon member. It also has the added benefit of allowing platoons to communicate with RSUs when they become available.

Human behaviors and interactions with CACC vehicles have been studied [21] as have packet loss [23] and delays in wireless communication [14] [17] [24]. This thesis will not discuss these problems; it will be assumed that the driver's only interaction with the longitudinal controller is to set the desired velocity set point. It will also be assumed that the states received from other vehicles wirelessly will not experience delay or packet loss. Platoons with both lateral and longitudinal control have been studied [23], but this thesis will only consider longitudinal control, leaving lateral control to the driver.

Typically, string stability analysis involves defining the intervehicle distance error as a transfer function [3] [4] [6] [7] [12] [14] [16] [17] [20] [24]. This is apparently standard practice. As also noted in [19], there is an inherent drawback in this method of analysis: transfer functions are a representation of the system dynamics with zero initial conditions [20]. In the context of platoons, zero initial conditions means that the platoon's string stability can only be analyzed with every vehicle starting from a complete stop and with zero intervehicle distance error. This is an unrealistic scenario. We must be able to analyze string stability in the event of vehicles entering and exiting a platoon while moving, thus a method to analyze a platoon with non-zero initial conditions and non-zero initial errors is desirable.

Section 2.1 – Statement of Purpose

In existing literature, the leader is treated as an external source pinning in to or otherwise externally affecting the follower vehicles and the leader is controlled independently from the platoon. In this thesis, a novel approach to platooning is used which utilizes consensus theory: the leader is treated as an internal information source and the controller for the leader is designed simultaneously with the controllers for the followers. Chapter 2 provides background information on consensus theory, information flow between vehicles in a platoon and the vehicle model dynamics used in this thesis. Chapter 3 defines the 1-Leader Type graph which allows us to treat the leader as an internal member of the platoon and suggests a consensus value for this type of graph when there is no spatial offset from the leader position. Chapter 4 provides simulations as evidence to support ideas presented in Chapter 3. Chapter 5 defines a platoon consensus protocol for the 1-Leader Type graph in both local and global form and suggests a resulting consensus value when there *is* spatial offset from the leader position. Chapters 6, 7, and 8 provide simulations as evidence to support ideas presented in Chapter 4.

As previously stated, it is currently considered a requirement that control system designers choose algorithms and gains such that the platoon is closed-loop stable as well as string stable. However, as this thesis will demonstrate in Chapter 9, string stability does not guarantee collision avoidance and therefore the primary design consideration for longitudinal controllers in platooning vehicles should instead be to ensure convergence and to ensure collision avoidance, regardless of whether the platoon topology is string stable and while considering non-zero initial conditions. Chapter 9 suggests a method to design such controllers. Chapter 10 provides a summary of the work presented in this thesis and provides suggestions for future work.

Chapter 2:

Preliminaries

This chapter provides notations, an explanation of the information flow in platoons, background information for communication graphs, and information regarding the model for the vehicle dynamics, and an introduction to consensus theory using communication graphs.

Section 2.1 – Document Notations

For the sake of being clear about which ideas are my own and which are not, the reader will notice throughout the document that four key terms will be bolded: theorem, lemma, definition, and conjecture. Please note that the theorems are not my own and proper credit is given. They are bolded to denote important starting points for my work. The lemmas, definitions, and conjectures are of my own deduction and design, but stem from the theorems and other documented background information. The term ‘assumption’ is also bolded for easy reference location.

Section 2.2 – Mathematical and Symbolic Notations

The transpose of a matrix or vector A is denoted by A^T. The cofactor of an element of a matrix is denoted by $cof(m_{i,j})$. An $m \times n$ real matrix is denoted by $R^{m \times n}$. A real vector of length n is denoted by R^n. A real scalar value is denoted by R. Let $A \in R^{m \times n}$ and $B \in R^{p \times q}$, then the Kronecker product of A and B is denoted by $A \otimes B$ and $A \otimes B = \begin{bmatrix} a_{11}B & \cdots & a_{m1}B \\ \vdots & \ddots & \vdots \\ a_{1n}B & \cdots & a_{mn}B \end{bmatrix} \in R^{mp \times nq}$. A diagonal matrix with entries $a_1, a_2, \ldots a_n$ is denoted by $diag\{a_1, a_2, \ldots a_n\} \in R^{n \times n}$. An identity matrix of dimension $n \times n$ is denoted by I_n.

Section 2.3 - Information Flowing in a Platoon

In the context of platooning, it is possible to define a formation protocol which does not require a pinning matrix. This allows one to not have to consider the dynamics of the leader differently. Leader dynamics can be considered simultaneously with the follower dynamics. As stated in the literature review it is common to treat the leader (and sometimes the caboose) as a special case or as different from the followers, even if they have the same dynamics. This does not allow for expansion into lateral control, followers becoming leaders, or leaders becoming followers without changing the controller protocol or controller gain. This means that while using a pinning matrix, the leader always must be the leader and can never be a follower. If the lead vehicle needs to become a follower, then the controllers and gains for all vehicles must change.

It is important to distinguish the key difference in the analysis of the topologies in existing literature [2] [17] [18] [25] [26] [27] and in this thesis. In existing literature, the leader is treated as an *external* source pinning in to or otherwise externally affecting the follower vehicles and the leader is controlled independently from the platoon. In this thesis, the leader is treated as an *internal* information source and the controller for the leader is designed simultaneously with the controller for the followers. This allows the leader to become a follower and any follower to become the leader. This is important because it allows for much greater flexibility in platooning.

This thesis includes the leader in the communication graph and does not treat it separately. A new protocol is defined such that the leader is the origin of an inertial frame of reference, rather than being pinned from a virtual leader at the formation center. As with other experiments in the platooning literature, it is a requirement that the number of nodes be known and the order of vehicles be known. The method developed in this thesis allows for any vehicle to be the leader, follower, or caboose while maintaining the

same gains and controller structure. Any vehicle can assume any node number (leader or non-leader) and the controller does not change.

Although there are many different topologies for vehicle platoons, we will only analyze six commonly used communication topologies in this thesis [25]. The platoon has N vehicles *including* the leader. The six topologies we will analyze in this thesis are

1. Predecessor-Following (PF)
2. Predecessor-Leader-Following (PLF)
3. Bidirectional (BD)
4. Bidirectional-Leader (BDL)
5. Two-Predecessor-Following (TPF)
6. Two-Predecessor-Leader-Following (TPLF)

Figure 1 shows these six common vehicle platooning communication topologies. Each vehicle, or node, is represented as a black dot. Node 1 is the lead vehicle and is shown on the far right. Node N is the last vehicle of the platoon and is shown on the far left. The white dot with three black dots in the middle represents vehicles 4 through $N-4$. The arrows represent the direction of information flow. The tail of the arrow connected to a node means information comes from that node. The head of the arrow pointing into a node means information comes into that node. For example, and arrow from node 1 to node 3 means that vehicle 3 gets information from the lead vehicle. Note that in each of these topologies, the lead vehicle does not receive information from any follower vehicles.

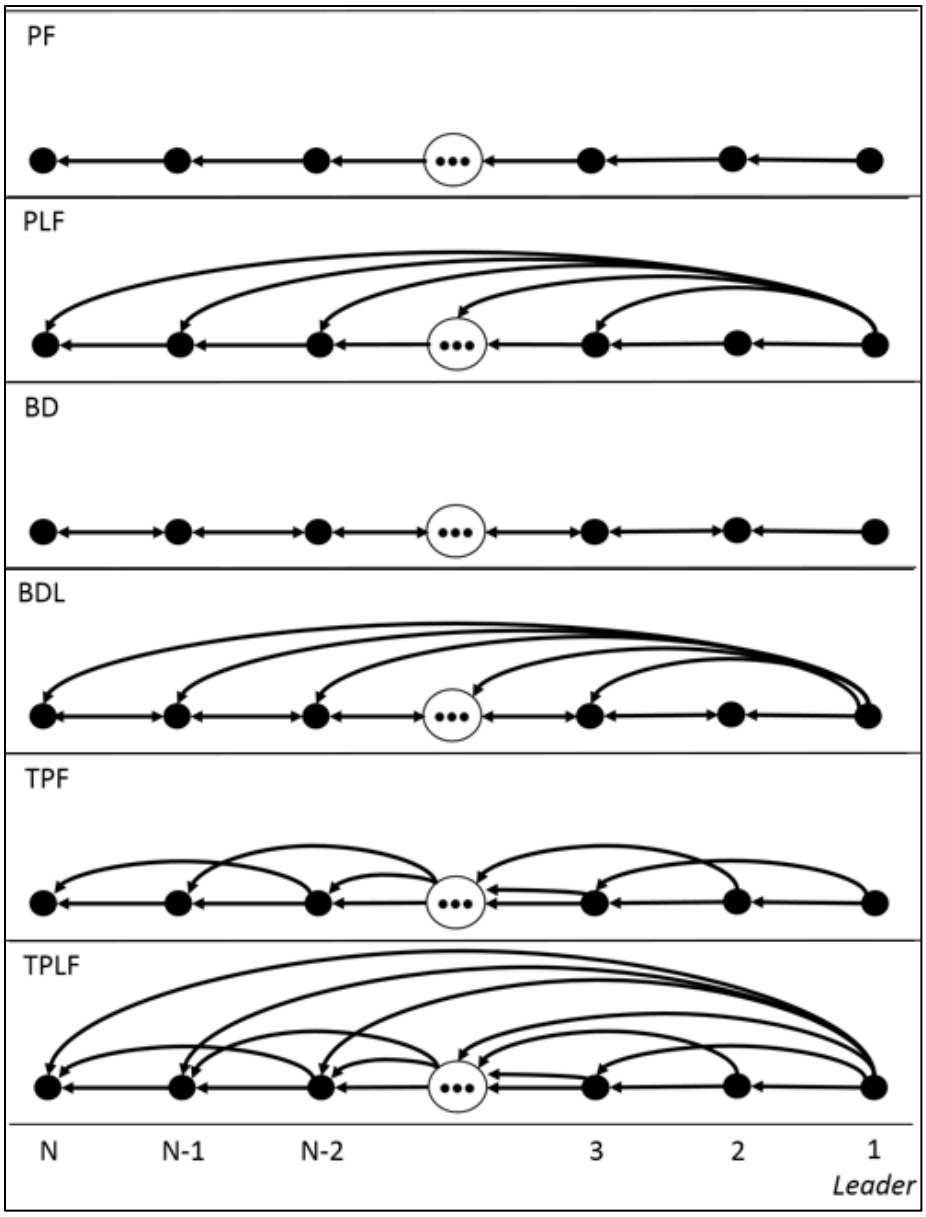

Figure 1 - Six common vehicle platooning communication topologies with the leader (node 1) shown on the far right.

Predecessor-Following (PF), Predecessor-Leader-Following (PLF),

Bidirectional (BD), Bidirectional-Leader (BDL),

Two-Predecessor-Following (TPF), Two-Predecessor-Leader-Following (TPLF).

Section 2.4 - Vehicle Longitudinal Dynamics

The vehicles are all assumed to have homogeneous dynamics. To represent the vehicle dynamics, we will use Newton's law agent dynamics. The agent dynamics are $\dot{x}_i = v_i$, $\dot{v}_i = u_i$ with position $x_i \in R$, velocity $v_i \in R$, and acceleration input $u_i \in R$. We use the script $\mathcal{A}$ to distinguish the node dynamics from the adjacency matrix A. The state space model for each vehicle is derived as (1).

$$\dot{z}_i = \mathcal{A} z_i + B u_i \quad (1)$$

where $z_i = \begin{bmatrix} x_i \\ v_i \end{bmatrix}$, $\mathcal{A} = \begin{bmatrix} 0 & 1 \\ 0 & 0 \end{bmatrix}$, $B = \begin{bmatrix} 0 \\ 1 \end{bmatrix}$. More accurate models exist and have been used in literature such as [10] [16] [25] but that is beyond the scope of this thesis.

Tying this into Figure 1, the information that flows along the communication arrows is vehicle position x_i and velocity v_i. This thesis will use only SI units such that position is in meters, velocity is in meters per second, and acceleration is in meters per second-squared. Note that each vehicle is treated as a point mass with no physical length and width dimensions.

Section 2.5 - Communication Graphs

A communication graph $\mathcal{G}$ can be used to model the information flow between agents in a group. See [28] [29] for a thorough treatment of communication graphs in the context of distributed controls. The properties of $\mathcal{G}$ are known to affect the collective behavior of the group including platoon stability, string stability, and scalability [25]. Throughout this thesis, the terms agent, node, and vehicle will be used interchangeably. The platoon has N vehicles, including the leader.

The directed graph (digraph) model $\mathcal{G}$ is represented as follows. $\mathcal{G} = (V, E)$ where $V = \{v_1, \ldots, v_N\}$ is a set of N nodes and $E = (v_i, v_j)$ is a set of edges from v_i to v_j with

edge weights a_{ij}. A neighborhood set $N_i = \{v_j : (v_j, v_i) \in E\}$ is the set of nodes from which i gets information.

The adjacency matrix $A = [a_{ij}] \in R^{N \times N}$ is the matrix representation of $\mathcal{G}$. The in-degree of node i, d_i, is the total number of neighbors a node gets information from and is $d_i = \sum_{j=1}^{N} a_{ij}$. The graph Laplacian is defined as $L = D - A, \in R^{N \times N}$, where $D = diag\{d_i\}, \in R^{N \times N}$. In this thesis, we will assume $\mathcal{G}$ has the following properties:

Assumption 1.1: Binary edge weights, i.e. $a_{ij} \in \{0,1\}$.

Assumption 1.2: It is a digraph, i.e. $A \neq A^T$.

Assumption 1.3: There are no self-loops, i.e. $a_{ij} = 0, \forall\, i = j$.

A directed tree, also known as a spanning tree, is a subset of edges where every node except one, called the root node or leader node, has in-degree equal to one. A graph is connected if it contains at least one directed tree [29]. Depending on the graph, it is possible for there to exist multiple directed trees with more than one node root node. If the graph is not connected, it has no root nodes.

Chapter 3:

1-Leader Type Graphs and Consensus Values without Offset

This chapter defines a 1-Leader Type (1LT) graph, establishes a mathematical method to use the graph Laplacian to identify a 1LT graph, identifies an error in [29] regarding the consensus value for 1LT graphs, and proposes a formula for consensus values which relates to counting the number of directed trees in a graph.

Section 3.1 – Defining and Identifying 1-Leader Type Graphs

Definition 1*:* For ease of discussion throughout this thesis, we will define a connected graph $\mathcal{G}$ as 1-Leader Type (1LT) if node 1 is the only root node in the graph. It may have multiple directed trees rooted in node 1, but node 1 must be the only node which roots a directed tree. Node 1 will be called the leader.

Theorem 1*:* The Directed Matrix Tree Theorem states that given a graph $\mathcal{G}$, the so-called "Kirchoff in-matrix" S is (2) and the number of directed trees τ rooted at node i is equal to the value of *any* cofactor in the i^{th} *column* of S, as shown in (3).

$$S = D - A^T \in R^{N \times N} \quad (2)$$

$$\tau_i = cof\left(S_{j,i}\right) \forall j \quad (3)$$

Proof: The Directed Matrix Tree Theorem is stated as a theorem and described in [30]. A proof is not directly provided in [30] nor will it be provided in this thesis.

Lemma 1: The number of directed trees τ in $\mathcal{G}$ rooted at node i is (4).

$$\tau_i = cof(L_{i,1}) \quad (4)$$

Proof: Extending from *Theorem 1*, we can relate the Kirchoff in-matrix S to the communication graph Laplacian matrix L. Recall from Section 2.5 that the graph Laplacian is defined as (5).

$$L = D - A \quad (5)$$

Applying the transpose to both sides of (5) we arrive at (6). Applying the commutative property to (6), we arrive at (7).

$$L^T = (D - A)^T \quad (6)$$

$$L^T = D^T - A^T \quad (7)$$

Since D is a diagonal matrix, then (8) allows (7) to become (9).

$$D = D^T \quad (8)$$

$$L^T = D - A^T \quad (9)$$

Combining (2) and (9) we arrive at a direct relation between the Kirchoff in-matrix S to the communication graph Laplacian matrix L with (10) and (11).

$$S = L^T \quad (10)$$

$$L = S^T \quad (11)$$

Utilizing the definition of transpose, the elements of the L and S matrices are related as (12) such that (13).

$$L_{i,j} = S_{j,i} \quad (12)$$

$$cof(L_{i,j}) = cof(S_{j,i}) \quad (13)$$

Combining (3) and (13) we arrive at (14). The number of directed trees rooted at node i is equal to the value of any cofactor in the i^{th} *row* of L.

$$\tau_i = cof\left(L_{i,j}\right) \forall j \quad (14)$$

For ease of use, we will choose the cofactor in the first column ($j = 1$) in the i^{th} row of L to arrive at (4). This concludes the proof for *Lemma 1*.

Definition 2*:* Define the tree count vector T as (15).

$$T = [\tau_1 \quad \tau_2 \quad \dots \quad \tau_N]^T = \left[cof\left(L_{1,1}\right) \quad cof\left(L_{2,1}\right) \quad \dots \quad cof\left(L_{N,1}\right)\right]^T \in R^N \quad (15)$$

The tree count vector T is simply a single vector which tells the number of directed trees rooted at all nodes.

Definition 3*:* Define the normalized tree count vector C as (16).

$$C = \frac{T}{\|T\|_\infty} \in R^N \qquad (16)$$

The normalized tree count vector C is simply a single vector which tells us which nodes are the root of at least one directed tree. By *Definition 3*, $0 \leq C_i \leq 1$. If $C_i > 0$, then node i is the root of at least one directed tree. If $C_i = 0$ then node i does not root any directed trees.

Lemma 2*:* If $\mathcal{G}$ is 1-Leader Type (1LT), then $C = [1 \quad 0 \quad 0 \quad ... \quad 0]^T$.

Proof: By *Definition 1* and *Definition 2*, $T_{i=1} > 0$ and $T_{i\neq 1} = 0$ for a 1LT graph since there is at least 1 directed tree at node 1 and there are no directed trees rooted at any other node. Therefore, the normalized tree count vector is always $C = [1 \quad 0 \quad 0 \quad ... \quad 0]^T$ for a 1LT graph.

Table 1 displays T and C for the six platoon topologies, which indicates that they are all 1LT graphs. The fact that they are all 1LT graphs can also be visually cross-checked with Figure 1. Recall the platoon topologies are Predecessor-Following (PF), Predecessor-Leader-Following (PLF), Bidirectional (BD), Bidirectional-Leader (BDL), Two-Predecessor-Following (TPF) an Two-Predecessor-Leader-Following (TPLF) as shown in Figure 1.

Table 1 - T and C for each platoon topology.

	PF		PLF		BD		BDL		TPF		TPLF	
Node	T	C	T	C	T	C	T	C	T	C	T	C
1	1	1	256	1	1	1	2,584	1	256	1	4,374	1
2	0	0	0	0	0	0	0	0	0	0	0	0
3	0	0	0	0	0	0	0	0	0	0	0	0
4	0	0	0	0	0	0	0	0	0	0	0	0
5	0	0	0	0	0	0	0	0	0	0	0	0
6	0	0	0	0	0	0	0	0	0	0	0	0
7	0	0	0	0	0	0	0	0	0	0	0	0
8	0	0	0	0	0	0	0	0	0	0	0	0
9	0	0	0	0	0	0	0	0	0	0	0	0
10	0	0	0	0	0	0	0	0	0	0	0	0

In the next section, we will utilize the normalize tree count vector C from *Definition 2* to assist in development of a formula to determine the position and velocity consensus values for 1LT graphs such as the above platoon topologies.

Section 3.2 – Consensus Values of 1-Leader-Type Graphs without Offset

This section defines the distributed control protocol which will be utilized throughout this thesis and provides proof that consensus occurs for all 1LT graphs without position offset from the leader when said control protocol is utilized. This section also introduces both a documented theorem and a new conjecture to determine consensus values of position and speed.

Theorem 2*:* As derived in [29], for any connected graph, agent consensus (without an offset from the leader position) of second order systems using the distributed position/velocity feedback protocol (17) will occur if the following assumptions hold:

$$u_i = c\sum_{j\in N_i} a_{ij}\left(x_j - x_i\right) + c\gamma\sum_{j\in N_i} a_{ij}\left(v_j - v_i\right) \qquad (17)$$

Assumption 2.1: $L\underline{1} = 0$, where $\underline{1} = [1 \quad \dots \quad 1] \in R^N$.

Assumption 2.2: $w_1\underline{1} = 1$, where w_1 is the normalized first left eigenvector of L and $w_1 = [p_1 \quad \cdots \quad p_N]^T \in R^N$.

Assumption 2.3: $c > 0$ and $c\gamma > 0$, where c is termed the stiffness gain and $c\gamma$ is called the damping gain.

Proof: See [29] and the references therein.

Lemma 3*:* If $\mathcal{G}$ is 1LT, and protocol (17) is used, and *Assumption 2.3* holds, then consensus (without offset) will occur when $w_1 = C$.

Proof: *Assumption 1.3* confirms that *Assumption 2.1* holds. Given *Lemma 2*, it is easy to see that $C\underline{1} = 1$, thus *Assumption 2.2* holds. Since the three criteria have been met for *Theorem 2*, consensus will occur when $w_1 = C$, confirming *Lemma 3*.

Lemma 4: For any 1LT graph, $p_{i=1} = 1$ and $p_{i\neq 1} = 0$.

Proof: Since $w_1 = C$ by *Lemma 3* and $w_1 = [p_1 \quad \cdots \quad p_N]^T$ by *Assumption 2.2*, then $C = [p_1 \quad \cdots \quad p_N]^T$. Since $C = [1 \quad 0 \quad 0 \quad \ldots \quad 0]$ by *Lemma 2*, then *Lemma 4* is confirmed.

Theorem 3*:* In [29] it has been shown that for a connected graph that meets the criteria of *Theorem 2*, the consensus values of position and speed are given by (18) and (19). Note t_f is the final time in seconds, and must occur after $u_i = 0, \forall i$ [29]. That is to say, t_f must occur after convergence.

$$\overline{x}_A = \frac{1}{N}\sum_{i=1}^{N} p_i x_i(0) + t_f \overline{v}_A \qquad (18)$$

$$\overline{v}_A = \frac{1}{N}\sum_{i=1}^{N} p_i v_i(0) \qquad (19)$$

Proof: No proof will be provided for *Theorem 3*. In fact, Chapter 4 provides six examples which confirm that *Theorem 3* is invalid for a 1LT graph. Thus, Chapter 4 serves to *dis*prove *Theorem 3*. *Conjecture 1* provides a possible correction to *Theorem 3.*

Conjecture 1: If $\mathcal{G}$ is 1LT and *Assumption 2.3* holds, then the consensus values of position and speed are given by (20) and (21), where $\overline{x}_B$ and $\overline{v}_B$ are both scalar values.

$$\overline{x}_B = \sum_{i=1}^{N} p_i x_i(0) + t_f \overline{v}_B \qquad (20)$$

$$\overline{v}_B = \sum_{i=1}^{N} p_i v_i(0) \qquad (21)$$

Proof: Chapter 4 provides simulation evidence to support *Conjecture 1.*

Given *Lemma 4*, (18) and (19) can be simplified to (22) and (23).

$$\overline{x}_A = \frac{1}{N} x_1(0) + t_f \overline{v}_A \quad (22)$$

$$\overline{v}_A = \frac{1}{N} v_1(0) \quad (23)$$

Likewise, (20) and (21) can be simplified to (24) and (25).

$$\overline{x}_B = x_1(0) + t_f \overline{v}_B \quad (24)$$

$$\overline{v}_B = v_1(0) \quad (25)$$

Therefore, the consensus values of a 1LT graph which utilizes the distributed position/velocity feedback protocol (17) are not (22) and (23) as theorized in [29], but instead are (24) and (25) as proposed in *Conjecture 1.* The following chapter (Chapter 4) provides evidence for this claim.

Chapter 4:

Evidence for Chapter 3

This chapter provides details and results of 6 simulations which simultaneously serve to disprove *Theorem 3* and provide support for *Conjecture 1*.

Section 4.1 – Explanation of Simulation Setup for Chapter 4

Protocol (17) was implemented using MATLAB/Simulink for each of the 6 platoon topologies. The Appendix provides details regarding how the simulation was performed. An important thing to note regarding the simulations in this chapter is that no restrictions or bounds were placed on the acceleration input or the vehicle velocity.

Per California PATH's automated highway system design and analysis, a platoon can consist of no more than 20 vehicles [3]. In all cases throughout this thesis, there are 10 vehicles including the leader so that $N = 10$. Let $x(0) = [x_i(0)] \in R^N$ be the initial position vector and $v(0) = [v_i(0)] \in R^N$ be the initial velocity vector, where x and v are functions of time in seconds. $\overline{x}_A$ and $\overline{v}_A$ from *Theorem 3* as well as $\overline{x}_B$and $\overline{v}_B$ from *Conjecture 1* were calculated for each platoon topology using (22), (23), (24), (25), respectively with the following initial conditions:

$$x(0) = [10 \quad 9 \quad 8 \quad 7 \quad 6 \quad 5 \quad 4 \quad 3 \quad 2 \quad 1]$$

$$v(0) = [1 \quad .9 \quad .8 \quad .7 \quad .6 \quad .5 \quad .4 \quad .3 \quad .2 \quad .1].$$

In this chapter, the gain values of the protocol (17) were arbitrarily chosen to be $c = 1$ and $\gamma = 1$, which satisfies *Assumption 2.3*. Notice that calculating $\overline{x}_A, \overline{x}_B, \overline{v}_A, \overline{v}_B$ requires final time t_f and recall that t_f must occur after $u_i = 0, \forall i$. The Appendix displays the code used in running the simulations. The code section titled "Determine Time to Convergence (ttc)" shows the code and method used for determining t_f in simulation.

Section 4.2 – Analysis of Results for Simulation 4.1

The results for t_f for each topology given the conditions described in Section 4.1 are provided in Table 2. Recall the platoon topologies are Predecessor-Following (PF), Predecessor-Leader-Following (PLF), Bidirectional (BD), Bidirectional-Leader (BDL), Two-Predecessor-Following (TPF) and Two-Predecessor-Leader-Following (TPLF) as shown in Figure 1.

Table 2 – Final Times for Simulations in Chapter 4

Topology	t_f
PF	50
PLF	19.27
BD	291.82
BDL	22.09
TPF	24.92
TPLF	18.37

Each subsection below presents a table. A description of the information presented in these tables follows. Column 1 (Node) shows the node number, where node 1 is the lead vehicle and node 10 is the last vehicle in the platoon. Column 2 ($\overline{x}_A$) displays the final position value for each node as calculated by (22). Column 3 ($\overline{x}_B$) displays the final position value for each node as calculated by (24). Column 4 ($x_i(t_f)_{sim}$) shows the final position value for each node as obtained by the simulation using the final time t_f from Table 2 . Column 5 ($\%error\ (\overline{x}_A)$) shows the error percentage between $\overline{x}_A$ and $x_i(t_f)_{sim}$. Column 6 ($\%error\ (\overline{x}_B)$) shows the error percentage between $\overline{x}_B$ and $x_i(t_f)_{sim}$. Column 7 ($\overline{v}_A$) displays the final velocity value for each node as calculated by (23). Column 8 ($\overline{v}_B$) displays the final velocity value for each node as calculated by (25). Column 9 ($v_i(t_f)_{sim}$) shows the final velocity value for each node as obtained by the

simulation using the final time t_f from Table 2 . Column 10 ($\%error\ (\overline{v}_A)$) shows the error percentage between $\overline{x}_A$ and $x_i(t_f)_{sim}$. Column 11 ($\%error\ (\overline{x}_B)$) shows the error percentage between $\overline{x}_B$ and $x_i(t_f)_{sim}$.

The subsections below also present three figures for each topology. The first figure shows the simulation results of position versus time for each node. The values $\overline{x}_A$ and $\overline{x}_B$ were superimposed on the position plots, where $\overline{x}_A$ is denoted by a red "x" and $\overline{x}_B$ is denoted by a blue "x". The second figure shows the simulation results of velocity versus time for each node. The values $\overline{v}_A$ and $\overline{v}_B$ were superimposed on the velocity plots, where $\overline{v}_A$ is denoted by a red "x" and $\overline{v}_B$ is denoted by a blue "x". The acceleration input plots show that the acceleration input $u_i = 0$ for all nodes at the at t_f listed in Table 2.

Table 3 through Table 8 along with Figure 2 through Figure 19 clearly show that *Theorem 3* is invalid for the 1-Leader Type (1LT) graph type and it is also clear that these simulations support *Conjecture 1.*

Predecessor-Following Topology

Table 3 – Analysis of PF Results for Chapter 4

Node	$\overline{x}_A$	$\overline{x}_B$	$x_i(t_f)_{sim}$	$\%error\ (\overline{x}_A)$	$\%error\ (\overline{x}_B)$	$\overline{v}_A$	$\overline{v}_B$	$v_i(t_f)_{sim}$	$\%error\ (\overline{v}_A)$	$\%error\ (\overline{v}_B)$
1	5.996	59.96	59.9600	900.000	0.000	0.1	1	1.0000	900.000	0.000
2	5.996	59.96	59.9600	900.000	0.000	0.1	1	1.0000	900.000	0.000
3	5.996	59.96	59.9600	900.000	0.000	0.1	1	1.0000	900.000	0.000
4	5.996	59.96	59.9600	900.000	0.000	0.1	1	1.0000	900.000	0.000
5	5.996	59.96	59.9600	900.000	0.000	0.1	1	1.0000	900.000	0.000
6	5.996	59.96	59.9600	900.000	0.000	0.1	1	1.0000	900.000	0.000
7	5.996	59.96	59.9600	900.000	0.000	0.1	1	1.0000	900.001	0.000
8	5.996	59.96	59.9600	900.000	0.000	0.1	1	1.0000	900.017	0.002
9	5.996	59.96	59.9600	900.000	0.000	0.1	1	1.0001	900.109	0.011
10	5.996	59.96	59.9597	899.994	0.001	0.1	1	1.0005	900.451	0.045

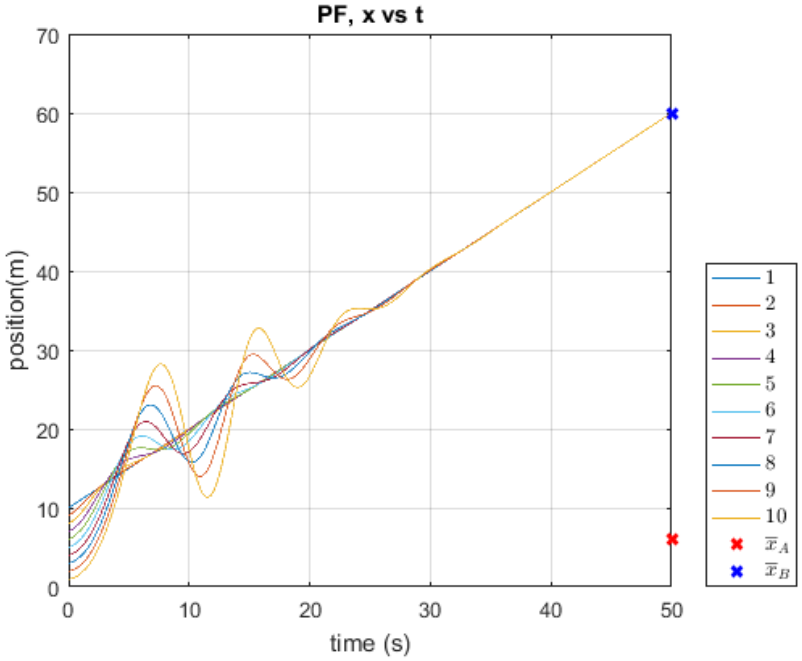

Figure 2 - PF Results for Chapter 4, position versus time.

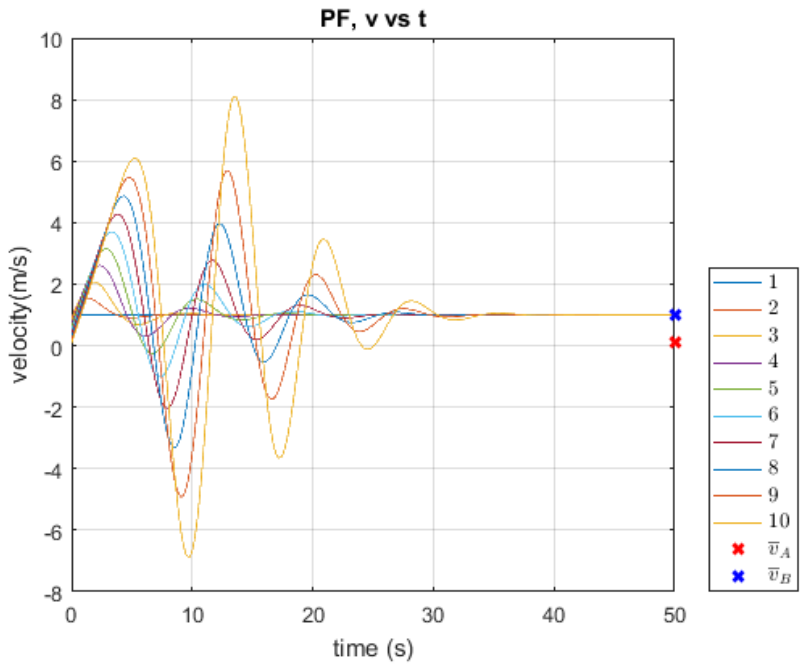

Figure 3 - PF Results for Chapter 4, velocity versus time.

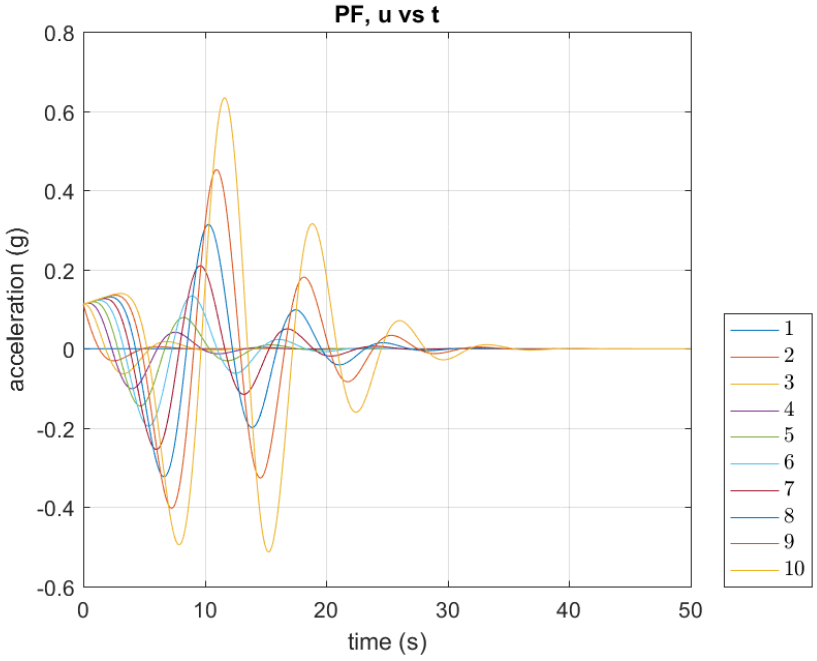

Figure 4 - PF Results for Chapter 4, acceleration input versus time.

Predecessor-Leader-Following Topology

Table 4 - Analysis of PLF Results for Chapter 4

Node	$\overline{x}_A$	$\overline{x}_B$	$x_i(t_f)_{sim}$	$\%error\ (\overline{x}_A)$	$\%error\ (\overline{x}_B)$	$\overline{v}_A$	$\overline{v}_B$	$v_i(t_f)_{sim}$	$\%error\ (\overline{v}_A)$	$\%error\ (\overline{v}_B)$
1	2.912	29.12	29.1200	900.000	0.000	0.1	1	1.0000	900.000	0.000
2	2.912	29.12	29.1201	900.003	0.000	0.1	1	0.9999	899.940	0.006
3	2.912	29.12	29.1201	900.003	0.000	0.1	1	0.9999	899.940	0.006
4	2.912	29.12	29.1201	900.003	0.000	0.1	1	0.9999	899.940	0.006
5	2.912	29.12	29.1201	900.003	0.000	0.1	1	0.9999	899.941	0.006
6	2.912	29.12	29.1201	900.003	0.000	0.1	1	0.9999	899.941	0.006
7	2.912	29.12	29.1201	900.003	0.000	0.1	1	0.9999	899.940	0.006
8	2.912	29.12	29.1201	900.003	0.000	0.1	1	0.9999	899.938	0.006
9	2.912	29.12	29.1201	900.002	0.000	0.1	1	0.9999	899.930	0.007
10	2.912	29.12	29.1201	900.002	0.000	0.1	1	0.9999	899.911	0.009

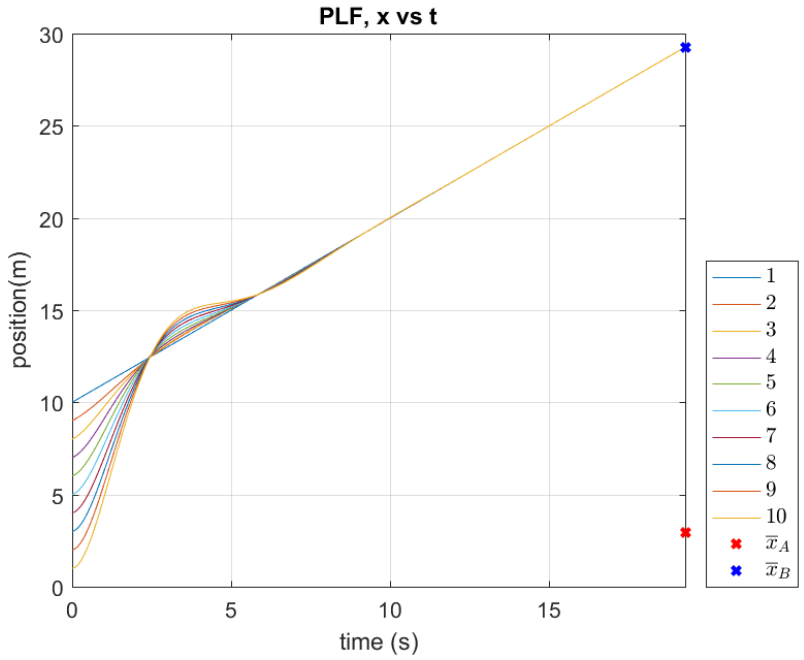

Figure 5 - PLF Results for Chapter 4, position versus time.

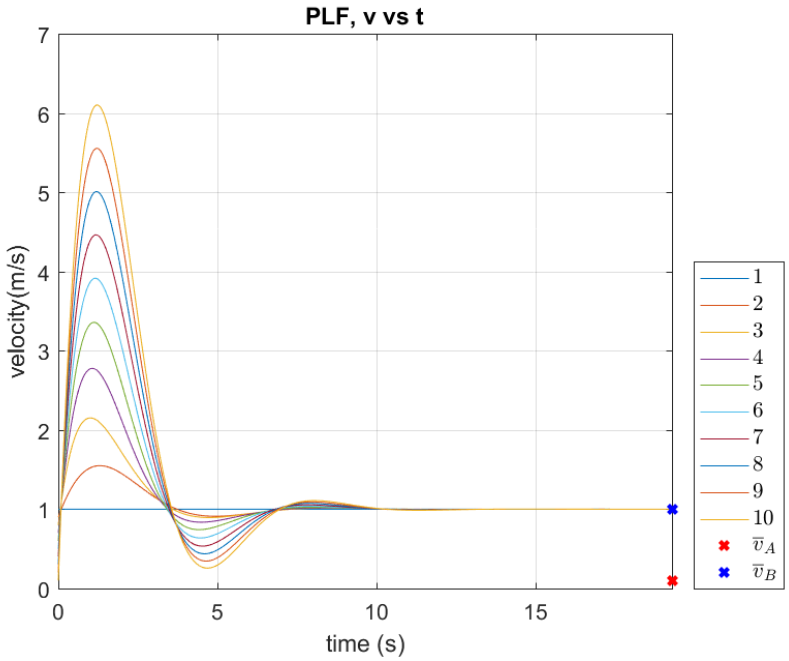

Figure 6 - PF Results for Chapter 4, velocity versus time.

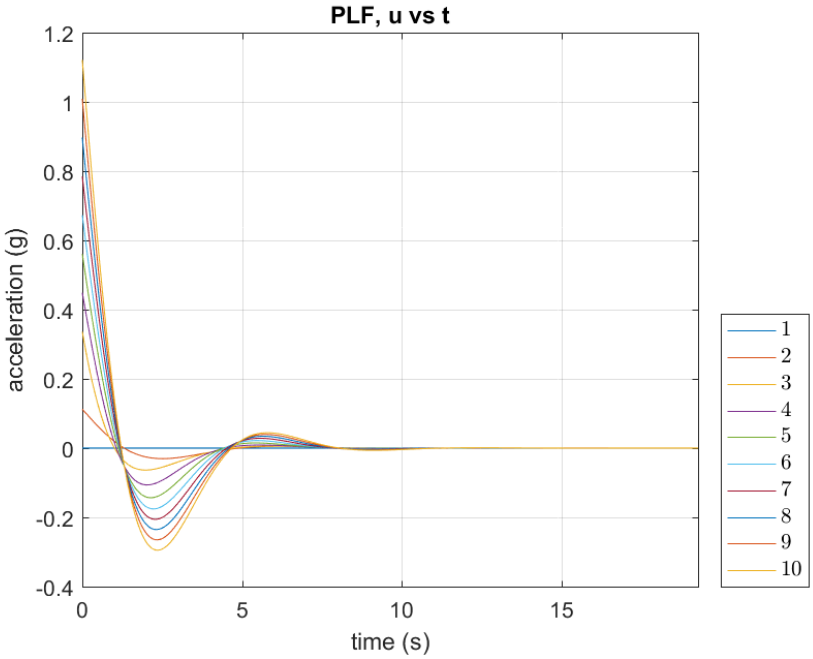

Figure 7 - PF Results for Chapter 4, acceleration input versus time.

Bidirectional Topology

Table 5 - Analysis for BD Results for Chapter 4

Node	$\overline{x}_A$	$\overline{x}_B$	$x_i(t_f)_{sim}$	$\%error\ (\overline{x}_A)$	$\%error\ (\overline{x}_B)$	$\overline{v}_A$	$\overline{v}_B$	$v_i(t_f)_{sim}$	$\%error\ (\overline{v}_A)$	$\%error\ (\overline{v}_B)$
1	30.182	301.82	301.8200	900.000	0.000	0.1	1	1.0000	900.000	0.000
2	30.182	301.82	301.8474	900.091	0.009	0.1	1	0.9982	898.210	0.179
3	30.182	301.82	301.8741	900.179	0.018	0.1	1	0.9965	896.470	0.353
4	30.182	301.82	301.8993	900.263	0.026	0.1	1	0.9948	894.825	0.517
5	30.182	301.82	301.9224	900.339	0.034	0.1	1	0.9933	893.322	0.668
6	30.182	301.82	301.9426	900.406	0.041	0.1	1	0.9920	892.001	0.800
7	30.182	301.82	301.9595	900.462	0.046	0.1	1	0.9909	890.898	0.910
8	30.182	301.82	301.9726	900.506	0.051	0.1	1	0.9900	890.043	0.996
9	30.182	301.82	301.9815	900.535	0.054	0.1	1	0.9895	889.460	1.054
10	30.182	301.82	301.9861	900.550	0.055	0.1	1	0.9892	889.164	1.084

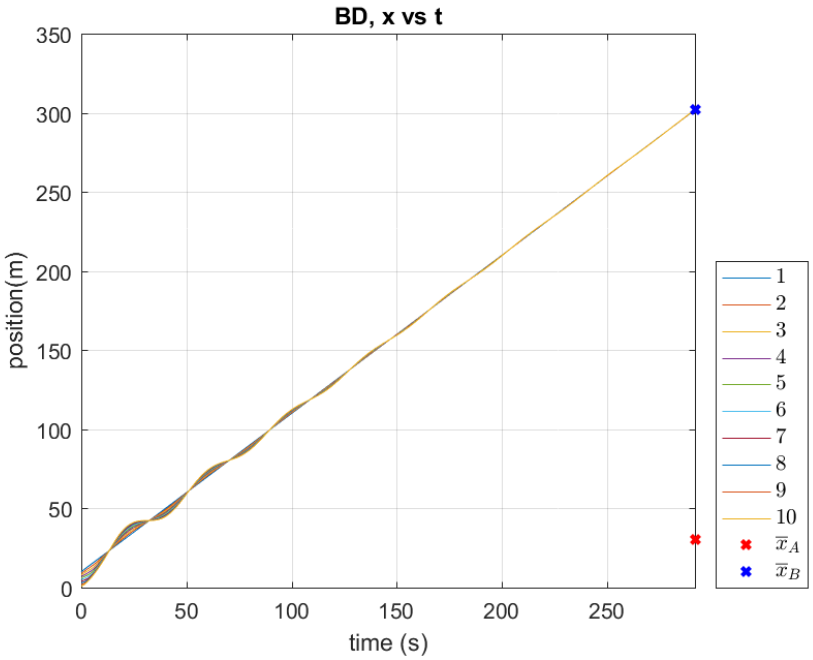

Figure 8 - BD Results for Chapter 4, position versus time.

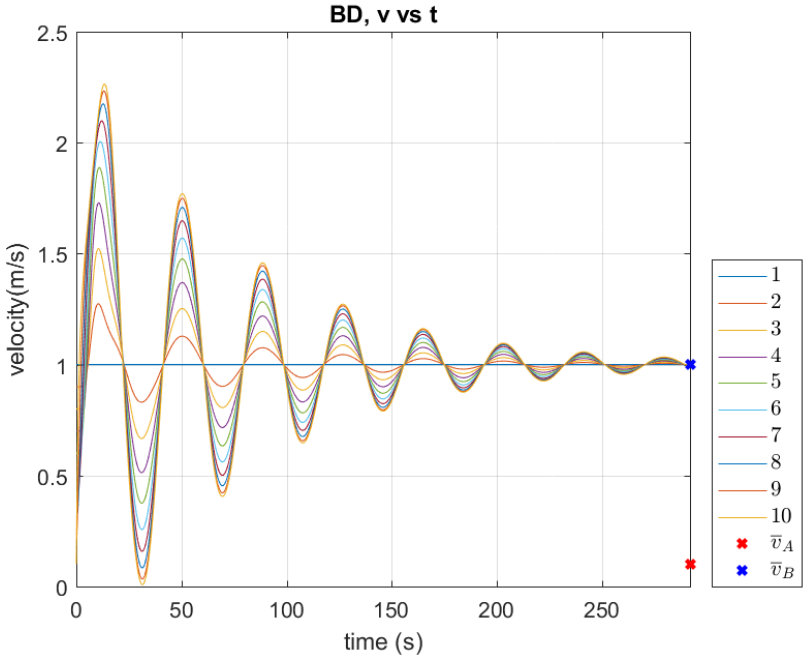

Figure 9 - BD Results for Chapter 4, velocity versus time.

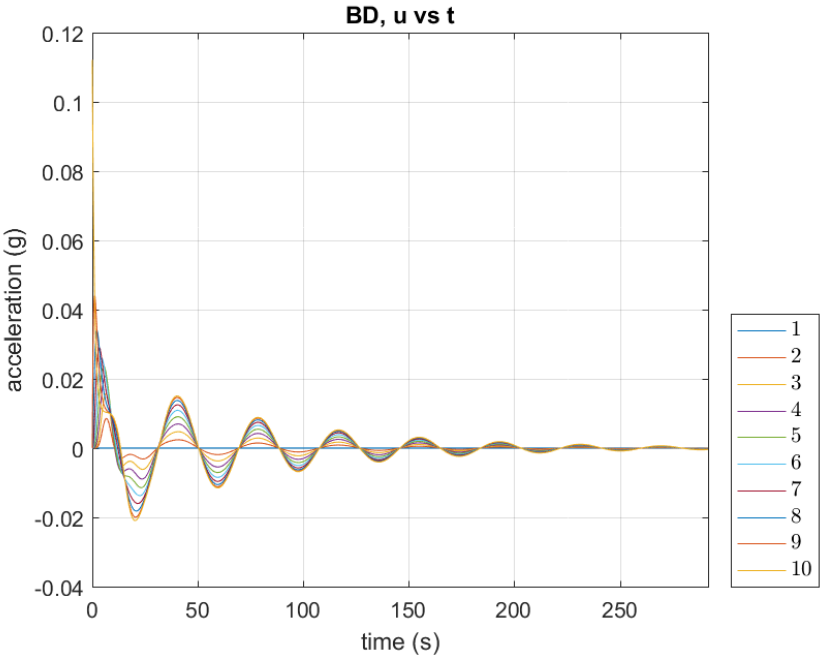

Figure 10 - BD Results for Chapter 4, acceleration input versus time.

Bidirectional-Leader Topology

Table 6 - Analysis for BDL Results for Chapter 4

Node	$\overline{x}_A$	$\overline{x}_B$	$x_i(t_f)_{sim}$	$\%error\ (\overline{x}_A)$	$\%error\ (\overline{x}_B)$	$\overline{v}_A$	$\overline{v}_B$	$v_i(t_f)_{sim}$	$\%error\ (\overline{v}_A)$	$\%error\ (\overline{v}_B)$
1	3.189	31.89	31.8900	900.000	0.000	0.1	1	1.0000	900.000	0.000
2	3.189	31.89	31.8899	899.998	0.000	0.1	1	1.0000	899.988	0.001
3	3.189	31.89	31.8899	899.998	0.000	0.1	1	1.0000	899.990	0.001
4	3.189	31.89	31.8899	899.997	0.000	0.1	1	1.0000	899.993	0.001
5	3.189	31.89	31.8899	899.997	0.000	0.1	1	1.0000	899.998	0.000
6	3.189	31.89	31.8899	899.997	0.000	0.1	1	1.0000	900.003	0.000
7	3.189	31.89	31.8899	899.997	0.000	0.1	1	1.0000	900.008	0.001
8	3.189	31.89	31.8899	899.997	0.000	0.1	1	1.0000	900.012	0.001
9	3.189	31.89	31.8899	899.996	0.000	0.1	1	1.0000	900.016	0.002
10	3.189	31.89	31.8899	899.996	0.000	0.1	1	1.0000	900.018	0.002

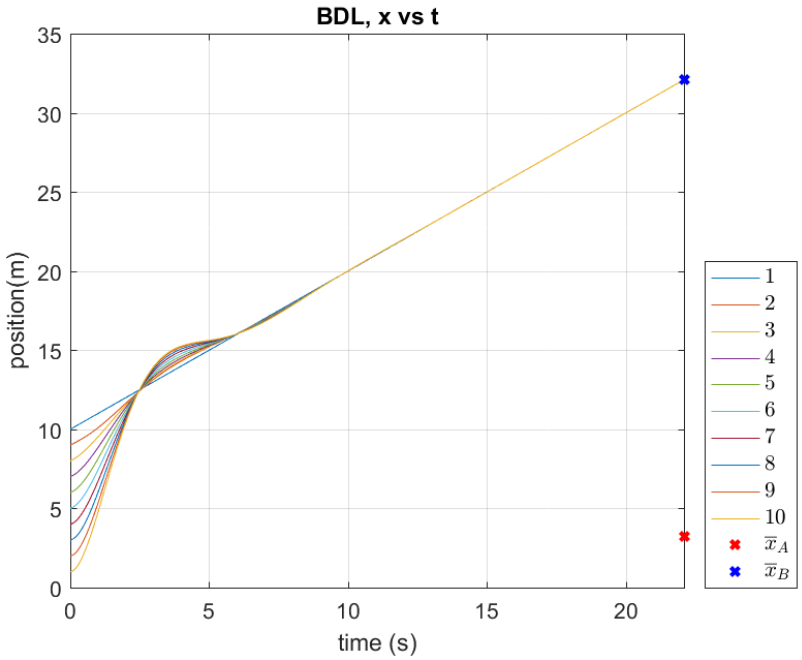

Figure 11 - BDL Results for Chapter 4, position versus time.

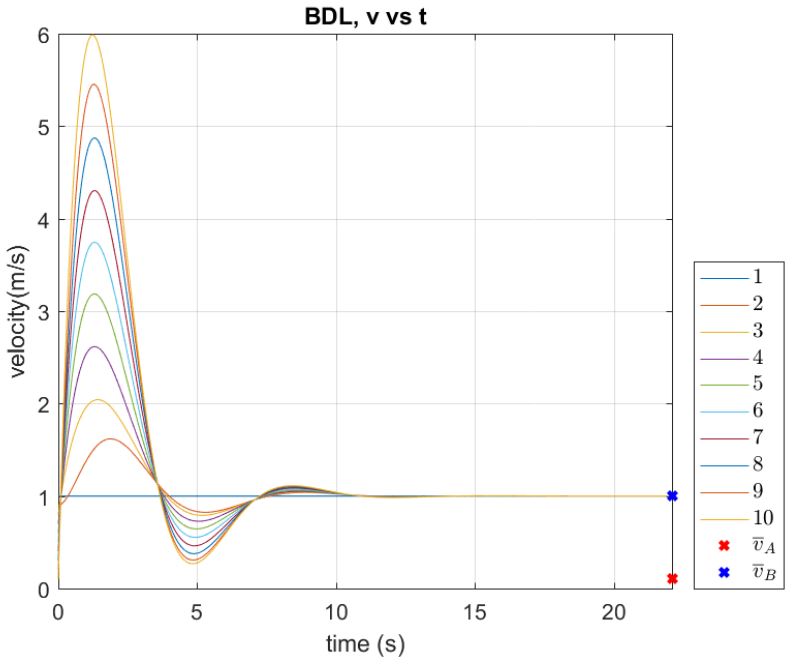

Figure 12 - BDL Results for Chapter 4, velocity versus time.

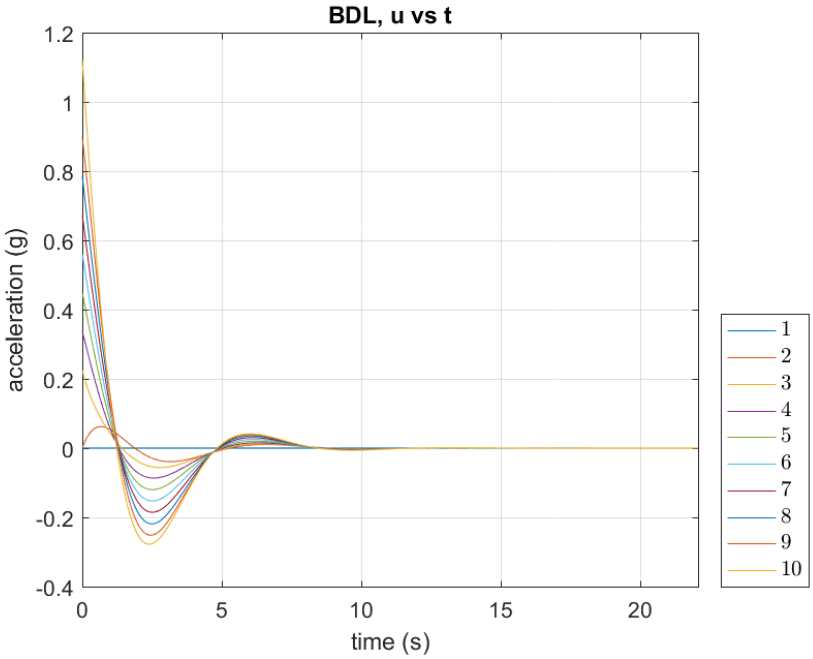

Figure 13 - BDL Results for Chapter 4, acceleration input versus time.

Two-Predecessor-Following Topology

Table 7 - Analysis for TPF Results for Chapter 4

Node	$\overline{x}_A$	$\overline{x}_B$	$x_i(t_f)_{sim}$	$\%error\ (\overline{x}_A)$	$\%error\ (\overline{x}_B)$	$\overline{v}_A$	$\overline{v}_B$	$v_i(t_f)_{sim}$	$\%error\ (\overline{v}_A)$	$\%error\ (\overline{v}_B)$
1	3.475	34.75	34.7500	900.000	0.000	0.1	1	1.0000	900.000	0.000
2	3.475	34.75	34.7500	900.000	0.000	0.1	1	1.0000	900.003	0.000
3	3.475	34.75	34.7500	900.000	0.000	0.1	1	1.0000	900.003	0.000
4	3.475	34.75	34.7500	900.000	0.000	0.1	1	1.0000	900.006	0.001
5	3.475	34.75	34.7500	900.000	0.000	0.1	1	1.0000	900.009	0.001
6	3.475	34.75	34.7500	900.000	0.000	0.1	1	1.0000	900.015	0.002
7	3.475	34.75	34.7500	900.000	0.000	0.1	1	1.0000	900.024	0.002
8	3.475	34.75	34.7500	900.001	0.000	0.1	1	1.0000	900.040	0.004
9	3.475	34.75	34.7500	900.001	0.000	0.1	1	1.0001	900.064	0.006
10	3.475	34.75	34.7501	900.002	0.000	0.1	1	1.0001	900.102	0.010

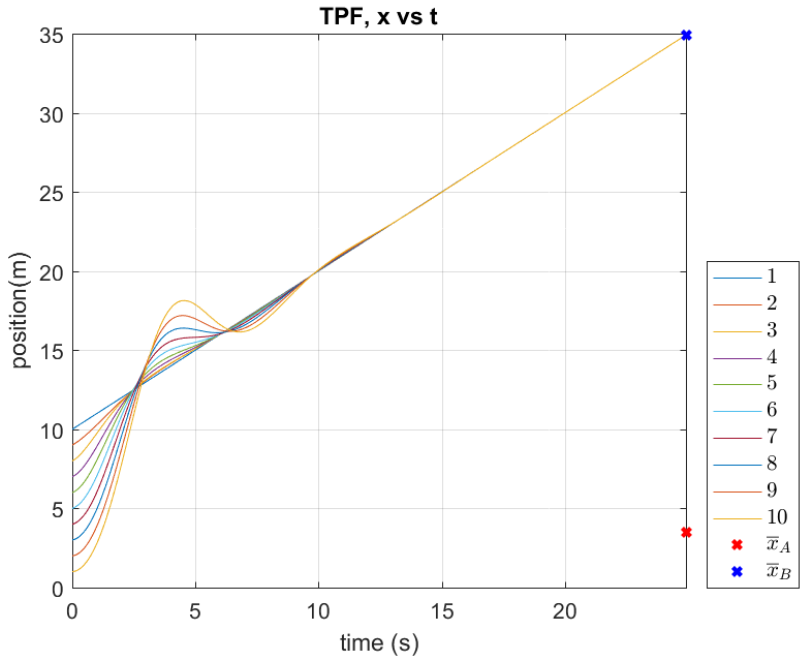

Figure 14 - TPF Results for Chapter 4, position versus time.

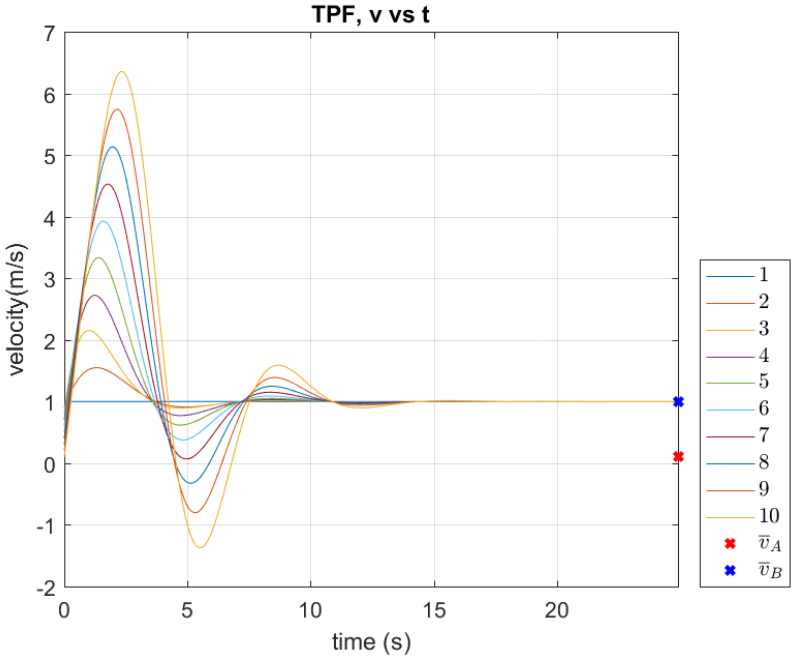

Figure 15 - TPF Results for Chapter 4, velocity versus time.

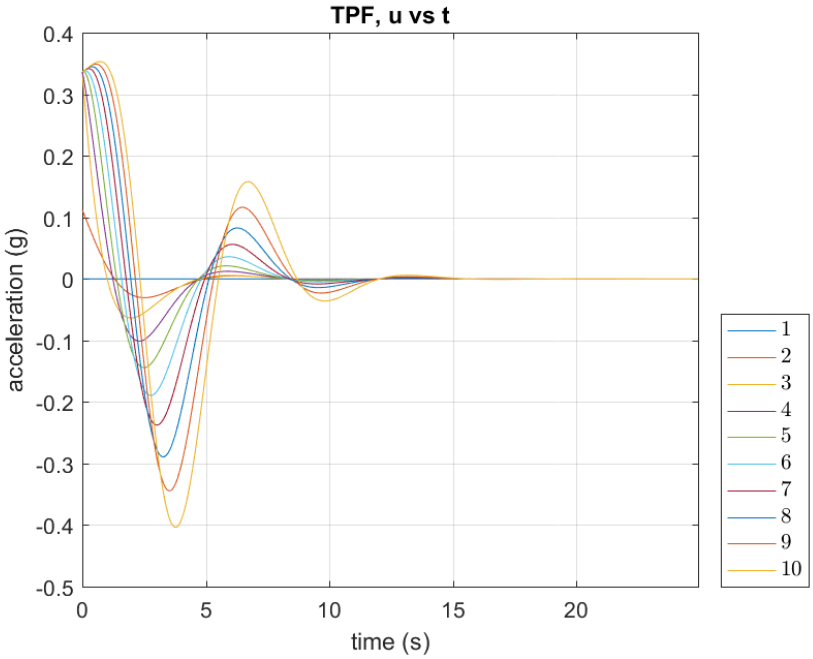

Figure 16 - TPF Results for Chapter 4, acceleration input versus time.

Two-Predecessor-Leader-Following Topology

Table 8 - Analysis for TPLF Results for Chapter 4

Node	$\overline{x}_A$	$\overline{x}_B$	$x_i(t_f)_{sim}$	$\%error\ (\overline{x}_A)$	$\%error\ (\overline{x}_B)$	$\overline{v}_A$	$\overline{v}_B$	$v_i(t_f)_{sim}$	$\%error\ (\overline{v}_A)$	$\%error\ (\overline{v}_B)$
1	2.82	28.20	28.2000	900.000	0.000	0.1	1	1.0000	900.000	0.000
2	2.82	28.20	28.2001	900.004	0.000	0.1	1	1.0000	900.004	0.000
3	2.82	28.20	28.2001	900.004	0.000	0.1	1	1.0000	900.004	0.000
4	2.82	28.20	28.2001	900.004	0.000	0.1	1	1.0000	900.004	0.000
5	2.82	28.20	28.2001	900.004	0.000	0.1	1	1.0000	900.004	0.000
6	2.82	28.20	28.2001	900.004	0.000	0.1	1	1.0000	900.004	0.000
7	2.82	28.20	28.2001	900.004	0.000	0.1	1	1.0000	900.004	0.000
8	2.82	28.20	28.2001	900.004	0.000	0.1	1	1.0000	900.004	0.000
9	2.82	28.20	28.2001	900.004	0.000	0.1	1	1.0000	900.004	0.000
10	2.82	28.20	28.2001	900.004	0.000	0.1	1	1.0000	900.003	0.000

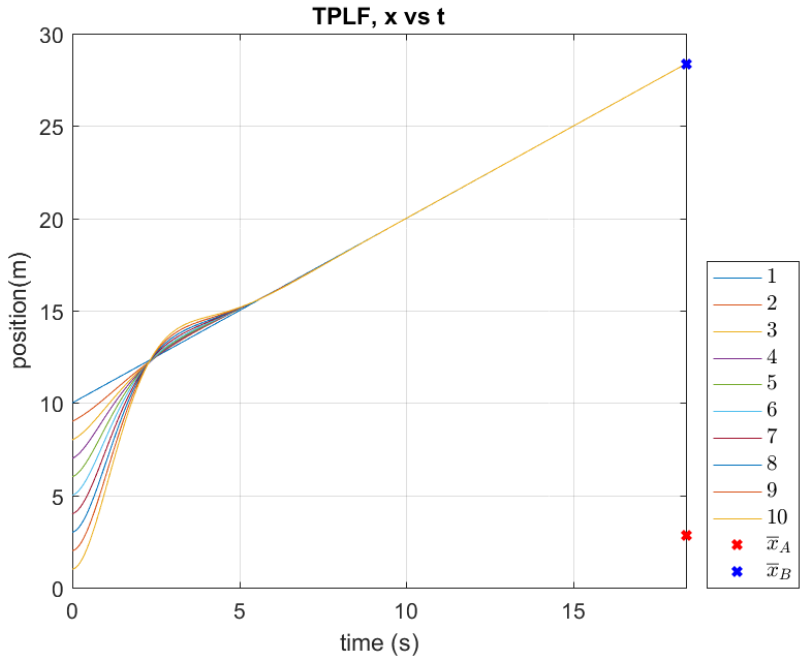

Figure 17 - TPLF Results for Chapter 4, position versus time.

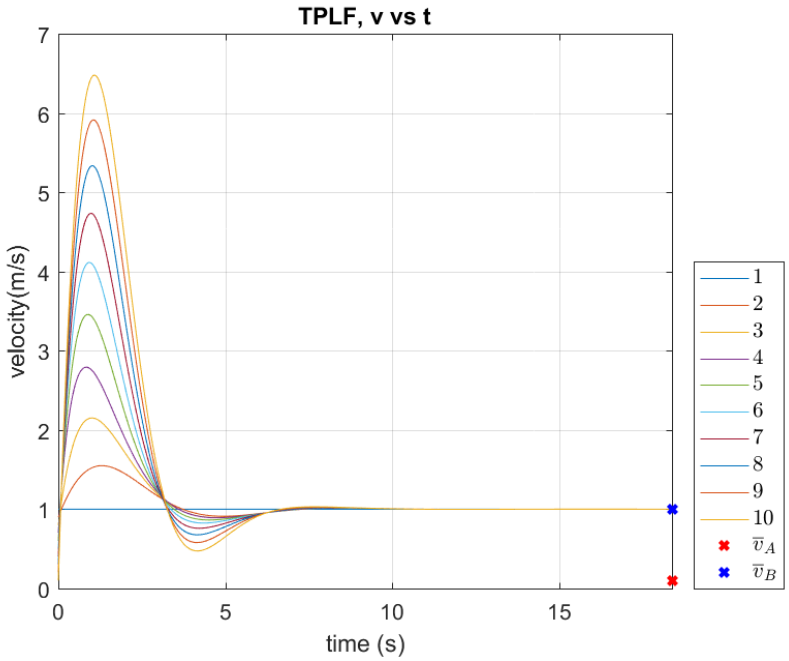

Figure 18 - TPLF Results for Chapter 4, velocity versus time.

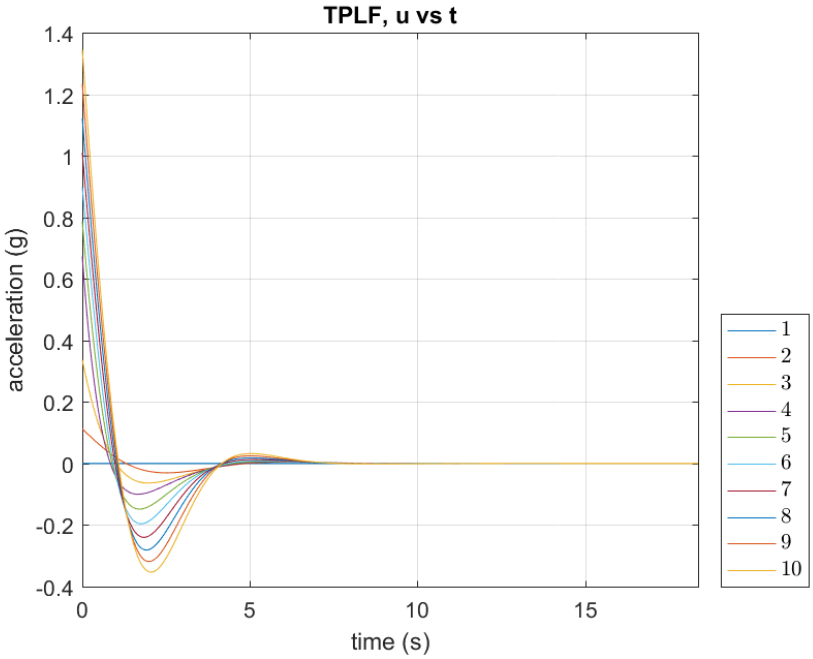

Figure 19 - TPLF Results for Chapter 4, acceleration input versus time.

Chapter 5:

1-Leader Type Graphs and Consensus with Offset

In the context of longitudinal control of platoons, the control objectives are for the vehicles to match velocities and for the distance between them to reach a desired distance. In this chapter and the remaining chapters, we will consider vehicles with homogeneous dynamics as described in Section 2.4 and a platoon with a constant distance policy, where h is the constant, velocity independent, desired distance between any follower and its immediate predecessor (the car directly in front of it). The length of the vehicle is assumed to be included in h.

To meet the control objectives without treating the leader separately or requiring a virtual leader at the formation center, we will use the distributed position/velocity feedback with offset protocol (26), as proposed by [26] [28]. Here, $\Delta_{ji} \in R$ represents the desired position offset of node i from node j.

$$u_i = c\sum_{j\in N_i} a_{ij}\left(x_j - x_i - \Delta_{ji}\right) + c\gamma\sum_{j\in N_i} a_{ij}\left(v_j - v_i\right) \qquad (26)$$

Conjecture 2*:* The global form of protocol (26) is $\dot{z} = \mathcal{A}_c z + Q$, where Q is a static constant.

Proof: It is easy to see in (26) that $u_i = 0$ when $x_j - x_i = \Delta_{ji}$ and $v_j = v_i$, so when the nodes have all reached the desired position offset from each other and the velocities all match, the acceleration of each node is zero. Since the vehicles are all travelling at the same acceleration when in formation, the leader position can be defined as the origin of an inertial frame of reference as shown in Figure 20. In Figure 20, the nodes or vehicles are represented by black dots with white numbers, where node 1 is the lead vehicle and is travelling in a positive direction to the right as indicated by the arrow to the right of node 1. Figure 20 represents the desired relative positions in consensus, which will be referred to as formation. The inertial frame of reference is of prime

importance because it provides the ability to define Δ_{ji} in such a way that protocol (26) can be written in global form.

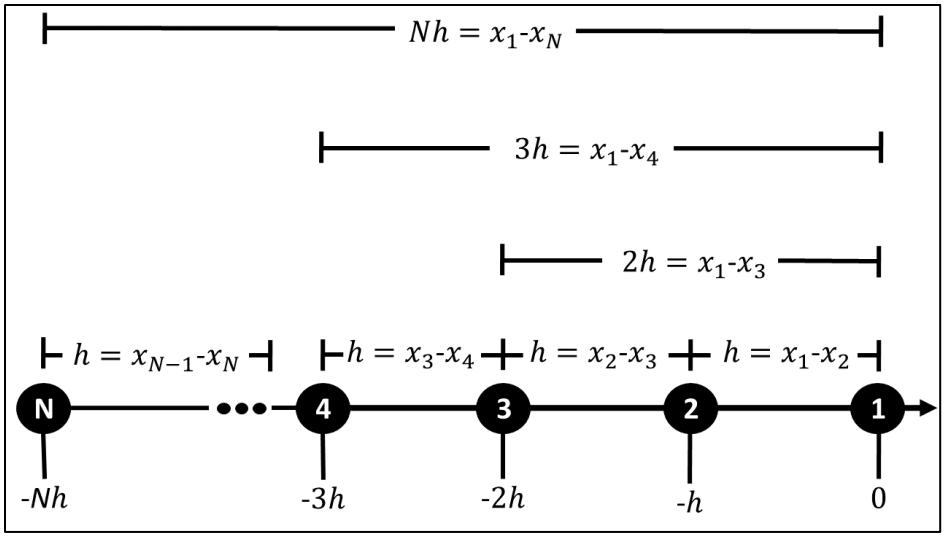

Figure 20 - Platoon formation with leader as origin of inertial frame of reference.

In formation as described by Figure 20, the actual distance between two nodes is equal to the desired distance (27). For example, using Figure 20, let $j = 1$ and $i = 3$.

$$x_j - x_i = \Delta_{ji} \quad (27)$$

$$x_1 - x_3 = (0h) - (-2h) \quad (28)$$

$$x_1 - x_3 = 2h \quad (29)$$

$$x_1 - x_3 = (3 - 1)h \quad (30)$$

As another example, let $j = 3$ and $i = 2$.

$$x_3 - x_2 = (-2h) - (-h) \quad (31)$$

$$x_3 - x_2 = -h \quad (32)$$

$$x_3 - x_2 = (2 - 3)h \quad (33)$$

We can generalize these examples such that Figure 20 allows (27) to become (34).

$$x_j - x_i = (i - j)h \quad (34)$$

Definition 4: The formation position vector H which corresponds to the formation shown in Figure 20 is (35) such that (36)

$$H = [0 \quad h \quad 2h \quad \cdots \quad (N-1)h]^T \in R^N, \tag{35}$$

$$H_j - H_i = (j-i)h. \tag{36}$$

Definition 5: The formation velocity vector G which corresponds to the formation shown in Figure 20 is (37) because in formation the velocities of each node are all equal such that (38).

$$G = [0 \quad 0 \quad 0 \quad \cdots \quad 0]^T \in R^N \tag{37}$$

$$G_j - G_i = 0 \tag{38}$$

Combining (34) and (36) the position error between any two nodes $e_{x_{ji}}$ is then defined as (39) and is zero when in formation. The velocity error between any two nodes $e_{v_{ji}}$ becomes (40) and is zero when in formation.

$$e_{x_{ji}} = (x_j - x_i) + (H_j - H_i) \tag{39}$$

$$e_{v_{ji}} = (v_j - v_i) + (G_j - G_i) \tag{40}$$

Considering (39) and (40), protocol (26) becomes (42).

$$u_i = c\sum_j^N a_{ij}\left((x_j - x_i) + (H_j - H_i)\right) + c\gamma\sum_j^N a_{ij}\left((v_j - v_i) + (G_j - G_i)\right) \tag{41}$$

Considering (42), (43) and (44), (41) becomes (45).

$$z_i = [x_i \quad v_i]^T \tag{42}$$

$$F_i = [H_i \quad G_i]^T \tag{43}$$

$$K = [1 \quad \gamma] \tag{44}$$

$$u_i = cK\sum_j^N a_{ij}\left((z_j - z_i) + (F_j - F_i)\right). \tag{45}$$

Considering (1), (46) and (47), (45) becomes (48).

$$z = [{z_1}^T \quad \dots \quad {z_N}^T]^T \in R^{2N} \tag{46}$$

$$F = \left[{F_1}^T \quad \dots \quad {F_N}^T\right]^T \in R^{2N} \tag{47}$$

$$\dot{z} = [(I_N \otimes \mathcal{A}) + (-cL \otimes BK)]z + (-cL \otimes BK)F \tag{48}$$

Considering (49), (50) and (51), (48) becomes (52).

$$\mathcal{A}_c = (I_N \otimes \mathcal{A}) + (-cL \otimes BK) \in R^{2N \times 2N} \tag{49}$$

$$F_c = -cL \otimes BK \in R^{2N \times 2N} \tag{50}$$

$$Q = F_c F \in R^{2N} \tag{51}$$

$$\dot{z} = \mathcal{A}_c z + Q. \tag{52}$$

Thus, the distributed position/velocity feedback with offset protocol (26) is written in global form as (52). This concludes the proof for *Conjecture 2.*

It is important to note in these above equations that Q does not change the eigenvalues of $\mathcal{A}_c$. Proof: Let $\dot{z_a} = \mathcal{A}_c z$ and $\dot{z} = \dot{z_a} + Q$. This clearly shows that Q is independent of the dynamics of the system $\mathcal{A}_c$ and therefore has no effect on the eigenvalues of the system. This is important because it means that adding a static position offset requirement to the *distributed position/velocity feedback* protocol (17) from Section 3.2 does not change the stability of the system and therefore convergence still occurs for 1-Leader Type (1LT) graphs.

***Conjecture 3*:** If $\mathcal{G}$ is 1LT and the global form of the distributed position/velocity feedback with offset protocol (52) is used at each node and *Assumption 2.3* holds, then the global formation consensus vectors $\overline{x} \in R^N$ and $\overline{v} \in R^N$ are (53) and (54), and the node states $\overline{x_i} \in R$ and $\overline{v_i} \in R$ at final time are (55) and (56).

$$\overline{x} = (x_1(0) - H) + t_f \overline{v} \tag{53}$$

$$\overline{v} = v_1(0) - G \tag{54}$$

$$\overline{x}_i = (x_1(0) - H_i) + t_f \overline{v}_i \quad (55)$$

$$\overline{v}_i = v_1(0) - G_i \quad (56)$$

Proof: Chapter 6 provides evidence to support *Conjecture 3.*

Chapter 6:

Evidence for Chapter 5

This chapter provides details and results of 6 simulations which simultaneously serve to provide evidence to support *Conjecture 1* and *Conjecture 2*.

Section 6.1 – Explanation of Simulation Setup for Chapter 6

The local node form of the distributed position/velocity feedback with offset protocol (26) as well as the global form of distributed position/velocity feedback with offset protocol (52) were implemented using MATLAB/Simulink for each of the 6 platoon topologies. The Appendix provides details regarding how the simulation was performed. An important note regarding the simulations in this chapter is that no restrictions or bounds were placed on the acceleration input or the vehicle velocity.

Protocols (26) and (52) were simulated with identical results, confirming correct derivation of *Conjecture 2*. For this simulation, the desired distance between vehicles in the platoon is 2 meters ($h = 2$) such that formation position vector H ((35) from Chapter 5), and formation velocity vector G ((37) from Chapter 5) become:

$$H = [0 \quad 2 \quad 4 \quad 6 \quad 8 \quad 10 \quad 12 \quad 14 \quad 16 \quad 18]$$

$$G = [0 \quad 0 \quad 0 \quad 0 \quad 0 \quad 0 \quad 0 \quad 0 \quad 0 \quad 0].$$

The initial conditions were chosen to be the same as in Chapter 4, and are

$$x(0) = [10 \quad 9 \quad 8 \quad 7 \quad 6 \quad 5 \quad 4 \quad 3 \quad 2 \quad 1],$$

$$v(0) = [1 \quad .9 \quad .8 \quad .7 \quad .6 \quad .5 \quad .4 \quad .3 \quad .2 \quad .1].$$

Section 6.2 – Analysis of Results for Simulation 6.1

In this chapter, the gain values of the protocol were arbitrarily chosen to be $c = 1$ and $\gamma = 1$, which satisfies *Assumption 2.3*. Notice that calculating $\overline{x}$ and $\overline{v}$ requires that

final time t_f be known. The method used for determining t_f in simulation is the same as described in Chapter 4. The results for t_f for each topology given the conditions described in Section 4.1 are provided in Table 9. Recall the platoon topologies are Predecessor-Following (PF), Predecessor-Leader-Following (PLF), Bidirectional (BD), Bidirectional-Leader (BDL), Two-Predecessor-Following (TPF) and Two-Predecessor-Leader-Following (TPLF) as shown in Figure 1.

Table 9 – Final Times for Simulations in Chapter 6

Topology	t_f
PF	49.96
PLF	19.12
BD	291.82
BDL	21.89
TPF	24.75
TPLF	18.20

Below are six subsections, one for each of the six topologies. Each subsection below presents a table. A description of the information presented in these tables follows. Column 1 (Node) shows the node number, where node 1 is the lead vehicle and node 10 is the last vehicle in the platoon. Column 2 (H_i) displays the i^{th} element of the formation position vector H, which is used to calculate (55). Column 3 ($\overline{x_i}$) displays the final position value for each node as calculated by (55). Column 4 ($x_i(t_f)_{sim}$) shows the final position value for each node as obtained by the simulation using the final time t_f from Table 9 . Column 5 ($\%error$ ($\overline{x_i}$)) shows the error percentage between $\overline{x_i}$ and $x_i(t_f)_{sim}$. Column 6 (G_i) displays the i^{th} element of the velocity vector G, which is used to calculate (56). Column 7 ($\overline{v_i}$) displays the final position value for each node as calculated by (56). Column 8 ($v_i(t_f)_{sim}$) shows the final position value for each node as obtained by the

simulation using the final time t_f from Table 9 . Column 9 ($\%error$ ($\overline{v}_i$)) shows the error percentage between $\overline{v}_i$ and $v_i(t_f)_{sim}$.

Each subsection below also presents three figures for each topology. The first figure shows the simulation results of position versus time for each node. The values $\overline{x}_i$ from the related table were superimposed on the position plots, where $\overline{x}_i$ is denoted by a blue "x". The second figure shows the simulation results of velocity versus time for each node. The values $\overline{v}_i$ were superimposed on the velocity plots, where $\overline{v}_i$ is denoted by a blue "x". The acceleration input plots show that the acceleration input $u_i = 0$ for all nodes at the at t_f listed in Table 9.

Table 10 through Table 15 along with Figure 21 through Figure 38 clearly show that these simulations support *Conjecture* 2 and *Conjecture 3* from Chapter 5.

Predecessor-Following Topology

Table 10 - Analysis of PF Results for Chapter 6

Node	H_i	$\overline{x}_i$	$x_i(t_f)_{sim}$	$\%error\ (\overline{x}_i)$	G_i	$\overline{v}_i$	$v_i(t_f)_{sim}$	$\%error\ (\overline{v}_i)$
1	0	59.96	59.9600	0.000	0	1	1.0000	0.000
2	2	57.96	57.9600	0.000	0	1	1.0000	0.000
3	4	55.96	55.9600	0.000	0	1	1.0000	0.000
4	6	53.96	53.9600	0.000	0	1	1.0000	0.000
5	8	51.96	51.9600	0.000	0	1	1.0000	0.000
6	10	49.96	49.9600	0.000	0	1	1.0000	0.000
7	12	47.96	47.9600	0.000	0	1	1.0000	0.000
8	14	45.96	45.9600	0.000	0	1	1.0000	0.001
9	16	43.96	43.9600	0.000	0	1	0.9999	0.009
10	18	41.96	41.9602	0.001	0	1	0.9996	0.042

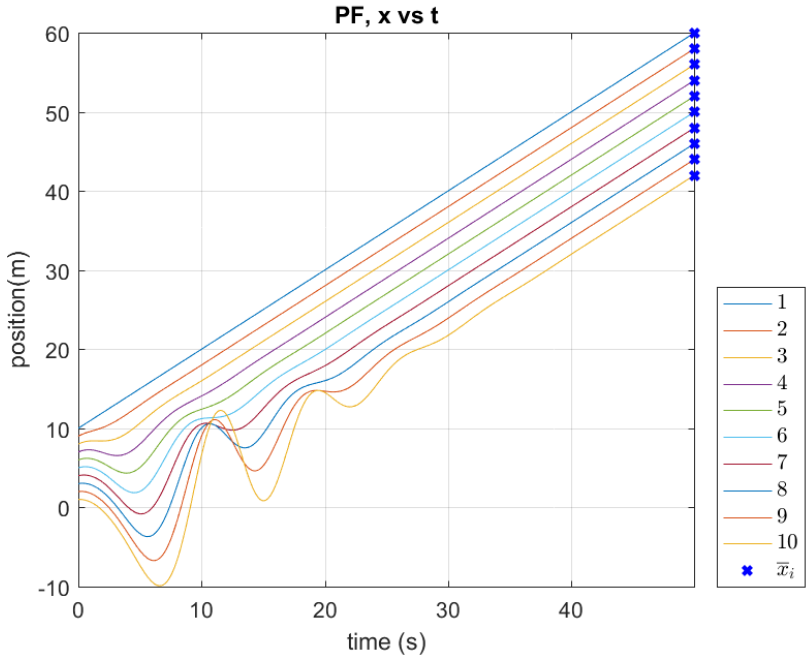

Figure 21 - PF Results for Chapter 6, position versus time.

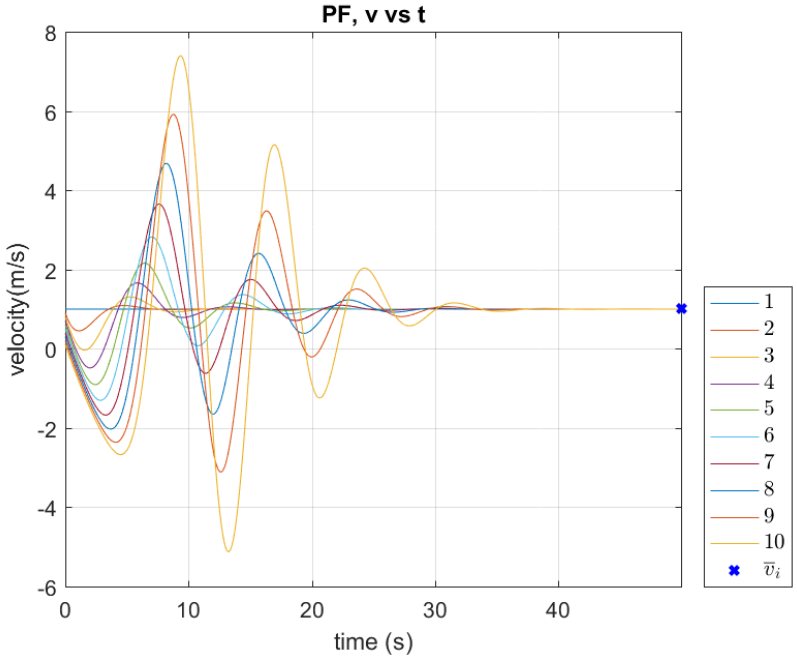

Figure 22 - PF Results for Chapter 6, velocity versus time.

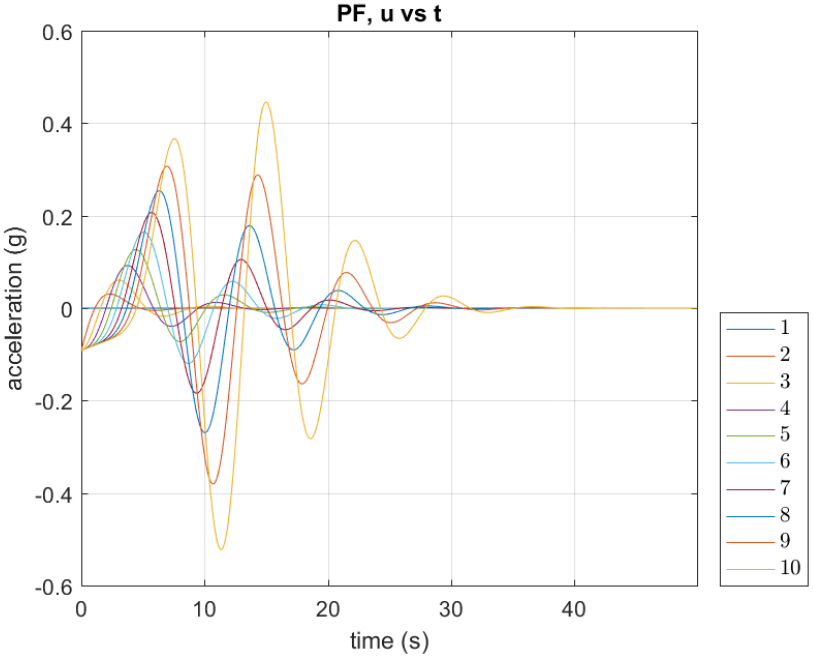

Figure 23 - PF Results for Chapter 6, acceleration input versus time.

Predecessor-Leader-Following Topology

Table 11 - Analysis of PLF Results for Chapter 6

Node	H_i	$\overline{x}_i$	$x_i(t_f)_{sim}$	$\%error\ (\overline{x}_i)$	G_i	$\overline{v}_i$	$v_i(t_f)_{sim}$	$\%error\ (\overline{v}_i)$
1	0	29.12	29.1200	0.000	0	1	1.0000	0.000
2	2	27.12	27.1199	0.000	0	1	1.0001	0.006
3	4	25.12	25.1199	0.000	0	1	1.0001	0.006
4	6	23.12	23.1199	0.000	0	1	1.0001	0.006
5	8	21.12	21.1199	0.000	0	1	1.0001	0.006
6	10	19.12	19.1199	0.000	0	1	1.0001	0.006
7	12	17.12	17.1199	0.000	0	1	1.0001	0.006
8	14	15.12	15.1199	0.000	0	1	1.0001	0.006
9	16	13.12	13.1199	0.000	0	1	1.0001	0.007
10	18	11.12	11.1200	0.000	0	1	1.0001	0.008

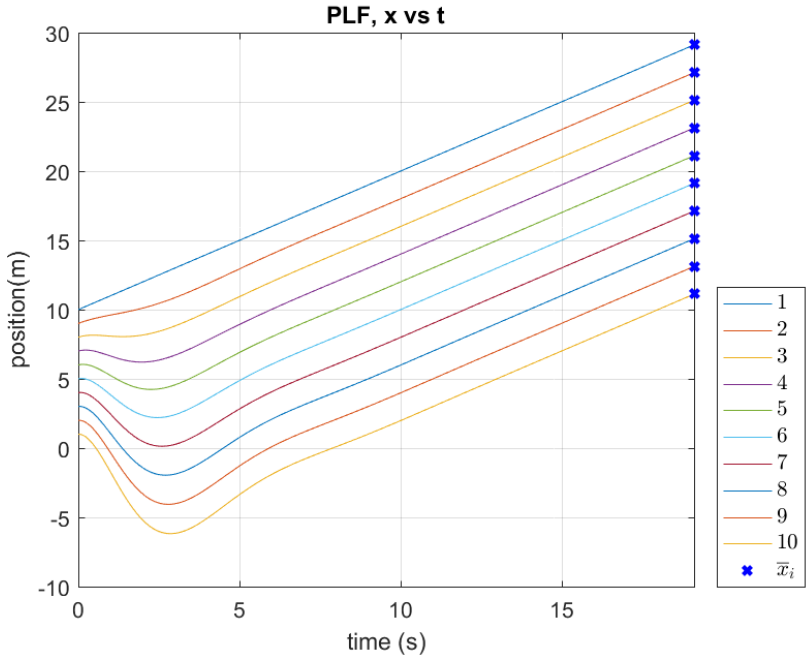

Figure 24 - PLF Results for Chapter 6, position versus time.

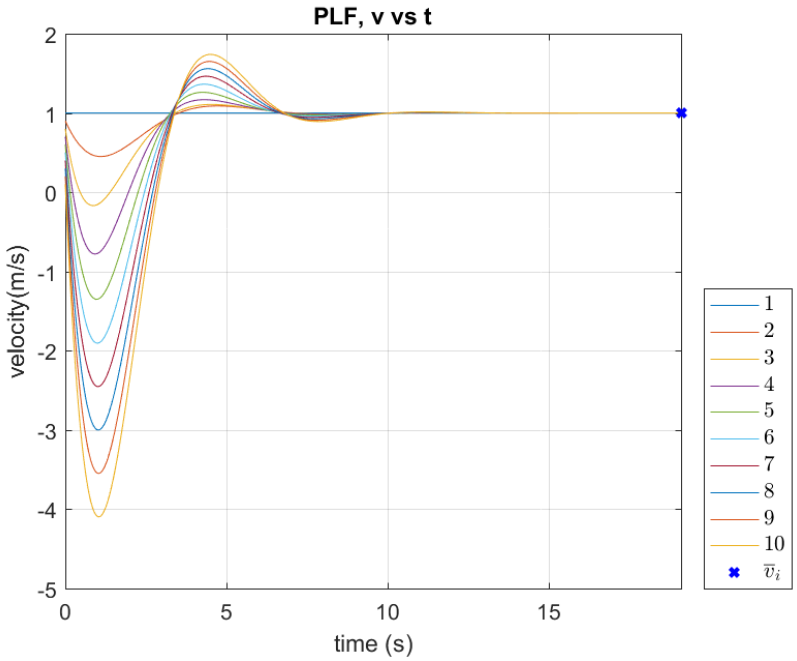

Figure 25 - PLF Results for Chapter 6, velocity versus time.

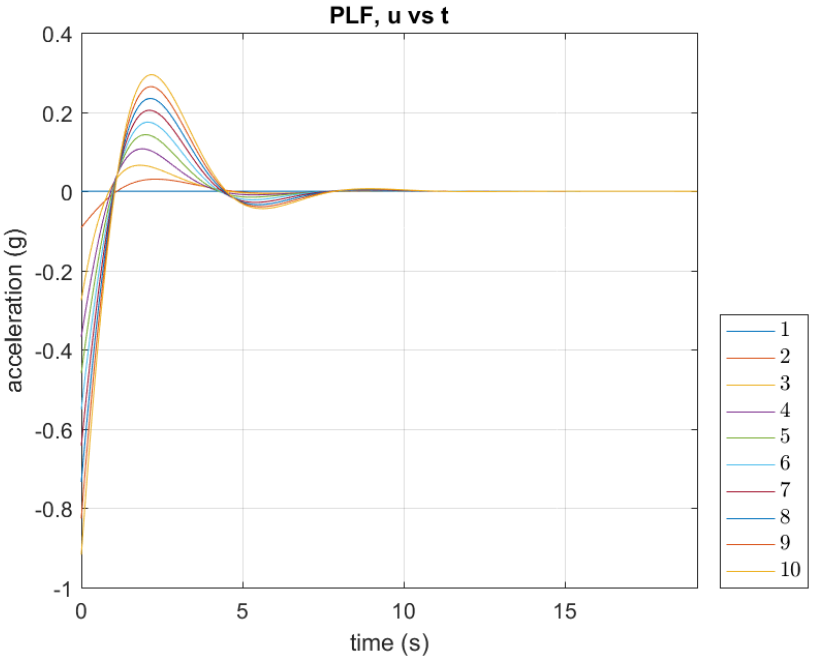

Figure 26 - PLF Results for Chapter 6, acceleration input versus time.

Bidirectional Topology

Table 12 - Analysis of BD Results for Chapter 6

Node	H_i	$\overline{x}_i$	$x_i(t_f)_{sim}$	$\%error\ (\overline{x}_i)$	G_i	$\overline{v}_i$	$v_i(t_f)_{sim}$	$\%error\ (\overline{v}_i)$
1	0	301.82	301.8200	0.000	0	1	1.0000	0.000
2	2	299.82	299.8152	0.002	0	1	1.0044	0.439
3	4	297.82	297.8106	0.003	0	1	1.0087	0.866
4	6	295.82	295.8062	0.005	0	1	1.0127	1.270
5	8	293.82	293.8022	0.006	0	1	1.0164	1.639
6	10	291.82	291.7987	0.007	0	1	1.0196	1.963
7	12	289.82	289.7957	0.008	0	1	1.0223	2.234
8	14	287.82	287.7935	0.009	0	1	1.0244	2.443
9	16	285.82	285.7919	0.010	0	1	1.0259	2.586
10	18	283.82	283.7911	0.010	0	1	1.0266	2.659

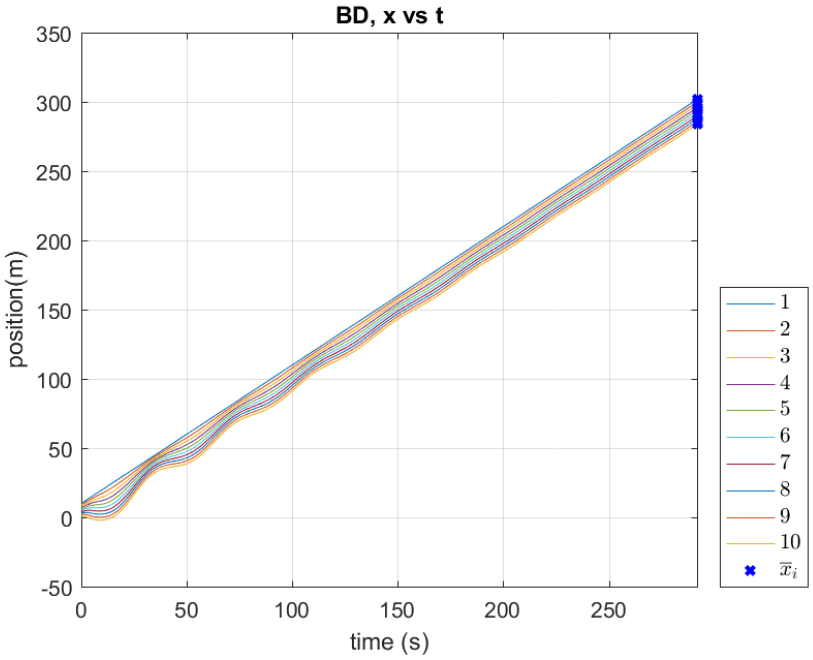

Figure 27 - BD Results for Chapter 6, position versus time.

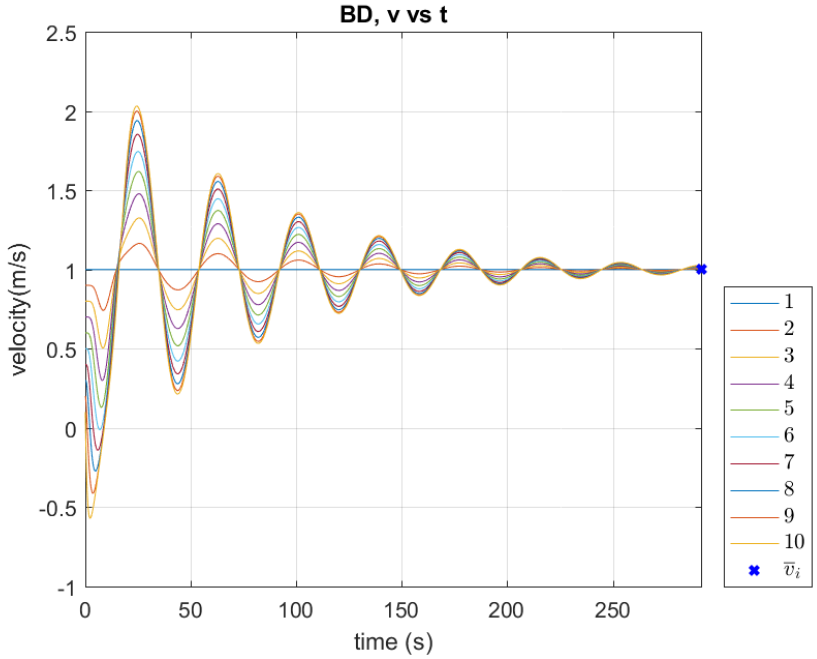

Figure 28 - BD Results for Chapter 6, velocity versus time.

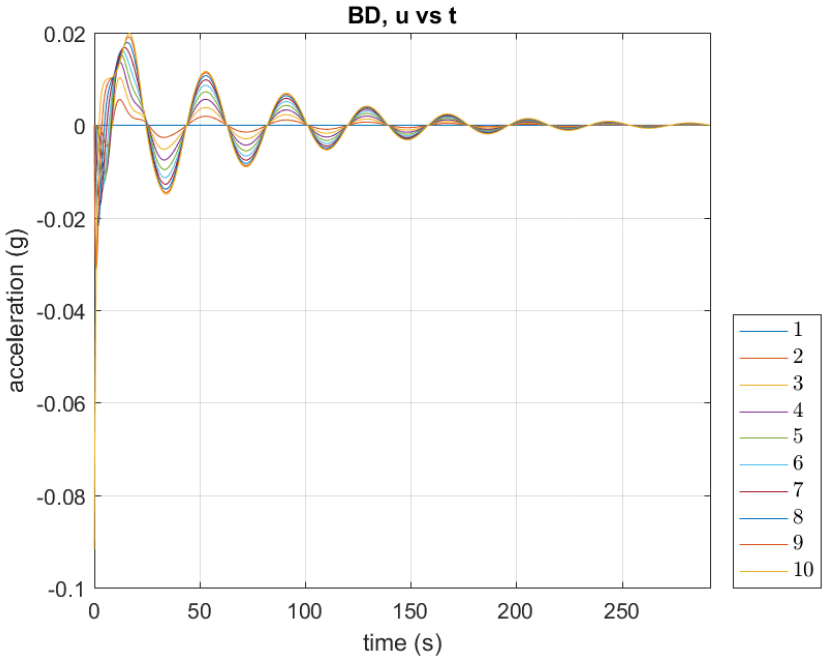

Figure 29 - BD Results for Chapter 6, acceleration input versus time.

Bidirectional-Leader Topology

Table 13 - Analysis of BDL Results for Chapter 6

Node	H_i	$\overline{x}_i$	$x_i(t_f)_{sim}$	$\%error\ (\overline{x}_i)$	G_i	$\overline{v}_i$	$v_i(t_f)_{sim}$	$\%error\ (\overline{v}_i)$
1	0	31.89	31.8900	0.000	0	1	1.0000	0.000
2	2	29.89	29.8901	0.000	0	1	1.0000	0.000
3	4	27.89	27.8901	0.000	0	1	1.0000	0.001
4	6	25.89	25.8901	0.000	0	1	1.0000	0.001
5	8	23.89	23.8901	0.000	0	1	1.0000	0.001
6	10	21.89	21.8901	0.000	0	1	1.0000	0.002
7	12	19.89	19.8901	0.000	0	1	1.0000	0.002
8	14	17.89	17.8901	0.001	0	1	1.0000	0.003
9	16	15.89	15.8901	0.001	0	1	1.0000	0.003
10	18	13.89	13.8901	0.001	0	1	1.0000	0.003

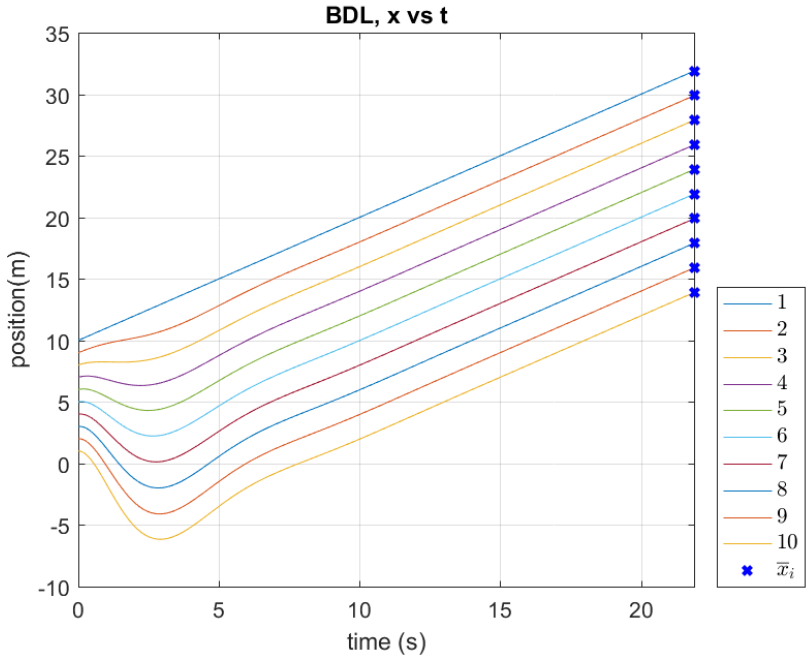

Figure 30 - BDL Results for Chapter 6, position versus time.

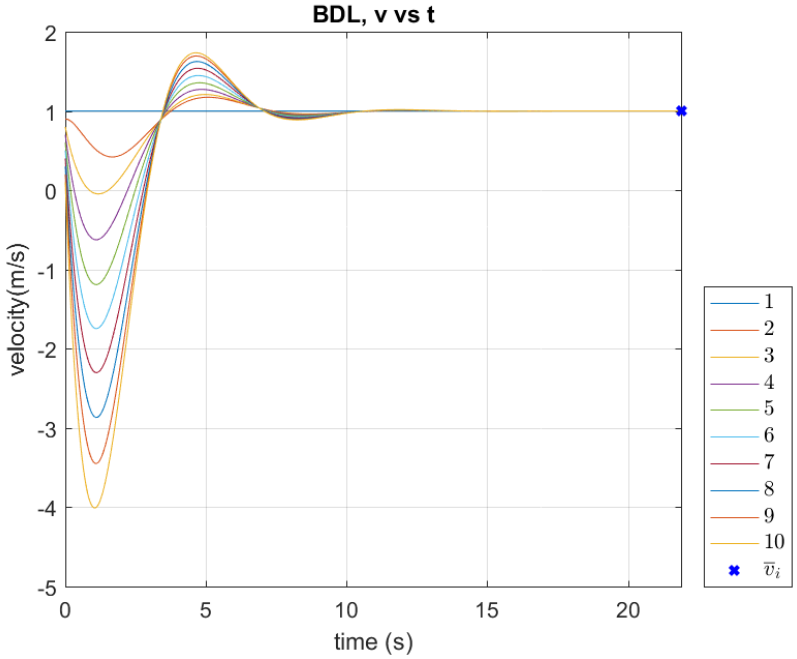

Figure 31 - BDL Results for Chapter 6, velocity versus time.

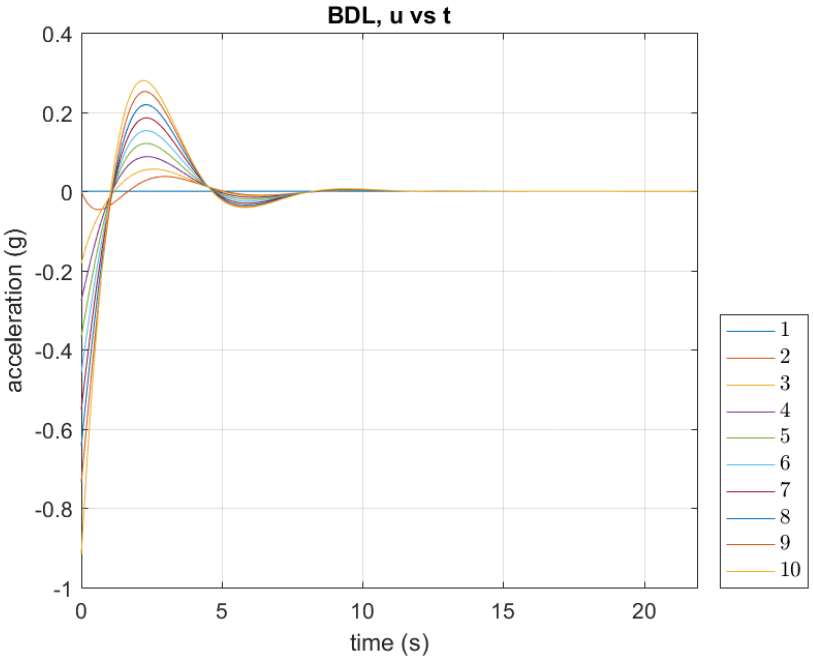

Figure 32 - BDL Results for Chapter 6, acceleration input versus time.

Two-Predecessor-Following Topology

Table 14 - Analysis of TPF Results for Chapter 6

Node	H_i	$\overline{x}_i$	$x_i(t_f)_{sim}$	$\%error\ (\overline{x}_i)$	G_i	$\overline{v}_i$	$v_i(t_f)_{sim}$	$\%error\ (\overline{v}_i)$
1	0	34.75	34.7500	0.000	0	1	1.0000	0.000
2	2	32.75	32.7500	0.000	0	1	1.0000	0.000
3	4	30.75	30.7500	0.000	0	1	1.0000	0.000
4	6	28.75	28.7500	0.000	0	1	1.0000	0.000
5	8	26.75	26.7500	0.000	0	1	1.0000	0.001
6	10	24.75	24.7500	0.000	0	1	1.0000	0.001
7	12	22.75	22.7500	0.000	0	1	1.0000	0.002
8	14	20.75	20.7500	0.000	0	1	1.0000	0.003
9	16	18.75	18.7499	0.000	0	1	1.0000	0.004
10	18	16.75	16.7499	0.001	0	1	0.9999	0.007

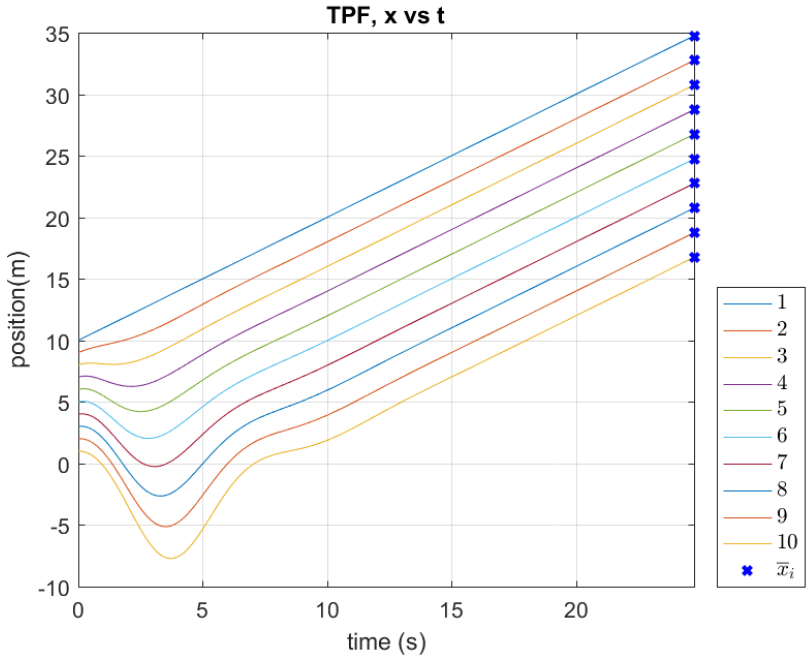

Figure 33 - TPF Results for Chapter 6, position versus time.

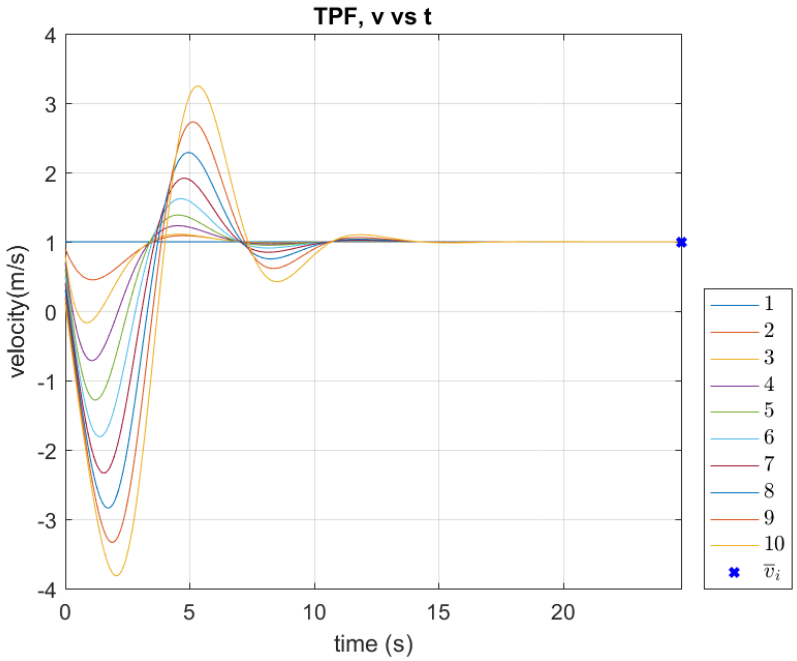

Figure 34 - TPF Results for Chapter 6, velocity versus time.

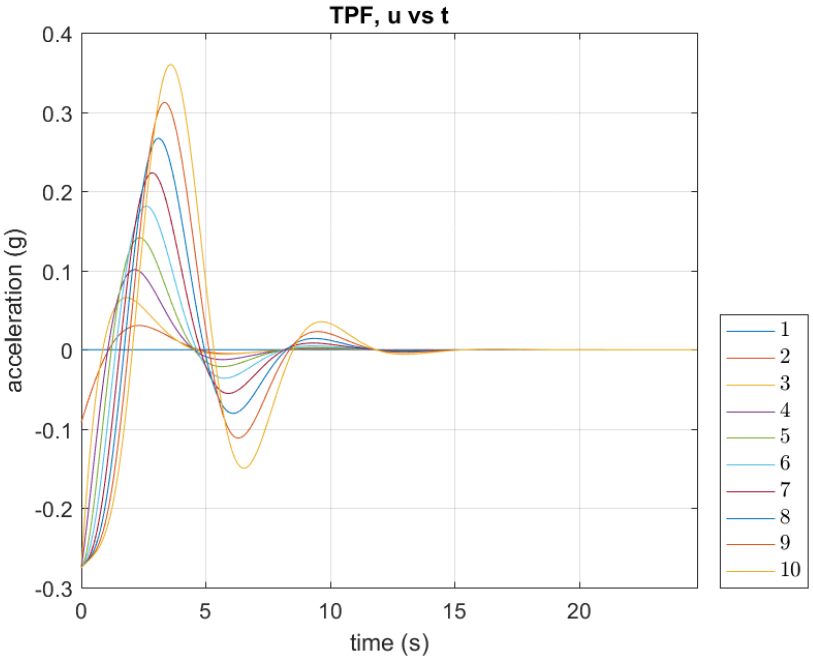

Figure 35 - TPF Results for Chapter 6, acceleration input versus time.

Two-Predecessor-Leader-Following Topology

Table 15 - Analysis of TPLF Results for Chapter 6

Node	H_i	$\overline{x}_i$	$x_i(t_f)_{sim}$	$\%error\ (\overline{x}_i)$	G_i	$\overline{v}_i$	$v_i(t_f)_{sim}$	$\%error\ (\overline{v}_i)$
1	0	28.20	28.2000	0.000	0	1	1.0000	0.000
2	2	26.20	26.1999	0.000	0	1	1.0000	0.002
3	4	24.20	24.1999	0.000	0	1	1.0000	0.002
4	6	22.20	22.1999	0.001	0	1	1.0000	0.002
5	8	20.20	20.1999	0.001	0	1	1.0000	0.002
6	10	18.20	18.1999	0.001	0	1	1.0000	0.002
7	12	16.20	16.1999	0.001	0	1	1.0000	0.002
8	14	14.20	14.1999	0.001	0	1	1.0000	0.002
9	16	12.20	12.1999	0.001	0	1	1.0000	0.002
10	18	10.20	10.1999	0.001	0	1	1.0000	0.002

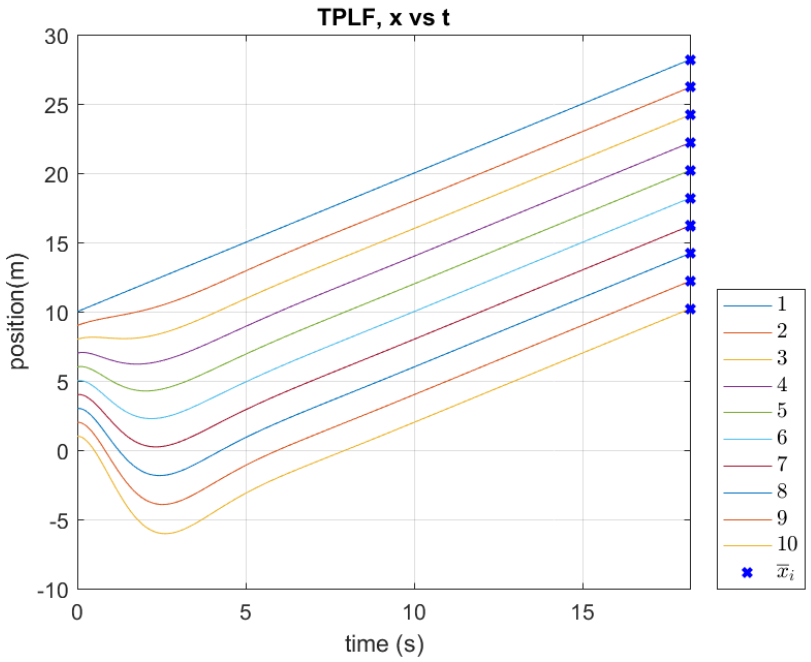

Figure 36 - TPLF Results for Chapter 6, position versus time.

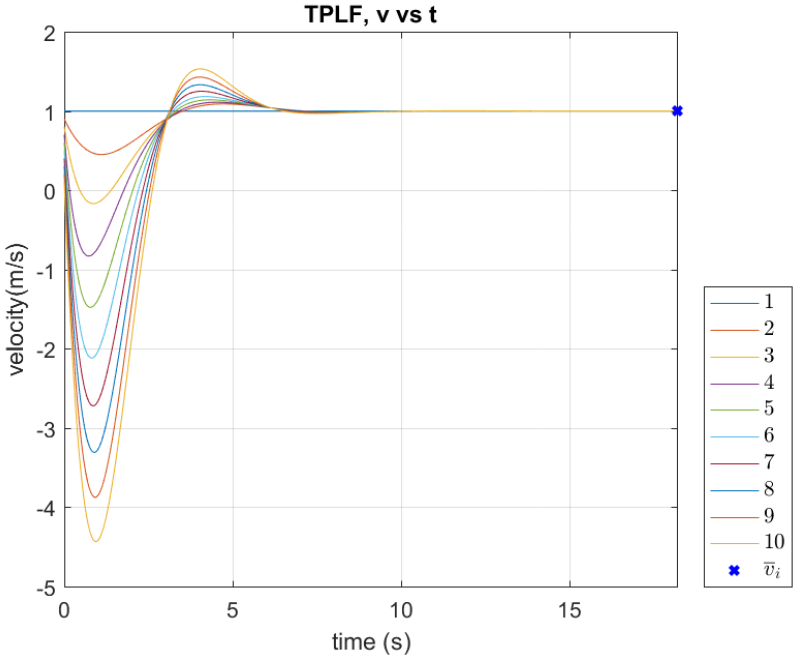

Figure 37 - TPLF Results for Chapter 6, velocity versus time.

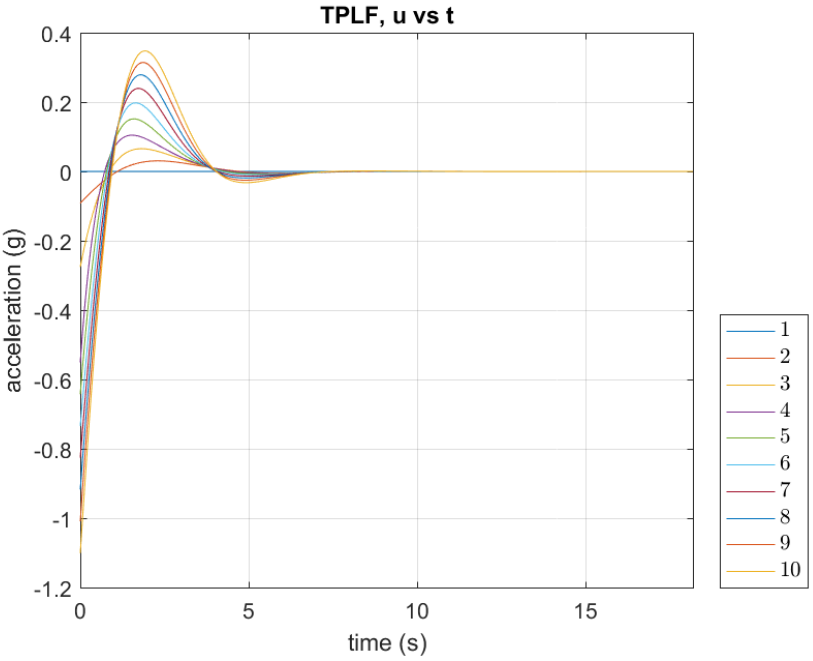

Figure 38 – TPLF Results for Chapter 6, acceleration input versus time.

Chapter 7:

Consensus with Limited Vehicle Dynamics

Recall that in Chapter 6, there are no limitations on the vehicle dynamics. In this chapter we seek to create more realistic vehicle dynamics and to verify convergence with offset still occurs.

Section 7.1 – Explanation of Simulation Setup for Chapter 7

The local node form of the distributed position/velocity feedback with offset protocol (26) as well as the global form of distributed position/velocity feedback with offset protocol (52) were implemented using MATLAB/Simulink for each of the 6 platoon topologies. The Appendix provides details regarding how the simulation was performed. Recall that in Chapter 6, no restrictions or bounds were placed on the acceleration input or the vehicle velocity. In this chapter, however, we assume the vehicles are generic passenger sedans driven at highway speeds and as such have an acceleration limitation of 0.3g's and deceleration limitation of 1.0g's. The vehicles must also not be allowed to drive in reverse so a lower limit of 0 m/s is placed on the velocity. An arbitrary upper limit of 100mph (44.704m/s) is also applied.

This chapter will rerun the simulations described in Section 6.1 and will show that the limitations on dynamics to not affect the $\overline{x}$ and $\overline{v}$ values. The simulation details of Section 6.1 are repeated here for convenience. Protocols (26) and (52) were simulated with identical results, confirming correct derivation of *Conjecture 2*. For this simulation, the desired distance between vehicles in the platoon is 2 meters ($h = 2$) such that formation position vector H ((35) from Chapter 5), and formation velocity vector G ((37) from Chapter 5) become:

$$H = [0 \quad 2 \quad 4 \quad 6 \quad 8 \quad 10 \quad 12 \quad 14 \quad 16 \quad 18]$$

$$G = [0 \quad 0 \quad 0 \quad 0 \quad 0 \quad 0 \quad 0 \quad 0 \quad 0 \quad 0].$$

The initial conditions were chosen to be the same as in Chapter 4 and Chapter 6, and are

$$x(0) = [10 \quad 9 \quad 8 \quad 7 \quad 6 \quad 5 \quad 4 \quad 3 \quad 2 \quad 1],$$

$$v(0) = [1 \quad .9 \quad .8 \quad .7 \quad .6 \quad .5 \quad .4 \quad .3 \quad .2 \quad .1].$$

Section 7.2 – Analysis of Results for Simulation 7.1

The results for t_f for each topology given the conditions described in Section 7.1 are provided in Table 16. Recall the platoon topologies are Predecessor-Following (PF), Predecessor-Leader-Following (PLF), Bidirectional (BD), Bidirectional-Leader (BDL), Two-Predecessor-Following (TPF) and Two-Predecessor-Leader-Following (TPLF) as shown in Figure 1

Table 16 – Final Times for Simulations in Chapter 7

Topology	t_f
PF	50.03
PLF	20.49
BD	256.65
BDL	23.65
TPF	23.35
TPLF	19.10

Below are six subsections, one for each of the six topologies. Each subsection below presents a table. A description of the information presented in these tables follows. Column 1 (Node) shows the node number, where node 1 is the lead vehicle and node 10 is the last vehicle in the platoon. Column 2 (H_i) displays the i^{th} element of the formation position vector H, which is used to calculate (55). Column 3 ($\overline{x_i}$) displays the final position value for each node as calculated by (55). Column 4 ($x_i(t_f)_{sim}$) shows the final position value for each node as obtained by the simulation using the final time t_f from Table 16 . Column 5 ($\%error\ (\overline{x_i})$) shows the error percentage between $\overline{x_i}$ and $x_i(t_f)_{sim}$. Column 6

(G_i) displays the i^{th} element of the velocity vector G, which is used to calculate (56). Column 7 ($\overline{v}_i$) displays the final position value for each node as calculated by (56). Column 8 ($v_i(t_f)_{sim}$) shows the final position value for each node as obtained by the simulation using the final time t_f from Table 16 . Column 9 ($\%error$ ($\overline{v}_i$)) shows the error percentage between $\overline{v}_i$ and $v_i(t_f)_{sim}$.

Each subsection below also presents three figures for each topology. The first figure shows the simulation results of position versus time for each node. The values $\overline{x}_i$ from the related table were superimposed on the position plots, where $\overline{x}_i$ is denoted by a blue "x". The second figure shows the simulation results of velocity versus time for each node. The values $\overline{v}_i$ were superimposed on the velocity plots, where $\overline{v}_i$ is denoted by a blue "x". The acceleration input plots show that the acceleration input $u_i = 0$ for all nodes at the at t_f listed in Table 16.

Table 17 through Table 22 along with Figure 39 through Figure 56 clearly show that these simulations support *Conjecture* 2 and *Conjecture 3* from Chapter 5, even with the limitations placed on the vehicle dynamics.

Predecessor-Following Topology

Table 17 – Analysis of PF Results for Chapter 7

Node	H_i	$\overline{x}_i$	$x_i(t_f)_{sim}$	$\%error\ (\overline{x}_i)$	G_i	$\overline{v}_i$	$v_i(t_f)_{sim}$	$\%error\ (\overline{v}_i)$
1	0	60.03	60.0300	0.000	0	1	1.0000	0.000
2	2	58.03	58.0300	0.000	0	1	1.0000	0.000
3	4	56.03	56.0300	0.000	0	1	1.0000	0.000
4	6	54.03	54.0300	0.000	0	1	1.0000	0.000
5	8	52.03	52.0300	0.000	0	1	1.0000	0.000
6	10	50.03	50.0300	0.000	0	1	1.0000	0.000
7	12	48.03	48.0300	0.000	0	1	1.0000	0.000
8	14	46.03	46.0300	0.000	0	1	1.0000	0.001
9	16	44.03	44.0300	0.000	0	1	0.9999	0.009
10	18	42.03	42.0302	0.001	0	1	0.9996	0.037

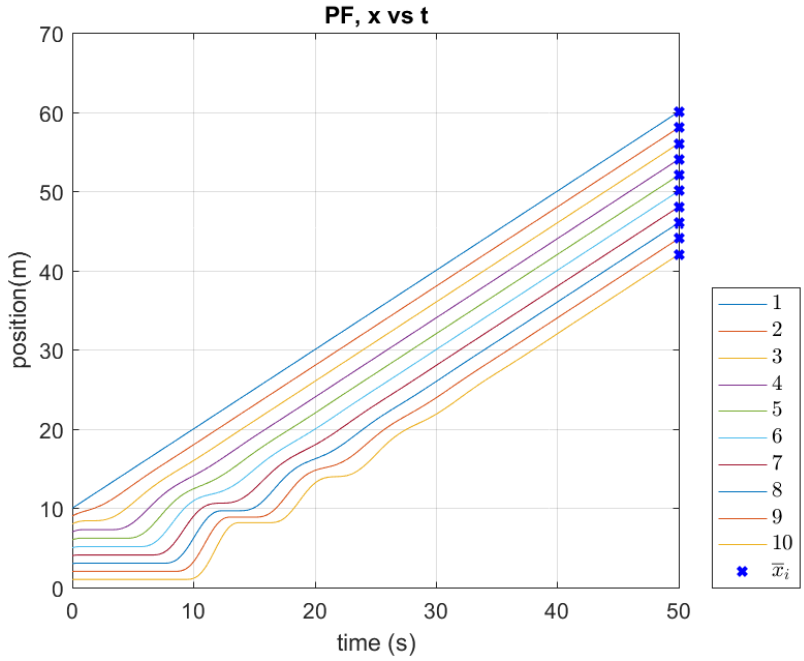

Figure 39 - PF Results for Chapter 7, position versus time.

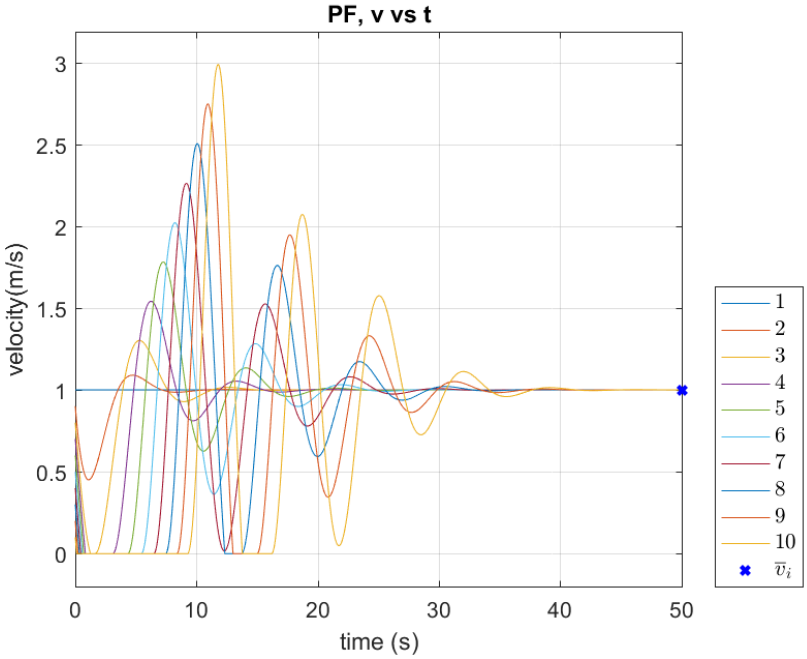

Figure 40 - PF Results for Chapter 7, velocity versus time.

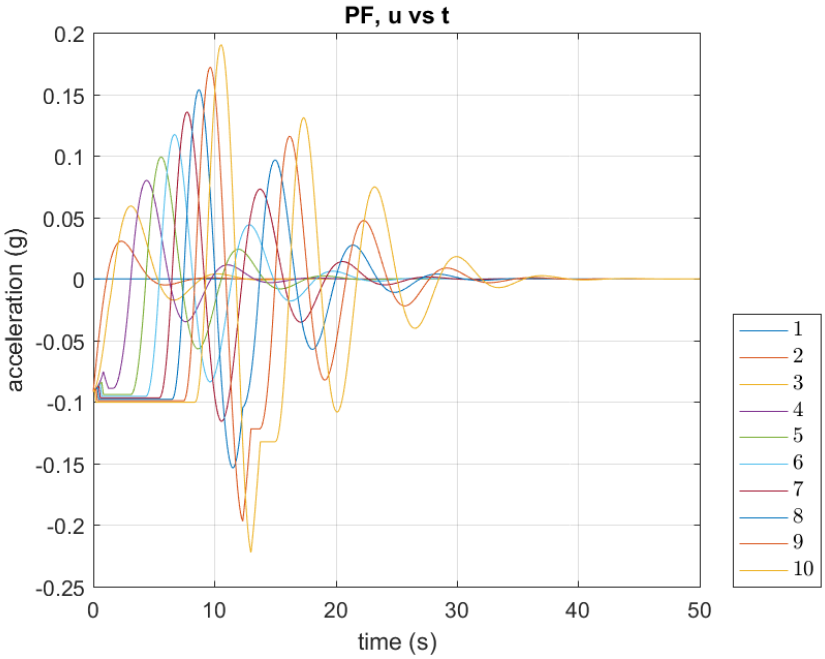

Figure 41 - PF Results for Chapter 7, acceleration input versus time.

Predecessor-Leader-Following Topology

Table 18 - Analysis of PLF Results for Chapter 7

Node	H_i	$\overline{x}_i$	$x_i(t_f)_{sim}$	$\%error\ (\overline{x}_i)$	G_i	$\overline{v}_i$	$v_i(t_f)_{sim}$	$\%error\ (\overline{v}_i)$
1	0	30.49	30.4900	0.000	0	1	1.0000	0.000
2	2	28.49	28.4900	0.000	0	1	1.0000	0.003
3	4	26.49	26.4900	0.000	0	1	1.0000	0.003
4	6	24.49	24.4900	0.000	0	1	1.0000	0.003
5	8	22.49	22.4900	0.000	0	1	1.0000	0.003
6	10	20.49	20.4900	0.000	0	1	1.0000	0.003
7	12	18.49	18.4900	0.000	0	1	1.0000	0.004
8	14	16.49	16.4900	0.000	0	1	1.0000	0.004
9	16	14.49	14.4900	0.000	0	1	1.0001	0.005
10	18	12.49	12.4900	0.000	0	1	1.0000	0.005

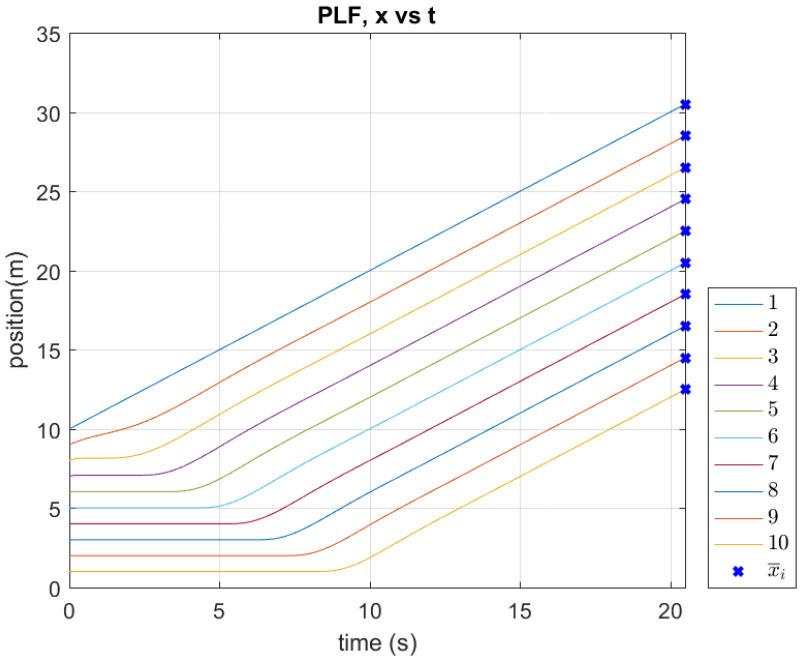

Figure 42 - PLF Results for Chapter 7, position versus time.

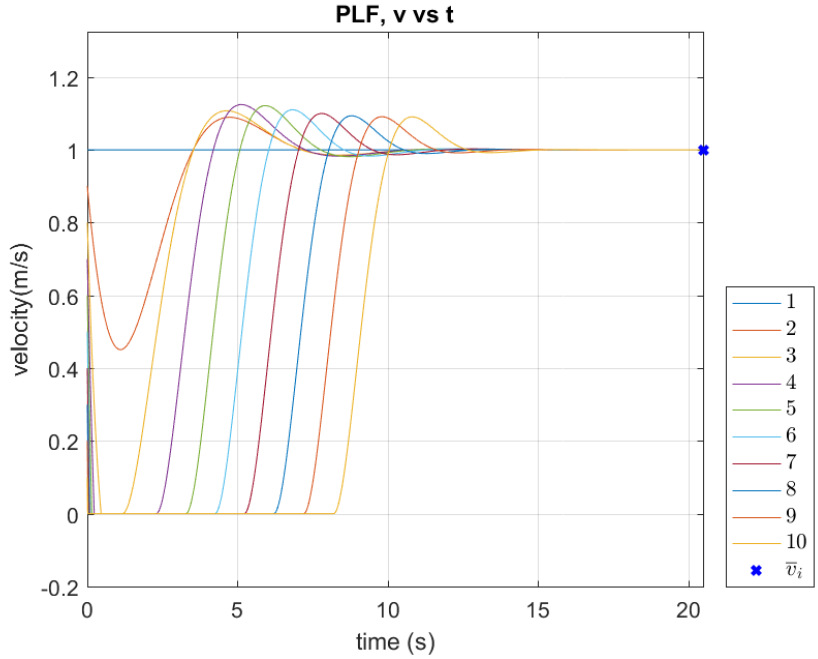

Figure 43 - PLF Results for Chapter 7, velocity versus time.

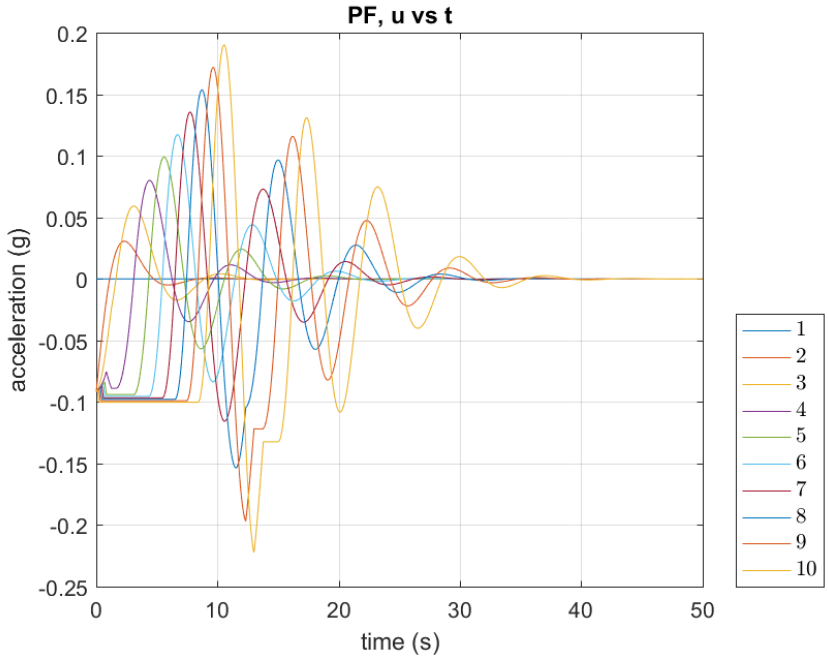

Figure 44 - PLF Results for Chapter 7, acceleration input versus time.

Bidirectional Topology

Table 19 - Analysis of BD Results for Chapter 7

Node	H_i	$\overline{x}_i$	$x_i(t_f)_{sim}$	$\%error\ (\overline{x}_i)$	G_i	$\overline{v}_i$	$v_i(t_f)_{sim}$	$\%error\ (\overline{v}_i)$
1	0	266.65	266.6500	0.000	0	1	1.0000	0.000
2	2	264.65	264.6476	0.001	0	1	1.0049	0.491
3	4	262.65	262.6452	0.002	0	1	1.0097	0.969
4	6	260.65	260.6430	0.003	0	1	1.0142	1.420
5	8	258.65	258.6410	0.003	0	1	1.0183	1.833
6	10	256.65	256.6392	0.004	0	1	1.0220	2.195
7	12	254.65	254.6377	0.005	0	1	1.0250	2.498
8	14	252.65	252.6365	0.005	0	1	1.0273	2.732
9	16	250.65	250.6357	0.006	0	1	1.0289	2.892
10	18	248.65	248.6353	0.006	0	1	1.0297	2.973

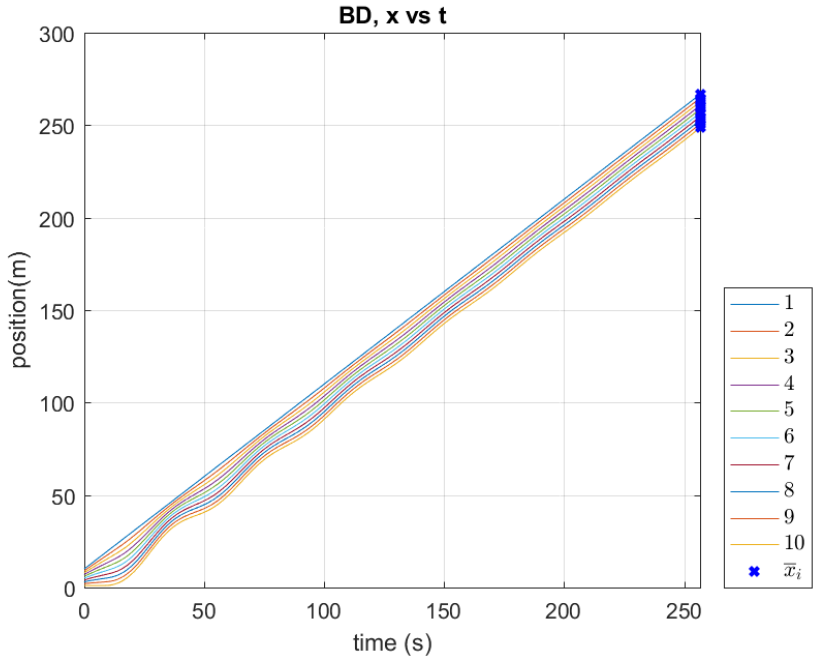

Figure 45 - BD Results for Chapter 7, position versus time.

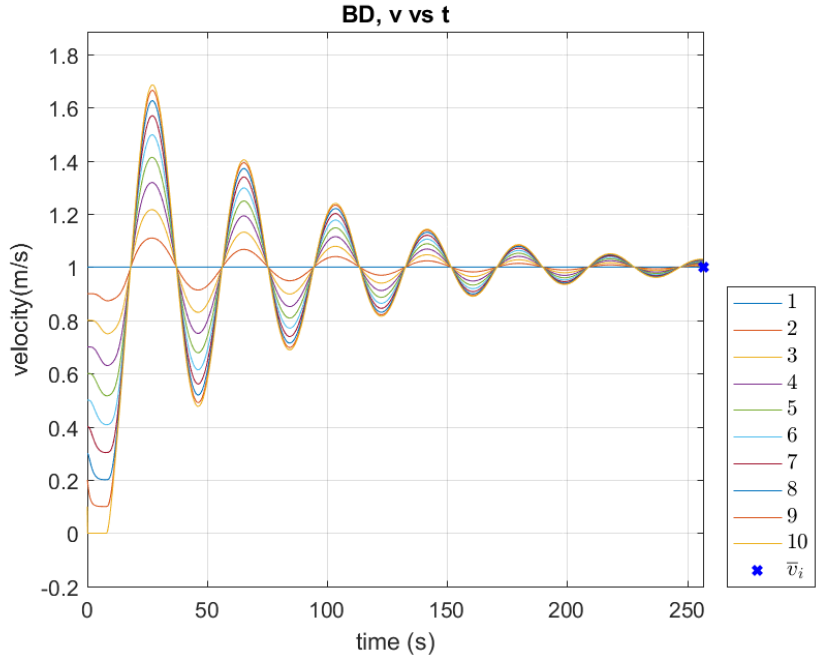

Figure 46 - BD Results for Chapter 7, velocity versus time.

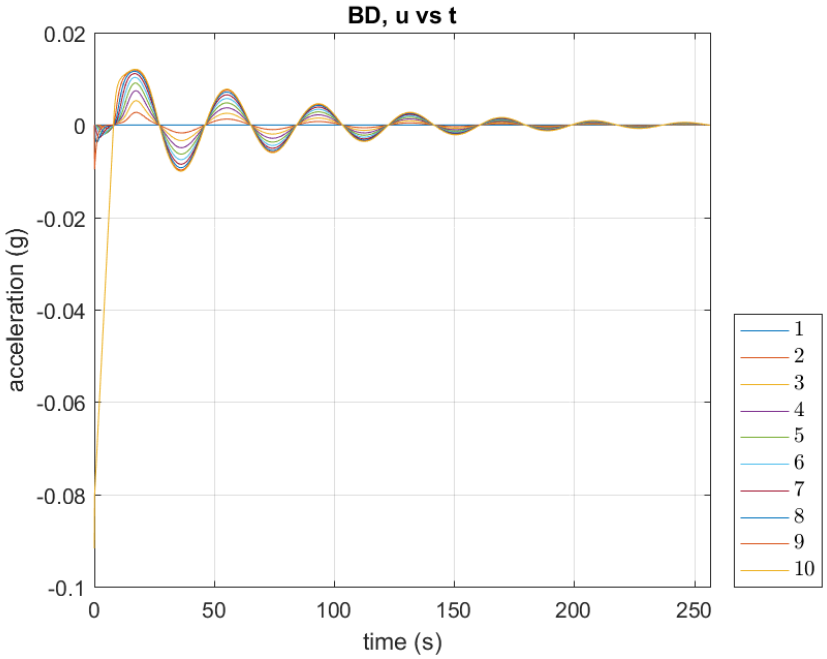

Figure 47 - BD Results for Chapter 7, acceleration input versus time.

Bidirectional-Leader Topology

Table 20 - Analysis of BDL Results for Chapter 7

Node	H_i	$\overline{x}_i$	$x_i(t_f)_{sim}$	$\%error\ (\overline{x}_i)$	G_i	$\overline{v}_i$	$v_i(t_f)_{sim}$	$\%error\ (\overline{v}_i)$
1	0	33.65	33.6500	0.000	0	1	1.0000	0.000
2	2	31.65	31.6500	0.000	0	1	1.0000	0.003
3	4	29.65	29.6500	0.000	0	1	1.0000	0.003
4	6	27.65	27.6500	0.000	0	1	1.0000	0.004
5	8	25.65	25.6500	0.000	0	1	0.9999	0.005
6	10	23.65	23.6500	0.000	0	1	0.9999	0.006
7	12	21.65	21.6500	0.000	0	1	0.9999	0.007
8	14	19.65	19.6500	0.000	0	1	0.9999	0.008
9	16	17.65	17.6500	0.000	0	1	0.9999	0.008
10	18	15.65	15.6500	0.000	0	1	0.9999	0.009

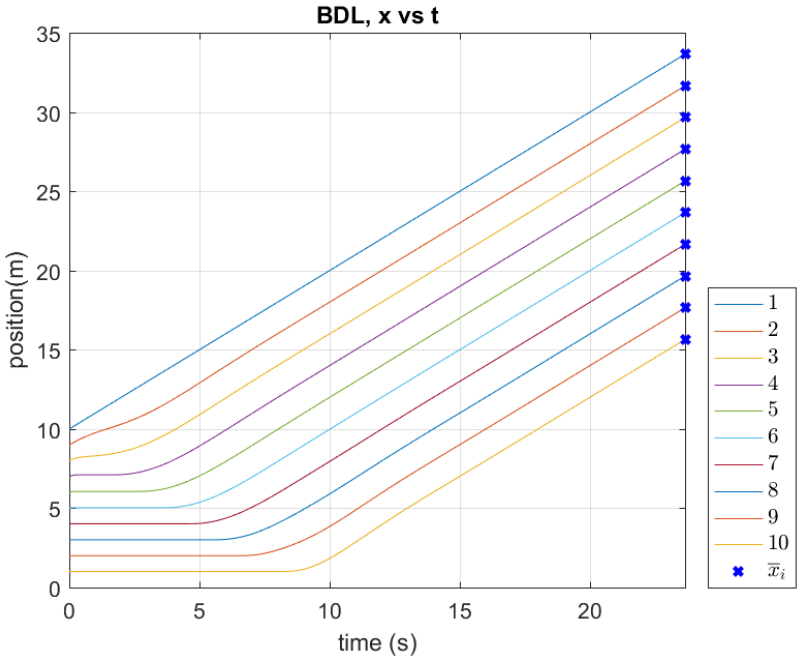

Figure 48 - BDL Results for Chapter 7, position versus time.

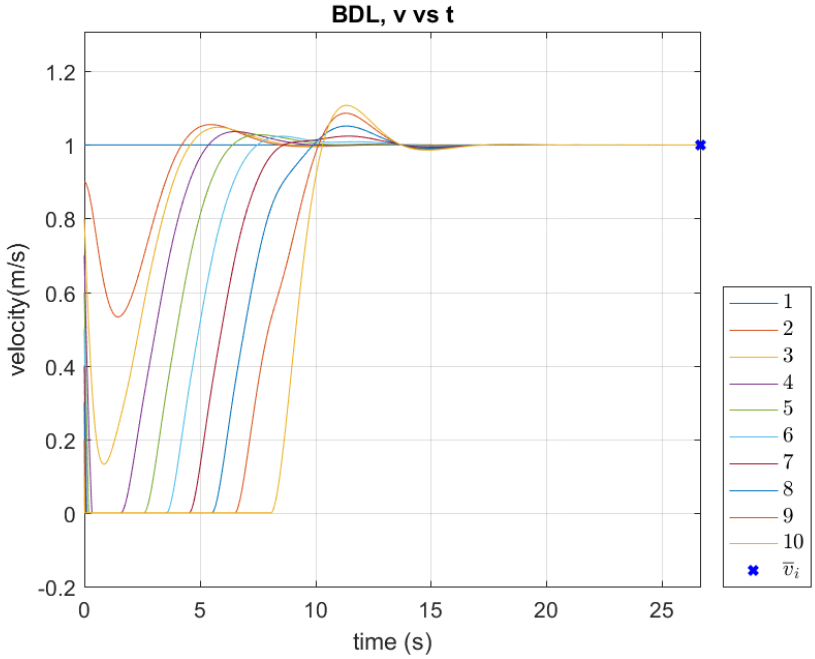

Figure 49 - BDL Results for Chapter 7, velocity versus time.

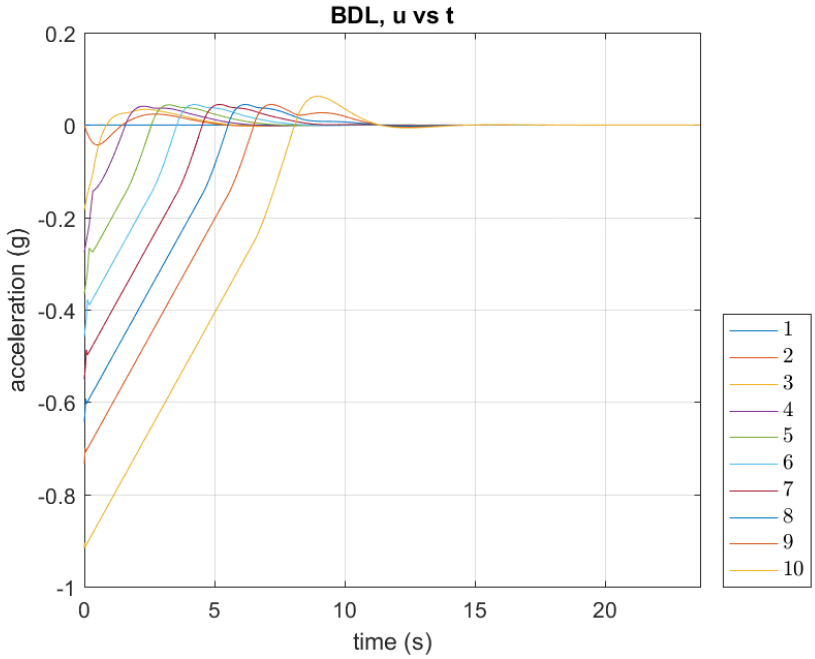

Figure 50 - BDL Results for Chapter 7, acceleration input versus time.

Two-Predecessor-Following Topology

Table 21 - Analysis of TPF Results for Chapter 7

Node	H_i	$\overline{x}_i$	$x_i(t_f)_{sim}$	$\%error\ (\overline{x}_i)$	G_i	$\overline{v}_i$	$v_i(t_f)_{sim}$	$\%error\ (\overline{v}_i)$
1	0	33.35	33.3500	0.000	0	1	1.0000	0.000
2	2	31.35	31.3500	0.000	0	1	1.0000	0.001
3	4	29.35	29.3500	0.000	0	1	1.0000	0.001
4	6	27.35	27.3500	0.000	0	1	1.0000	0.002
5	8	25.35	25.3500	0.000	0	1	1.0000	0.003
6	10	23.35	23.3500	0.000	0	1	1.0000	0.005
7	12	21.35	21.3500	0.000	0	1	0.9999	0.007
8	14	19.35	19.3501	0.000	0	1	0.9999	0.012
9	16	17.35	17.3501	0.001	0	1	0.9998	0.020
10	18	15.35	15.3502	0.001	0	1	0.9997	0.033

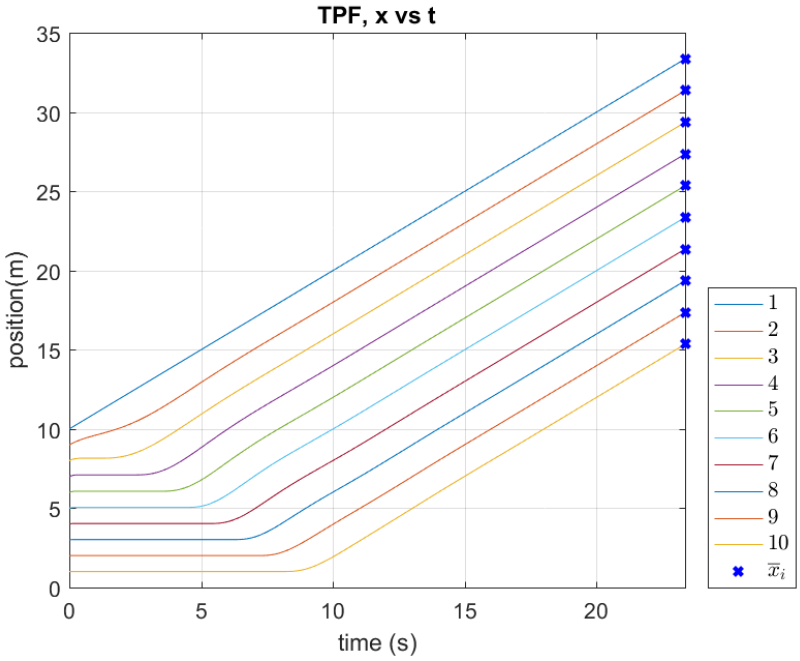

Figure 51 - TPF Results for Chapter 7, position versus time.

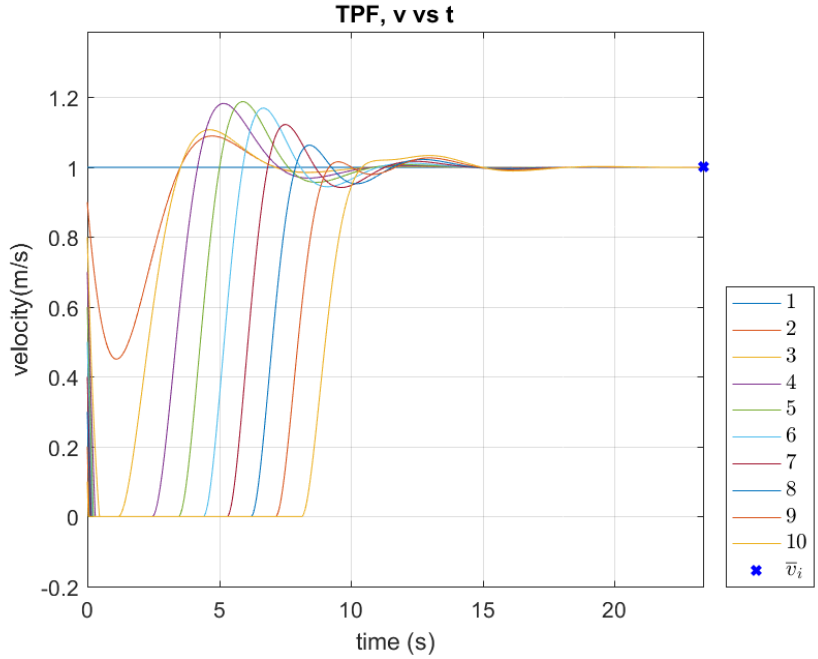

Figure 52 - TPF Results for Chapter 7, velocity versus time.

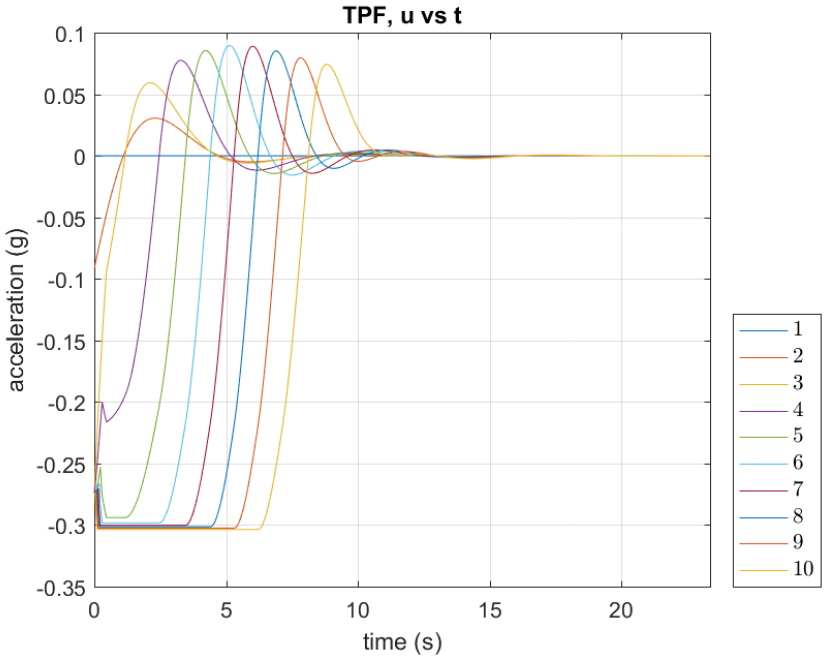

Figure 53 - TPF Results for Chapter 7, acceleration input versus time.

Two-Predecessor-Leader-Following Topology

Table 22 - Analysis of TPLF Results for Chapter 7

Node	H_i	$\overline{x}_i$	$x_i(t_f)_{sim}$	$\%error\ (\overline{x}_i)$	G_i	$\overline{v}_i$	$v_i(t_f)_{sim}$	$\%error\ (\overline{v}_i)$
1	0	29.10	29.1000	0.000	0	1	1.0000	0.000
2	2	27.10	27.0999	0.000	0	1	1.0001	0.006
3	4	25.10	25.0999	0.000	0	1	1.0001	0.006
4	6	23.10	23.0999	0.000	0	1	1.0001	0.006
5	8	21.10	21.0999	0.000	0	1	1.0001	0.006
6	10	19.10	19.0999	0.000	0	1	1.0001	0.006
7	12	17.10	17.0999	0.000	0	1	1.0001	0.006
8	14	15.10	15.0999	0.000	0	1	1.0001	0.006
9	16	13.10	13.0999	0.001	0	1	1.0001	0.006
10	18	11.10	11.0999	0.001	0	1	1.0001	0.006

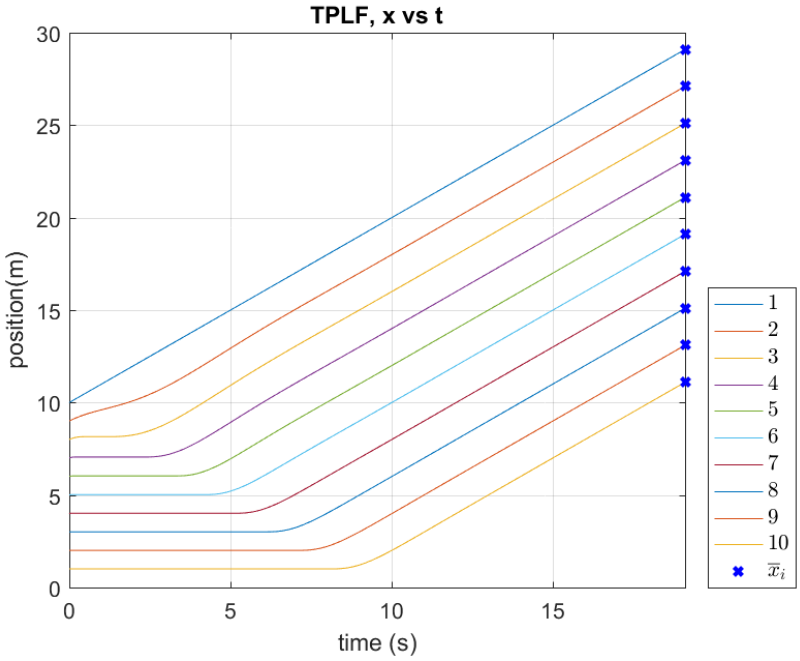

Figure 54 - TPLF Results for Chapter 7, position versus time.

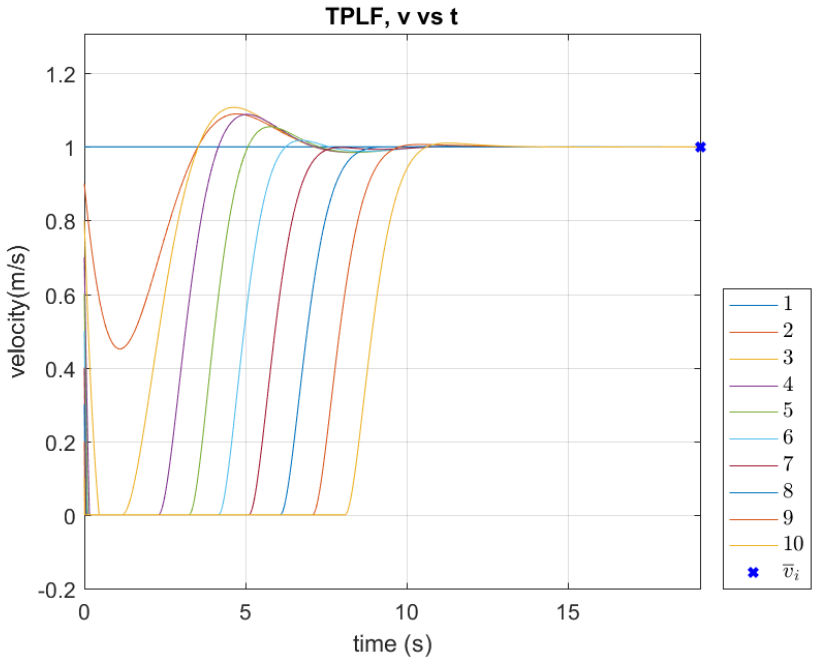

Figure 55 - TPLF Results for Chapter 7, velocity versus time.

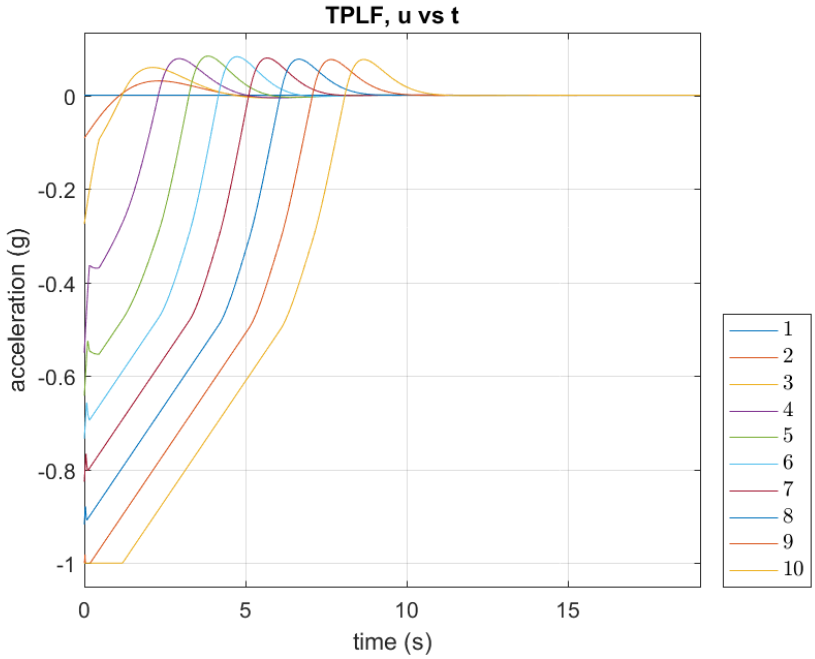

Figure 56 - TPLF Results for Chapter 7, acceleration input versus time.

Chapter 8:

Consensus in Highway On-ramp Merging Scenario

In this chapter, we simulate a highway-driving scenario with realistic limitations placed on the vehicle dynamics.

Section 8.1 – Explanation of Simulation for Chapter 8

The local node form of the distributed position/velocity feedback with offset protocol (26) as well as the global form of distributed position/velocity feedback with offset protocol (52) were implemented using MATLAB/Simulink for each of the 6 platoon topologies. The Appendix provides details regarding how the simulation was performed. Recall that in Chapter 7, restrictions were placed on the acceleration input and the vehicle velocity. We assume the vehicles are generic passenger sedans driven at highway speeds and as such have an acceleration limitation of 0.3g's and deceleration limitation of 1.0g's. The vehicles must also not be allowed to drive in reverse so a lower limit of 0 m/s is placed on the velocity. An arbitrary upper limit of 100mph (44.704m/s) is also applied.

For this simulation, the desired distance between vehicles in the platoon is 2 meters ($h = 2$) such that formation position vector H ((35) from Chapter 5), and formation velocity vector G ((37) from Chapter 5) become:

$$H = [0 \quad 2 \quad 4 \quad 6 \quad 8 \quad 10 \quad 12 \quad 14 \quad 16 \quad 18]$$

$$G = [0 \quad 0 \quad 0 \quad 0 \quad 0 \quad 0 \quad 0 \quad 0 \quad 0 \quad 0].$$

In the previous chapters, the desired velocity of 1 m/s was chosen so that the state versus time plots would be easy to read while working through the ideas that convergence value can be known for each vehicle even with limited vehicle dynamics. In this chapter, we will keep the initial conditions for vehicle position $x(0)$ the same as was used in previous chapters, but we will force the initial condition for vehicle velocity from

the previous velocity of 1m/s into highway speed, which is 29 m/s (64.8712 mph). The following initial conditions were used to simulate a highway on-ramp merging scenario:

$$x(0) = [10 \quad 9 \quad 8 \quad 7 \quad 6 \quad 5 \quad 4 \quad 3 \quad 2 \quad 1],$$

$$v(0) = [29 \quad 28 \quad 27 \quad 26 \quad 25 \quad 24 \quad 23 \quad 22 \quad 21 \quad 20].$$

Section 8.2 – Analysis of Results for Chapter 8

The results for t_f for each topology given the conditions described in Section 8.1 are provided in Table 23. Protocols (26) and (52) were simulated with identical results, confirming correct derivation of *Conjecture 2*. Recall the platoon topologies are Predecessor-Following (PF), Predecessor-Leader-Following (PLF), Bidirectional (BD), Bidirectional-Leader (BDL), Two-Predecessor-Following (TPF) and Two-Predecessor-Leader-Following (TPLF) as shown in Figure 1.

Table 23 – Final Time for Simulations in Chapter 8

Topology	t_f
PF	51.32
PLF	20.63
BD	419.27
BDL	23.07
TPF	25.08
TPLF	18.33

Below are six subsections, one for each of the six topologies. Each subsection below presents a table. A description of the information presented in these tables follows. Column 1 (Node) shows the node number, where node 1 is the lead vehicle and node 10 is the last vehicle in the platoon. Column 2 (H_i) displays the i^{th} element of the formation position vector H, which is used to calculate (55). Column 3 ($\overline{x_i}$) displays the final position value for each node as calculated by (55). Column 4 ($x_i(t_f)_{sim}$) shows the final position

value for each node as obtained by the simulation using the final time t_f from Table 16 . Column 5 ($\%error\ (\overline{x_i})$) shows the error percentage between $\overline{x_i}$ and $x_i(t_f)_{sim}$. Column 6 (G_i) displays the i^{th} element of the velocity vector G, which is used to calculate (56). Column 7 ($\overline{v_i}$) displays the final position value for each node as calculated by (56). Column 8 ($v_i(t_f)_{sim}$) shows the final position value for each node as obtained by the simulation using the final time t_f from Table 23 . Column 9 ($\%error\ (\overline{v_i})$) shows the error percentage between $\overline{v_i}$ and $v_i(t_f)_{sim}$.

Each subsection below also presents four figures for each topology. The first figure shows the simulation results of position versus time for each node from $t = 0$ to $t = t_f$. The values $\overline{x_i}$ from the related table were superimposed on the position plots, where $\overline{x_i}$ is denoted by a blue "x". If a collision occurs between two vehicles, then it is marked by a red "x". The second figure shows the simulation results of position versus time for the last few seconds of the simulation so that the desired offset can be visually inspected and referenced against the related table. The values $\overline{x_i}$ from the related table were superimposed on the position plots, where $\overline{x_i}$ is denoted by a blue "x". The third figure shows the simulation results of velocity versus time for each node. The values $\overline{v_i}$ were superimposed on the velocity plots, where $\overline{v_i}$ is denoted by a blue "x". The fourth figure shows the acceleration input plots show that the acceleration input $u_i = 0$ for all nodes at the at t_f listed in Table 23.

Table 24 through Table 29 along with Figure 39 through Figure 56 clearly show that these simulations support *Conjecture* 2 and *Conjecture 3* from Chapter 5, even with the limitations placed on the vehicle dynamics and in a realistic highway on-ramp merging scenario. The simulations in this chapter also serve to highlight that collisions can occur. Chapter 9 will elaborate more on collisions.

Predecessor-Following Topology

Table 24 - Analysis of PF Results for Chapter 8

Node	H_i	$\overline{x}_i$	$x_i(t_f)_{sim}$	$\%error\ (\overline{x}_i)$	G_i	$\overline{v}_i$	$v_i(t_f)_{sim}$	$\%error\ (\overline{v}_i)$
1	0	1498.28	1498.2800	0.000	0	29	29.0000	0.000
2	2	1496.28	1496.2800	0.000	0	29	29.0000	0.000
3	4	1494.28	1494.2800	0.000	0	29	29.0000	0.000
4	6	1492.28	1492.2800	0.000	0	29	29.0000	0.000
5	8	1490.28	1490.2800	0.000	0	29	29.0000	0.000
6	10	1488.28	1488.2800	0.000	0	29	29.0000	0.000
7	12	1486.28	1486.2800	0.000	0	29	29.0000	0.000
8	14	1484.28	1484.2800	0.000	0	29	29.0000	0.000
9	16	1482.28	1482.2799	0.000	0	29	29.0001	0.000
10	18	1480.28	1480.2797	0.000	0	29	29.0002	0.001

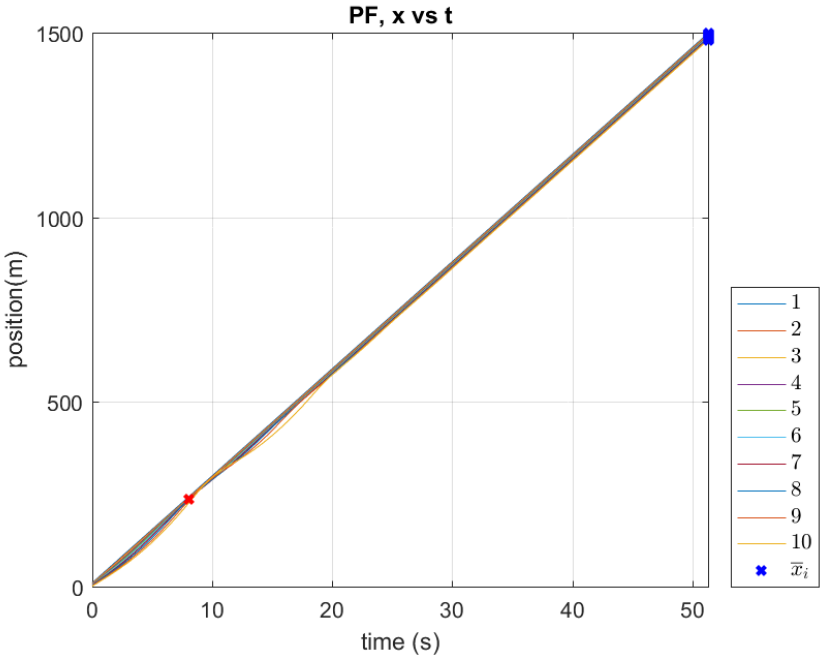

Figure 57 - PF Results for Chapter 8, position versus time.

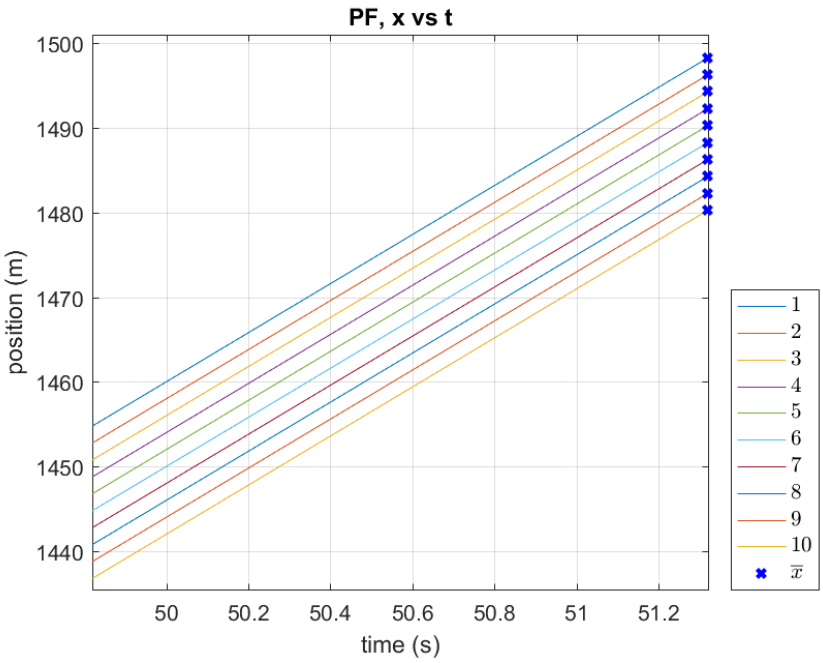

Figure 58 - PF Results for Chapter 8, position versus time, zoomed in.

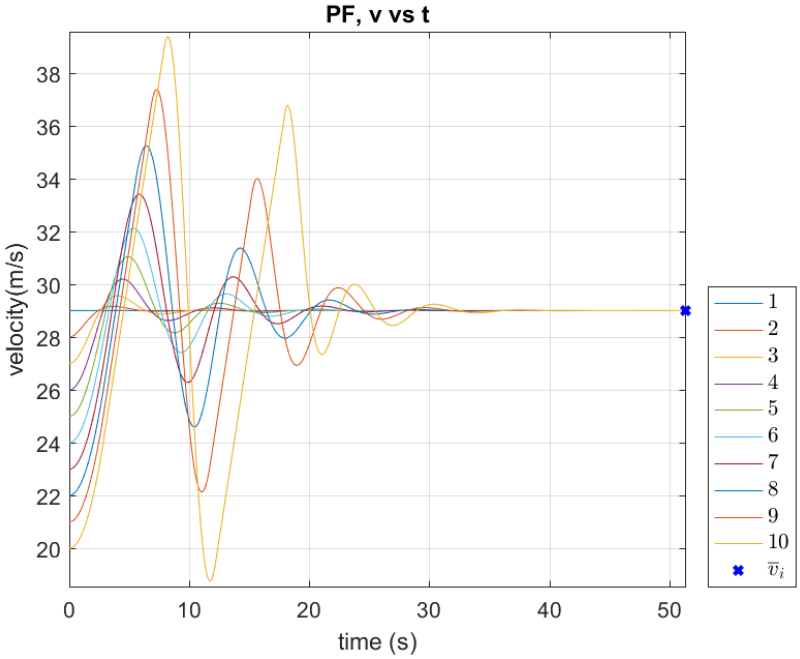

Figure 59 - PF Results for Chapter 8, velocity versus time.

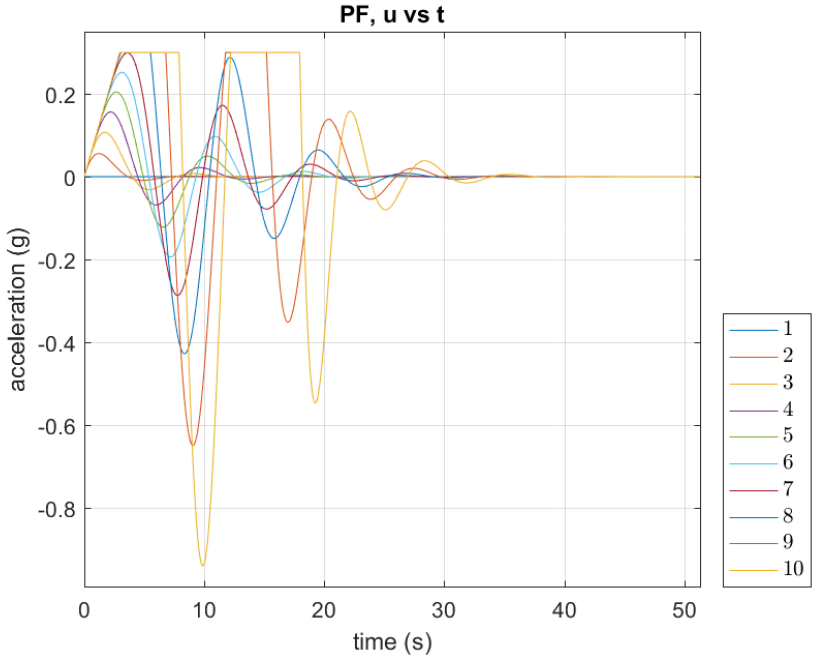

Figure 60 - PF Results for Chapter 8, acceleration input versus time.

Predecessor-Leader-Following Topology

Table 25 - Analysis of PLF Results for Chapter 8

Node	H_i	$\overline{x}_i$	$x_i(t_f)_{sim}$	$\%error\ (\overline{x}_i)$	G_i	$\overline{v}_i$	$v_i(t_f)_{sim}$	$\%error\ (\overline{v}_i)$
1	0	608.27	608.2700	0.000	0	29	29.0000	0.000
2	2	606.27	606.2700	0.000	0	29	29.0000	0.000
3	4	604.27	604.2700	0.000	0	29	29.0000	0.000
4	6	602.27	602.2700	0.000	0	29	29.0000	0.000
5	8	600.27	600.2700	0.000	0	29	29.0000	0.000
6	10	598.27	598.2700	0.000	0	29	29.0000	0.000
7	12	596.27	596.2700	0.000	0	29	29.0000	0.000
8	14	594.27	594.2700	0.000	0	29	29.0000	0.000
9	16	592.27	592.2700	0.000	0	29	29.0000	0.000
10	18	590.27	590.2700	0.000	0	29	29.0000	0.000

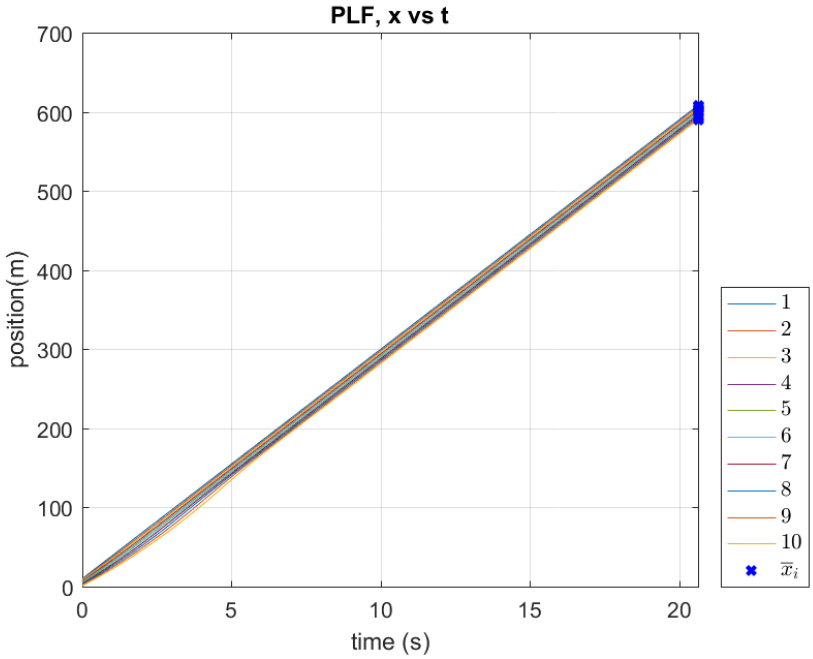

Figure 61 - PLF Results for Chapter 8, position versus time.

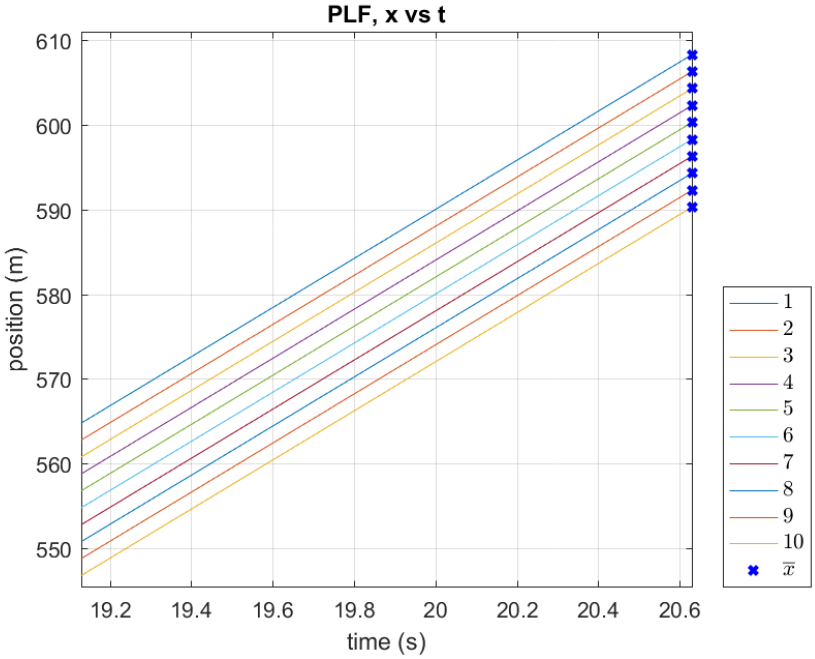

Figure 62 - PLF Results for Chapter 8, position versus time, zoomed in.

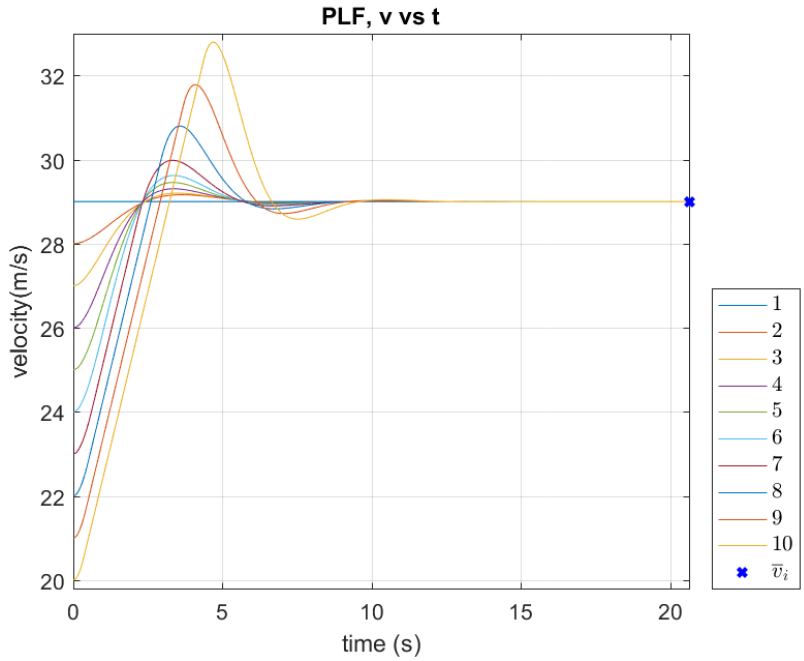

Figure 63 - PLF Results for Chapter 8, velocity versus time.

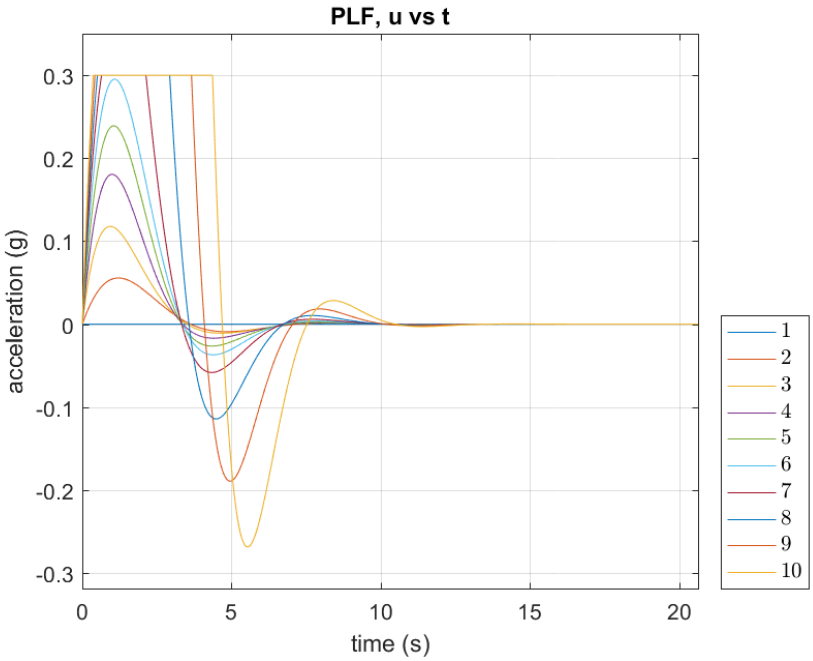

Figure 64 - PLF Results for Chapter 8, acceleration input versus time.

Bidirectional Topology

Table 26 - Analysis of BD Results for Chapter 8

Node	H_i	$\overline{x}_i$	$x_i(t_f)_{sim}$	$\%error\ (\overline{x}_i)$	G_i	$\overline{v}_i$	$v_i(t_f)_{sim}$	$\%error\ (\overline{v}_i)$
1	0	12168.83	12168.8300	0.000	0	29	29.0000	0.000
2	2	12166.83	12166.8368	0.000	0	29	28.9959	0.014
3	4	12164.83	12164.8433	0.000	0	29	28.9919	0.028
4	6	12162.83	12162.8495	0.000	0	29	28.9881	0.041
5	8	12160.83	12160.8552	0.000	0	29	28.9847	0.053
6	10	12158.83	12158.8602	0.000	0	29	28.9817	0.063
7	12	12156.83	12156.8644	0.000	0	29	28.9791	0.072
8	14	12154.83	12154.8676	0.000	0	29	28.9772	0.079
9	16	12152.83	12152.8698	0.000	0	29	28.9759	0.083
10	18	12150.83	12150.8709	0.000	0	29	28.9752	0.086

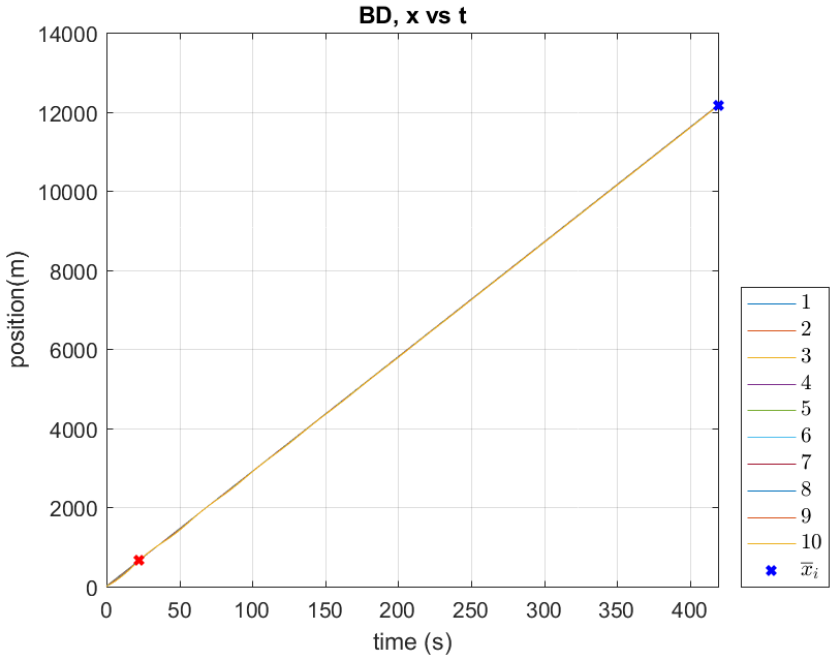

Figure 65 - BD Results for Chapter 8, position versus time.

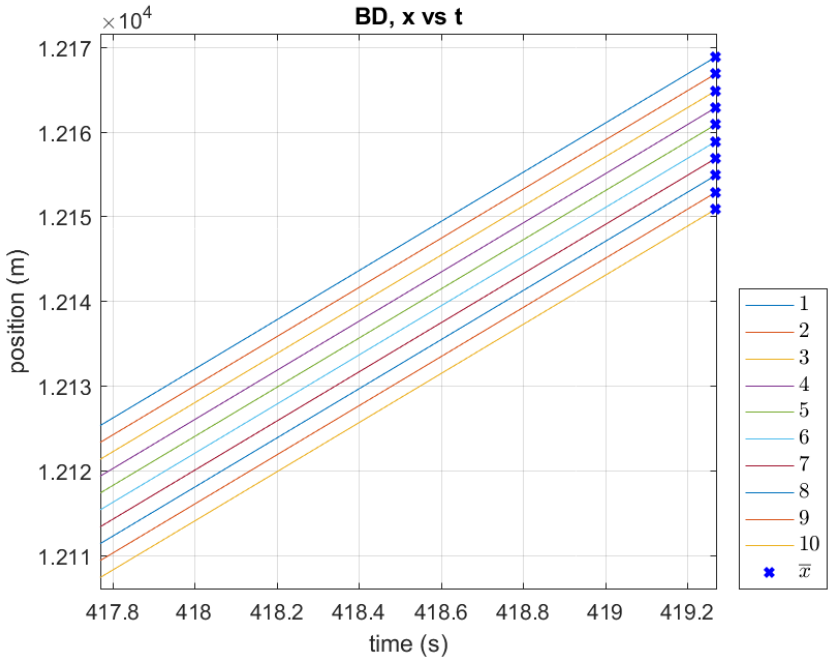

Figure 66 - BD Results for Chapter 8, position versus time, zoomed in.

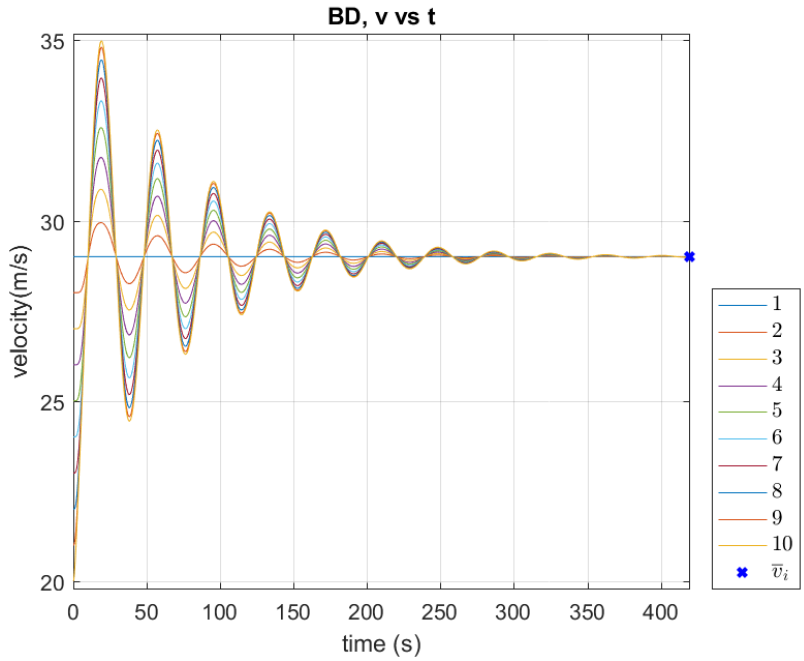

Figure 67 - BD Results for Chapter 8, velocity versus time.

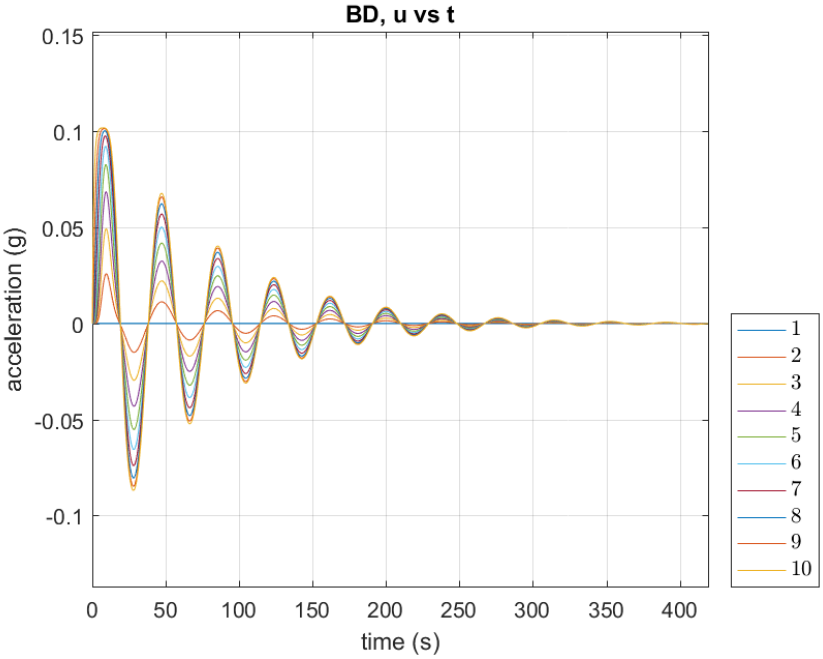

Figure 68 - BD Results for Chapter 8, acceleration input versus time.

Bidirectional-Leader Topology

Table 27 - Analysis of BDL Results for Chapter 8

Node	H_i	$\overline{x}_i$	$x_i(t_f)_{sim}$	$\%error\ (\overline{x}_i)$	G_i	$\overline{v}_i$	$v_i(t_f)_{sim}$	$\%error\ (\overline{v}_i)$
1	0	679.03	679.0300	0.000	0	29	29.0000	0.000
2	2	677.03	677.0301	0.000	0	29	28.9999	0.000
3	4	675.03	675.0301	0.000	0	29	28.9999	0.000
4	6	673.03	673.0301	0.000	0	29	28.9999	0.000
5	8	671.03	671.0301	0.000	0	29	28.9999	0.000
6	10	669.03	669.0301	0.000	0	29	28.9999	0.000
7	12	667.03	667.0301	0.000	0	29	28.9999	0.000
8	14	665.03	665.0301	0.000	0	29	28.9999	0.000
9	16	663.03	663.0301	0.000	0	29	28.9998	0.001
10	18	661.03	661.0301	0.000	0	29	28.9998	0.001

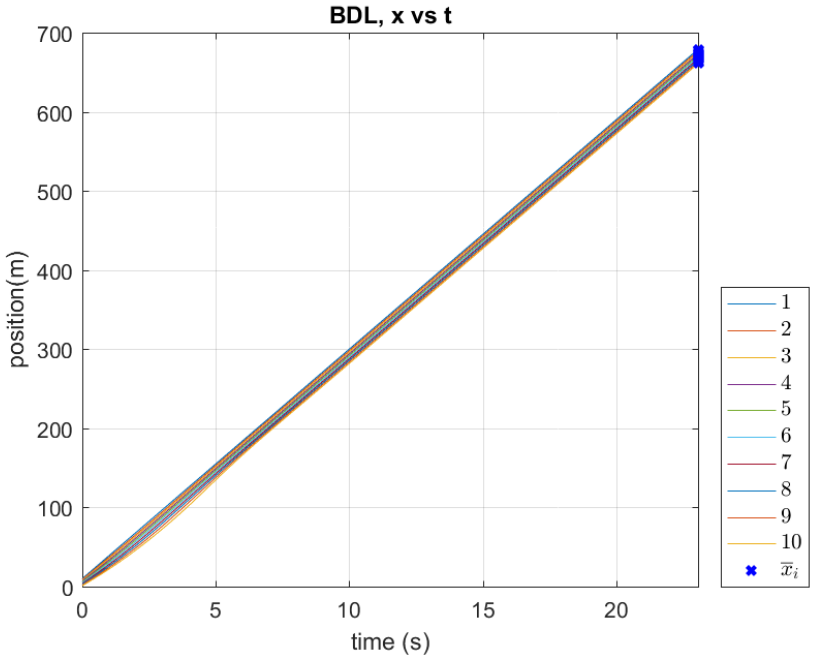

Figure 69 - BDL Results for Chapter 8, position versus time.

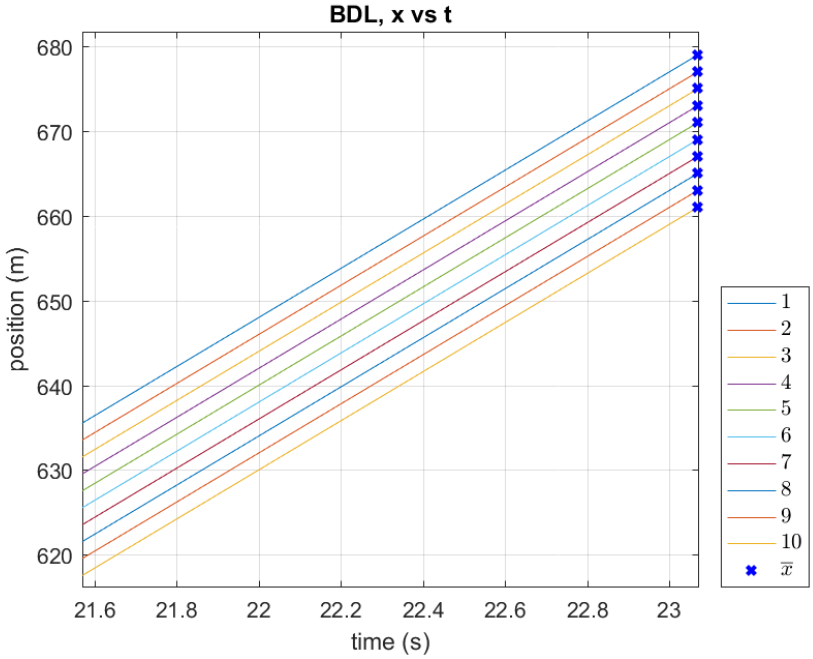

Figure 70 – BDL Results for Chapter 8, position versus time, zoomed in.

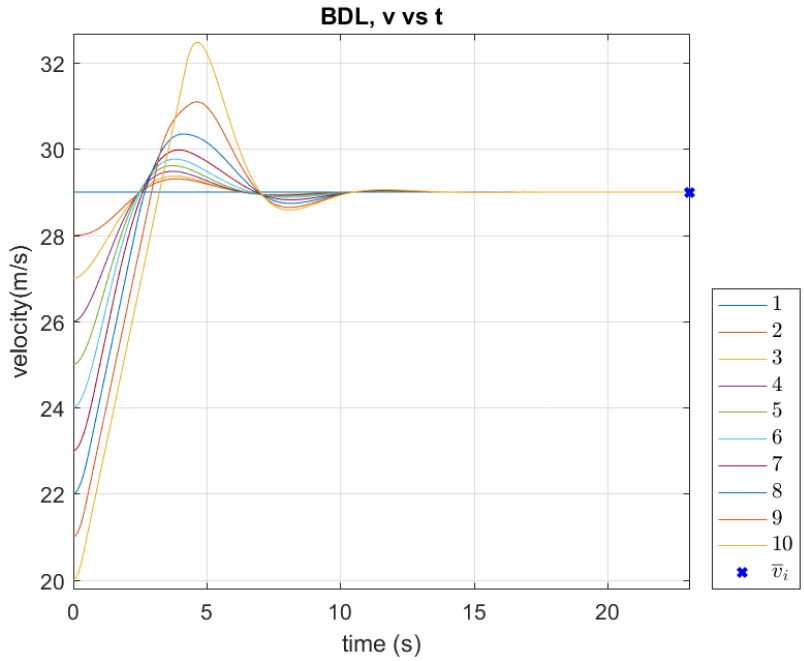

Figure 71 - BDL Results for Chapter 8, velocity versus time.

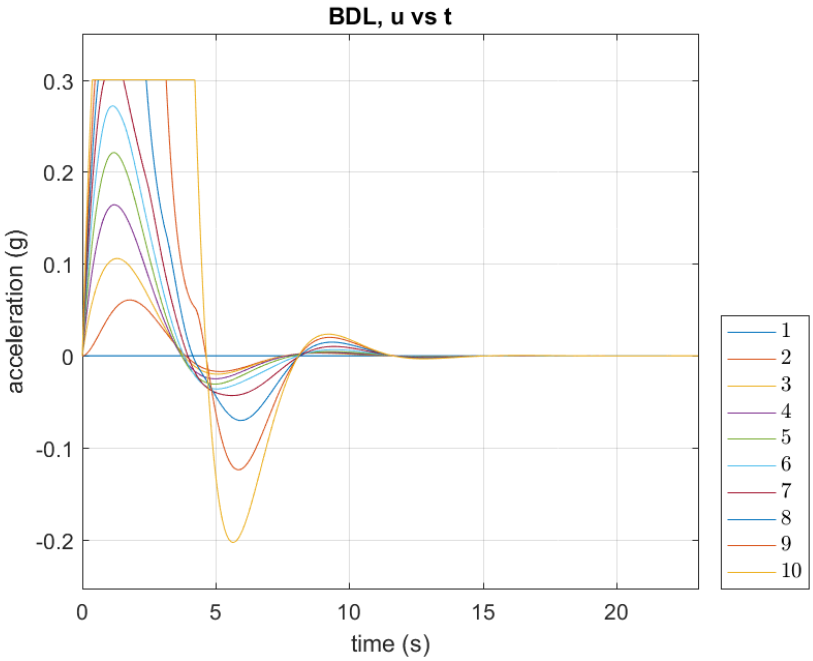

Figure 72 - BDL Results for Chapter 8, acceleration input versus time.

Two-Predecessor-Following Topology

Table 28 - Analysis of TPF Results for Chapter 8

Node	H_i	$\overline{x}_i$	$x_i(t_f)_{sim}$	$\%error\ (\overline{x}_i)$	G_i	$\overline{v}_i$	$v_i(t_f)_{sim}$	$\%error\ (\overline{v}_i)$
1	0	737.32	737.3200	0.000	0	29	29.0000	0.000
2	2	735.32	735.3200	0.000	0	29	29.0000	0.000
3	4	733.32	733.3200	0.000	0	29	29.0000	0.000
4	6	731.32	731.3200	0.000	0	29	29.0000	0.000
5	8	729.32	729.3200	0.000	0	29	29.0000	0.000
6	10	727.32	727.3200	0.000	0	29	29.0000	0.000
7	12	725.32	725.3200	0.000	0	29	29.0000	0.000
8	14	723.32	723.3199	0.000	0	29	29.0000	0.000
9	16	721.32	721.3199	0.000	0	29	29.0001	0.000
10	18	719.32	719.3199	0.000	0	29	29.0001	0.000

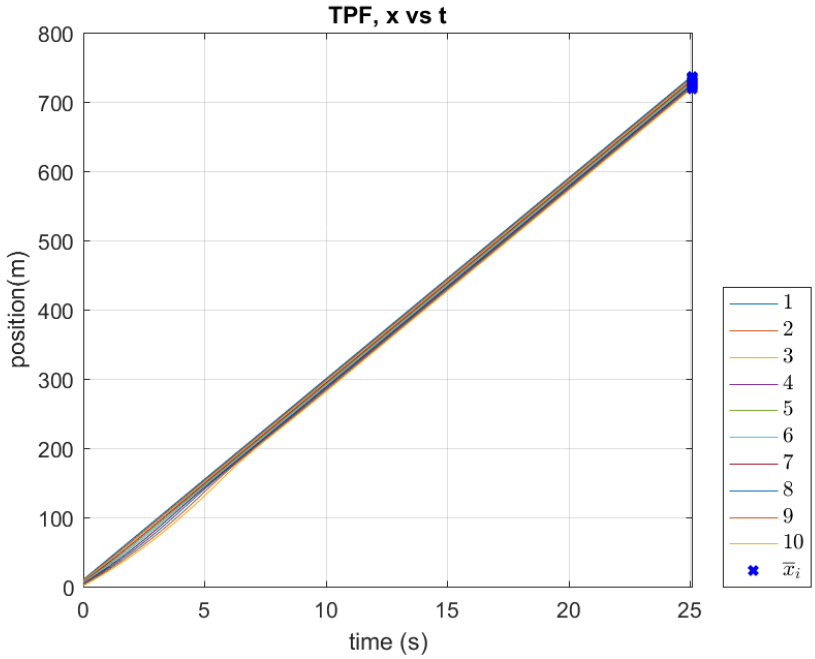

Figure 73 - TPF Results for Chapter 8, position versus time.

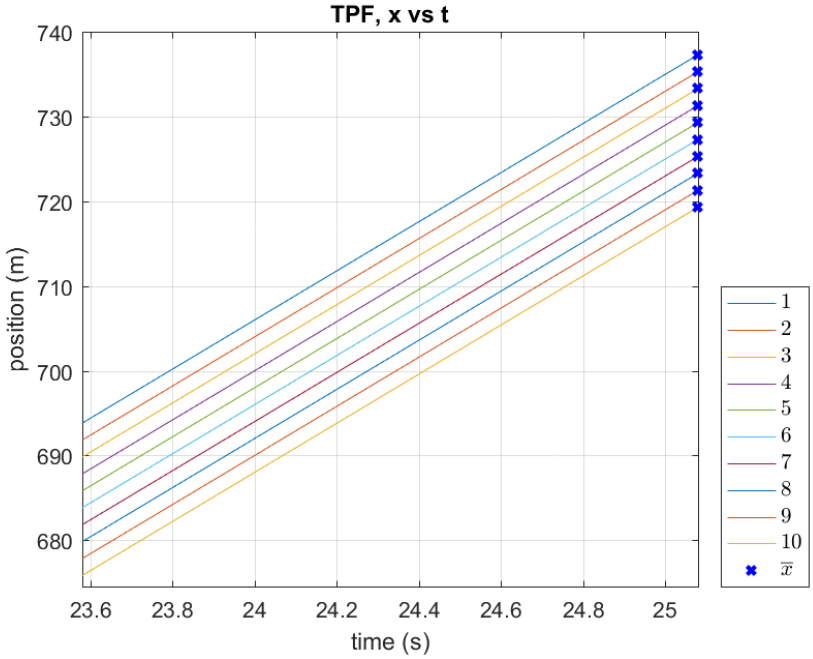

Figure 74 - TPF Results for Chapter 8, position versus time, zoomed in.

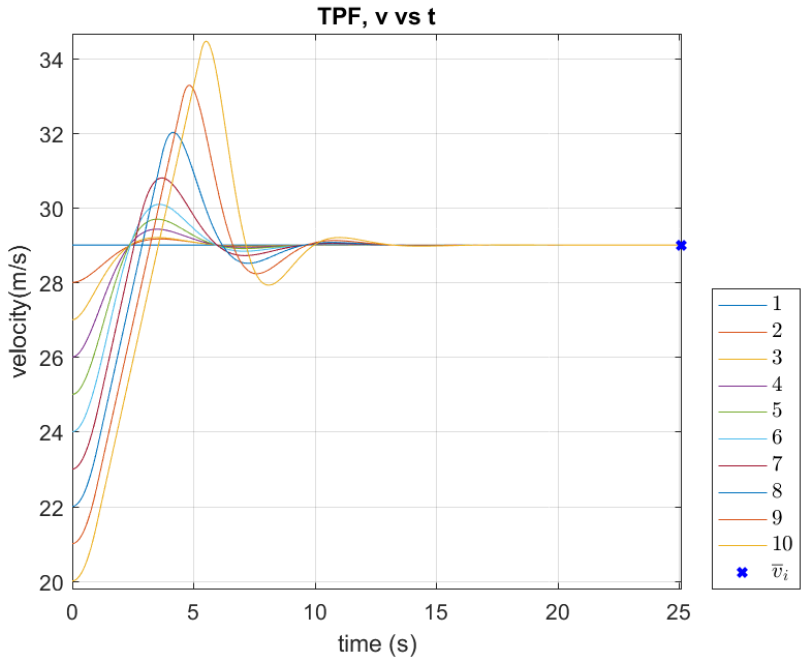

Figure 75 - TPF Results for Chapter 8, velocity versus time.

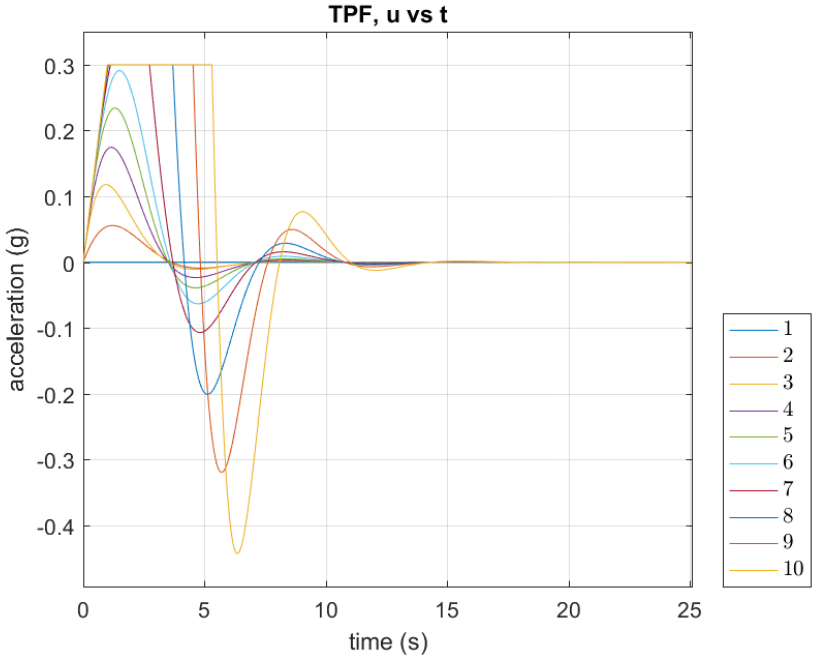

Figure 76 - TPF Results for Chapter 8, acceleration input versus time.

Two-Predecessor-Leader-Following Topology

Table 29 - Analysis of TPLF Results for Chapter 8

Node	H_i	$\overline{x}_i$	$x_i(t_f)_{sim}$	$\%error\ (\overline{x}_i)$	G_i	$\overline{v}_i$	$v_i(t_f)_{sim}$	$\%error\ (\overline{v}_i)$
1	0	541.57	541.5700	0.000	0	29	29.0000	0.000
2	2	539.57	539.5699	0.000	0	29	29.0001	0.000
3	4	537.57	537.5699	0.000	0	29	29.0001	0.000
4	6	535.57	535.5699	0.000	0	29	29.0001	0.000
5	8	533.57	533.5699	0.000	0	29	29.0001	0.000
6	10	531.57	531.5699	0.000	0	29	29.0001	0.000
7	12	529.57	529.5699	0.000	0	29	29.0001	0.000
8	14	527.57	527.5699	0.000	0	29	29.0001	0.000
9	16	525.57	525.5699	0.000	0	29	29.0001	0.000
10	18	523.57	523.5699	0.000	0	29	29.0001	0.000

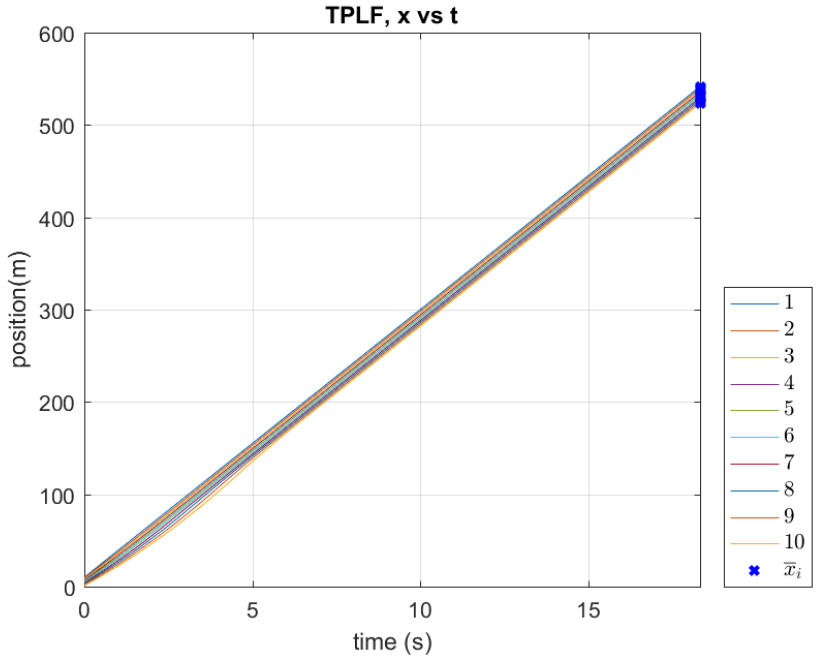

Figure 77 - TPLF Results for Chapter 8, position versus time.

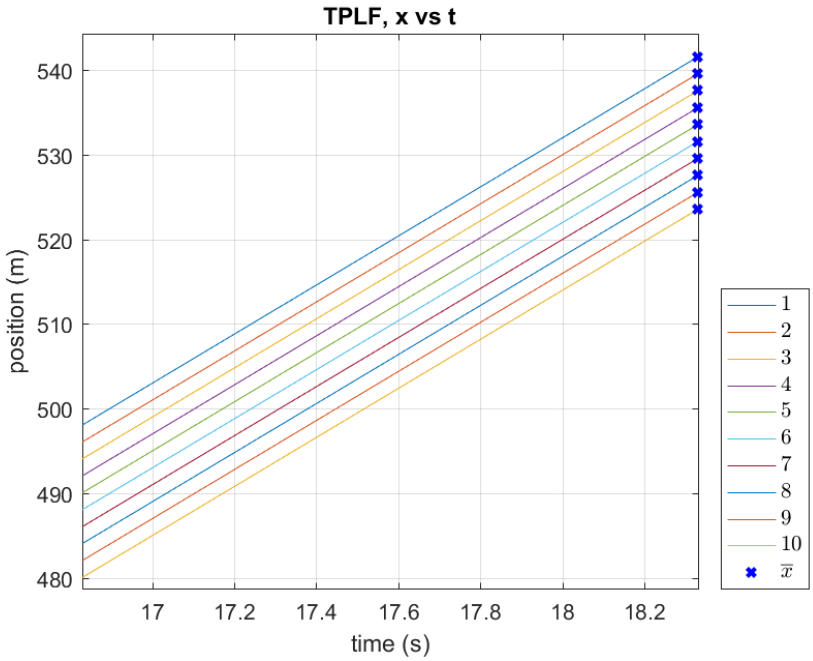

Figure 78 - TPLF Results for Chapter 8, position versus time, zoomed in.

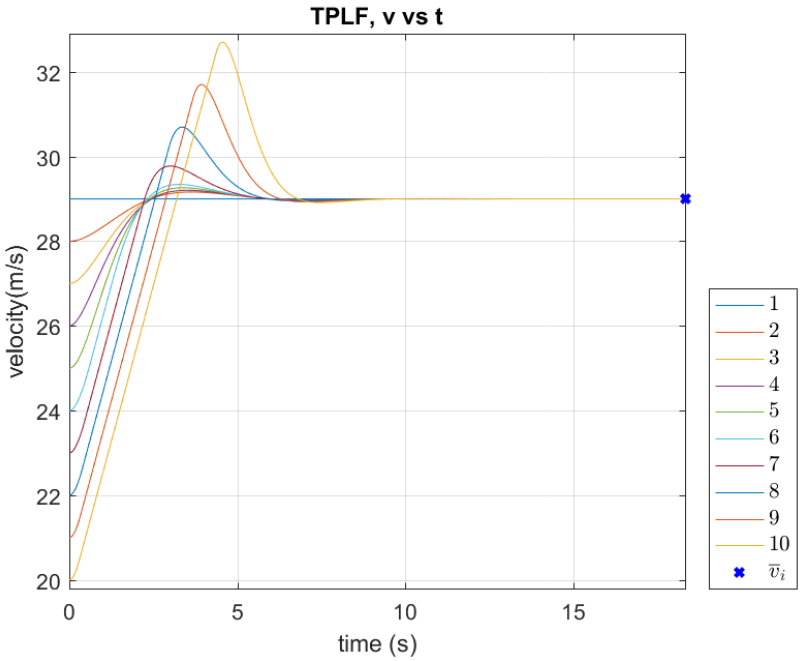

Figure 79 - TPLF Results for Chapter 8, velocity versus time.

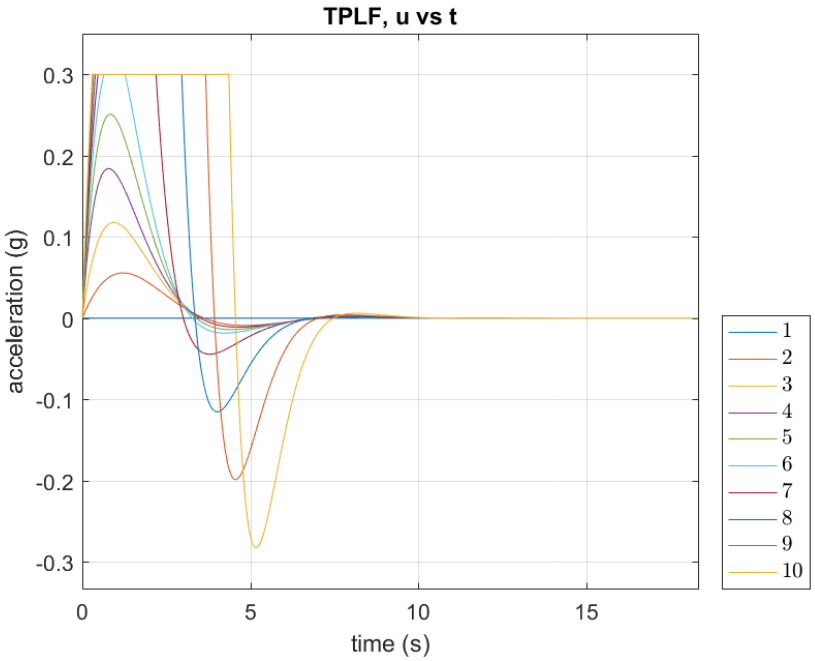

Figure 80 - TPLF Results for Chapter 8, acceleration input versus time.

Chapter 9:

String Stability and Collision Avoidance

Recall from Chapter 1 that string stability involves analyzing the intervehicle distance error. For any platoon topology, r is the intervehicle distance as shown in (57). The intervehicle distance error, e is defined as (58) as the desired intervehicle distance, h, minus the actual intervehicle distance, r. Note that this only considers the distance between adjacent vehicles.

$$r = [x_1 - x_2 \quad x_2 - x_3 \quad \cdots \quad x_{N-1} - x_N]^T, \in R^{(N-1)} \tag{57}$$

$$e = h - r, \in R^{(N-1)} \tag{58}$$

Existing literature places heavy emphasis on analyzing the intervehicle distance error e to design platoon controllers which provide string stability. However, this thesis uses the distributed position/velocity feedback with offset protocol (52) and seeks to tune the controller gains c and γ to provide collision avoidance rather than string stability. An emphasis is placed on collision avoidance rather than string stability because as will be seen in this chapter, string stability does not guarantee collision avoidance, and collision avoidance can be achieved even with string unstable platoons. Since consumer safety is the most important consideration in any design, this chapter focuses on collision avoidance rather than string stability.

To do this we will further analyze the two topologies which experienced collision in Chapter 8, the Predecessor-Follower (PF) and Bidirectional (BD) topologies. Recall that collisions are marked with a red “x” in the first occurrence where two vehicles occupy the same position. Figure 81 shows a zoomed in version of Figure 57, where a collision between car 6 and car 7 occurs at approximately 8.05 seconds. Likewise, Figure 82 shows a zoomed in version of Figure 65, where a collision between car 1 and car 2 occurs at approximately 22.27 seconds.

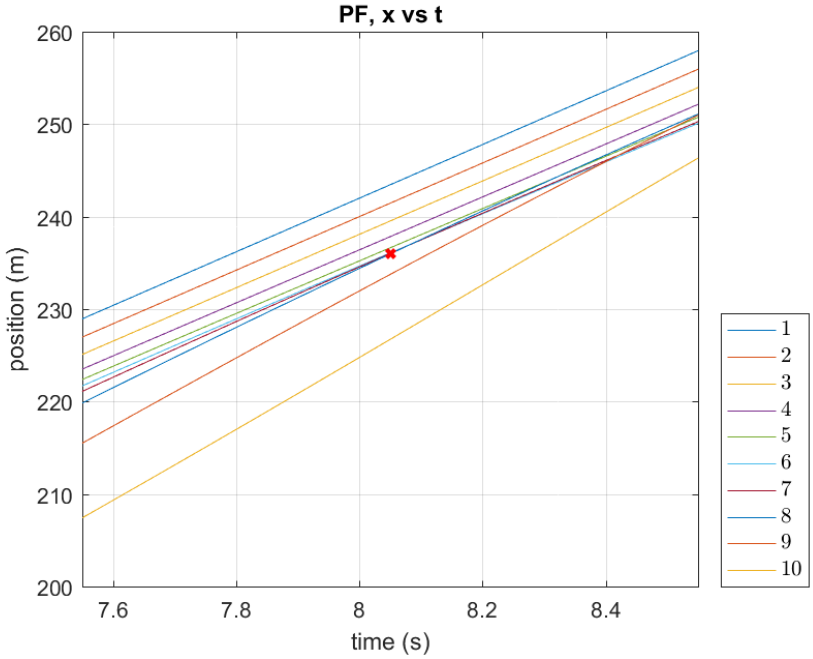

Figure 81 – PF Collision for Simulation 8.1.

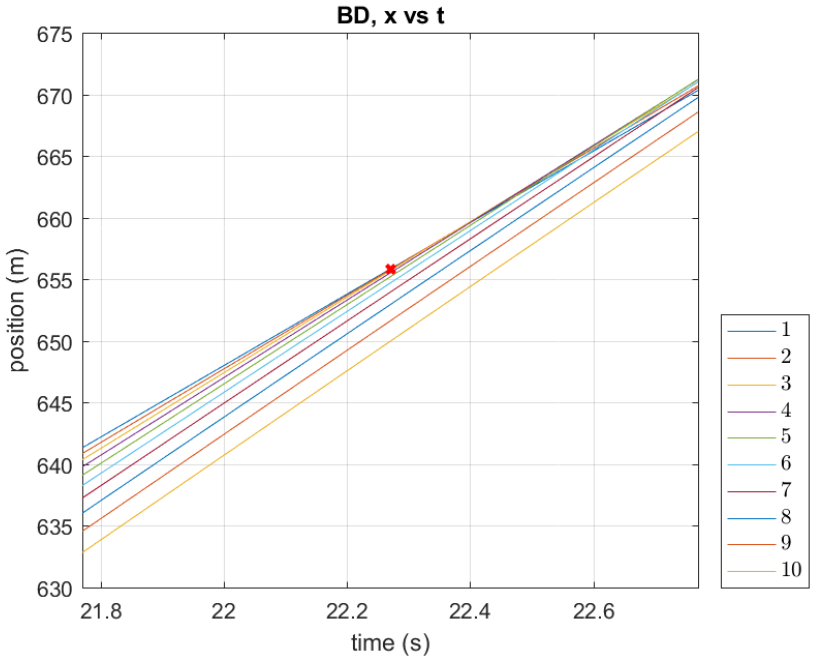

Figure 82 – BD Collision for Simulation 8.1.

Next we will look at the plots of intervehicle distance error e as well as intervehicle distance r and we will see which is more useful in terms of guaranteeing collision avoidance. Recall from Section 1.1 that string unstable behavior is characterized by intervehicle distance errors amplifying down the vehicle string, whereas string stable behavior is characterized by intervehicle distance errors attenuating down the vehicle string.

Figure 83 shows the intervehicle distance error e for the PF topology simulated in Chapter 8. It is quite easy to see from this figure that this platoon is string unstable; the error between car 9 and car 10 is consistently greater than the error between car 8 and car 9, which is consistently greater than the error between car 7 and car 8, and so on.

Figure 84 shows the intervehicle distance error e for the BD topology simulated in Chapter 8. It is likewise straightforward to see that this platoon is string stable; the error between car 9 and car 10 is consistently smaller than the error between car 8 and car 9, which is consistently smaller than the error between car 7 and car 8, and so on.

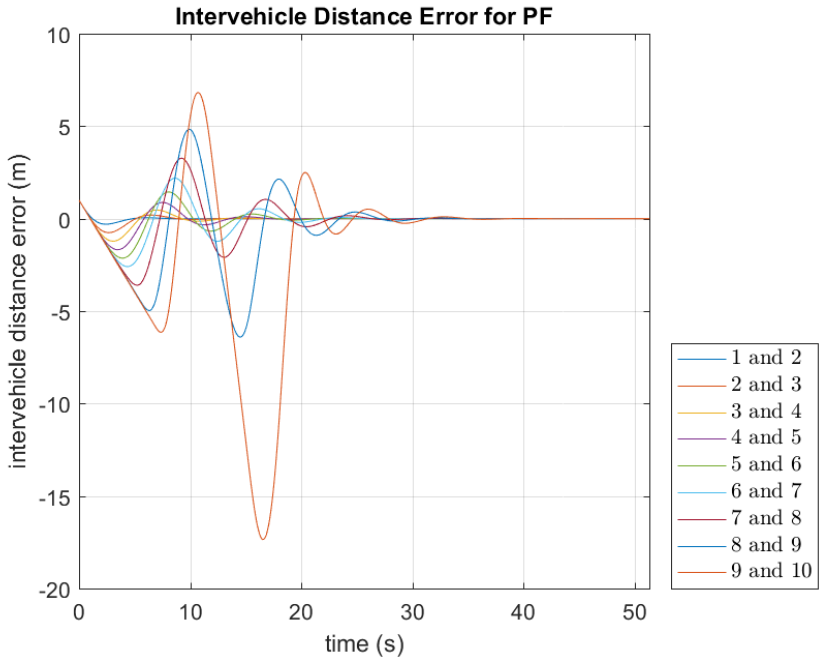

Figure 83 – PF Intervehicle Distance Error for Simulation 8.1.

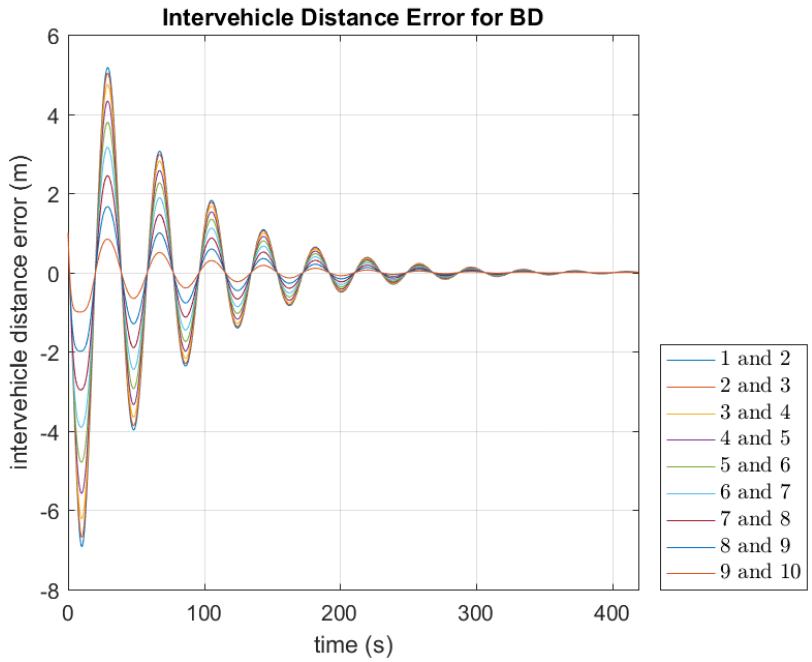

Figure 84 – BD Intervehicle Distance Error for Simulation 8.1.

However, neither Figure 83 nor Figure 84 provide clue as to how to proceed to eliminate the collision occurrence in this scenario. Instead of intervehicle distance error e, we need to look at the intervehicle distance r.

Figure 85 and Figure 86 show the intervehicle distance r for the PF and BD topologies (respectively) simulated in Chapter 8. The line $r = 0$ represents the line where collision occurs and is so-labeled as the "collision line". Note that we can plainly see that collision occurs when $r < 0$. As such, the intervehicle distance figures provide the clue as to how to proceed to eliminate the collision occurrence in this scenario. The controller gains c and γ are both unity in this simulation. Simply increasing them to $c = 2$ and $\gamma = 2$ yields a collision-free simulation for the PF topology as indicated by Figure 87 and for the BD topology as indicated by Figure 88. Both Figure 87 and Figure 88 indicate a collision-free simulation because $r > 0$ for all time.

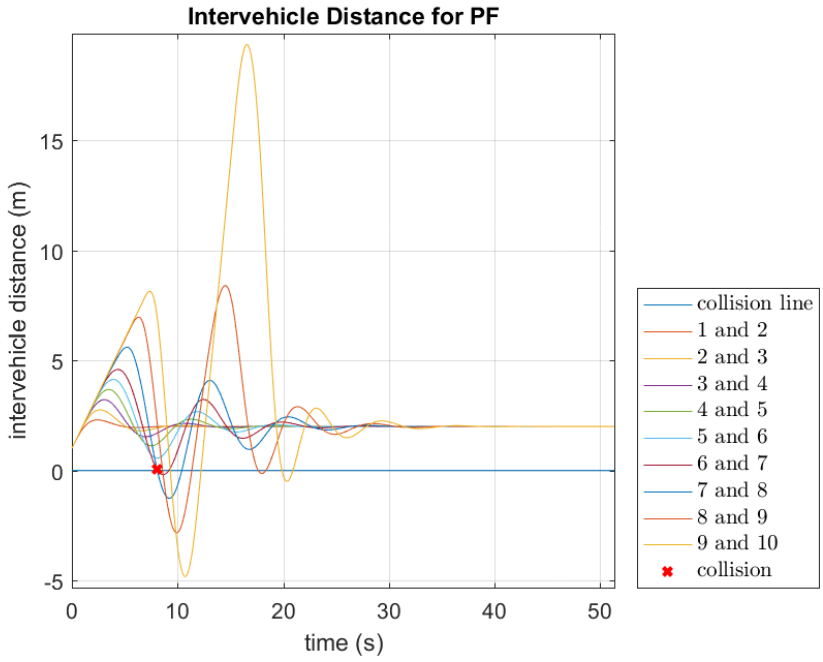

Figure 85 – PF Intervehicle Distance for Simulation 8.1.

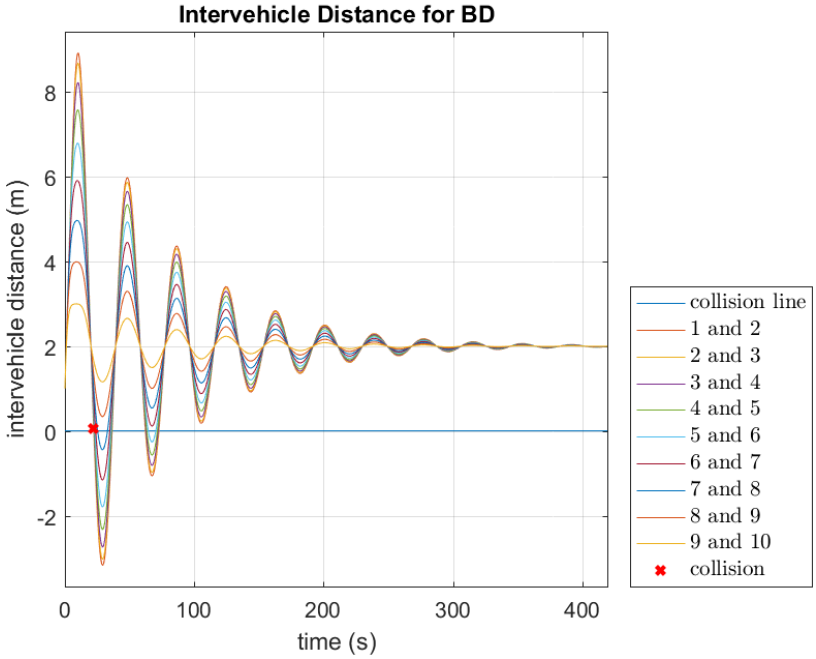

Figure 86 – BD Intervehicle Distance for Simulation 8.1.

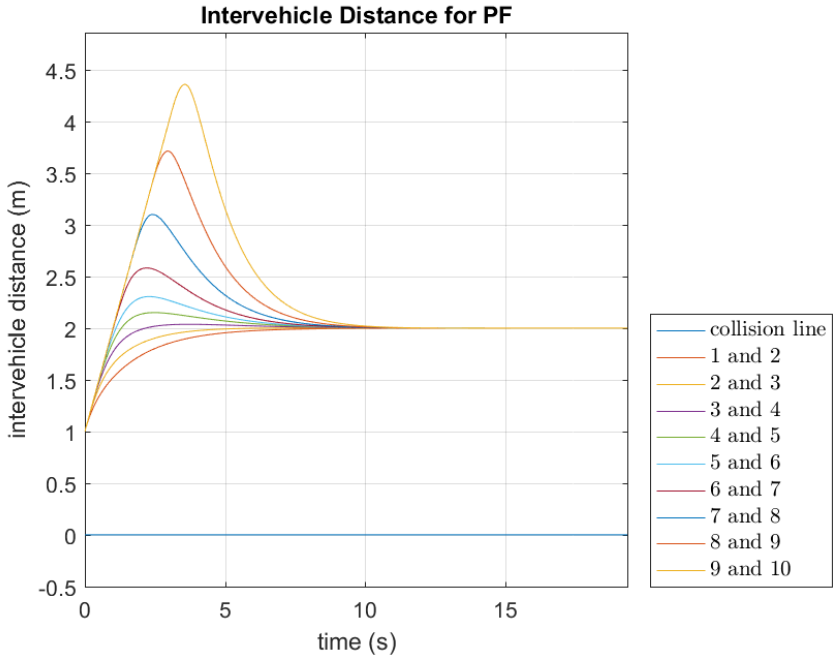

Figure 87 – PF Intervehicle distances for increased controller gains.

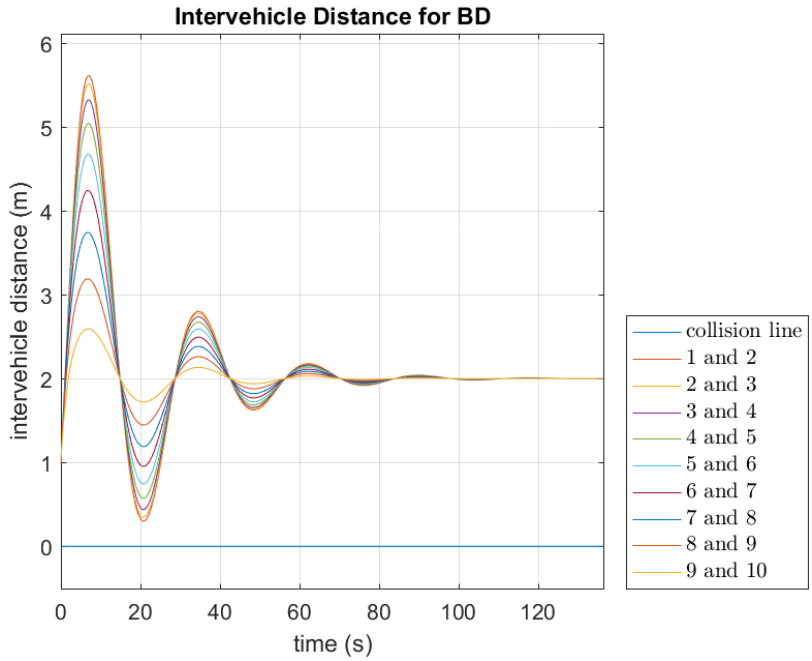

Figure 88 - BD Intervehicle distances for increased controller gains.

It is worth noting that $c = 2, \gamma = 2$ is not a universally applicable tune. For example, a Two-Predecessor-Leader-Follower (TPLF) platoon simulation was run with unity gains, $h = 2$, and the following initial conditions:

$$x(0) = [20 \quad 18 \quad 16 \quad 14 \quad 12 \quad 10 \quad 8 \quad 6 \quad 4 \quad 2],$$

$$v(0) = [29 \quad 32 \quad 28.4 \quad 28.1 \quad 25.5 \quad 32 \quad 28.4 \quad 28.7 \quad 29 \quad 33].$$

Figure 89 shows the intervehicle distance results with unity gains and it can be seen that a collision occurs between vehicles 5 and 6. Next, the gains $c = 2, \gamma = 2$ were simulated, and collision still occurs, as is shown in Figure 90. The collision can be avoided, however, with $c = 5$ and $\gamma = 1$, as shown in Figure 91.

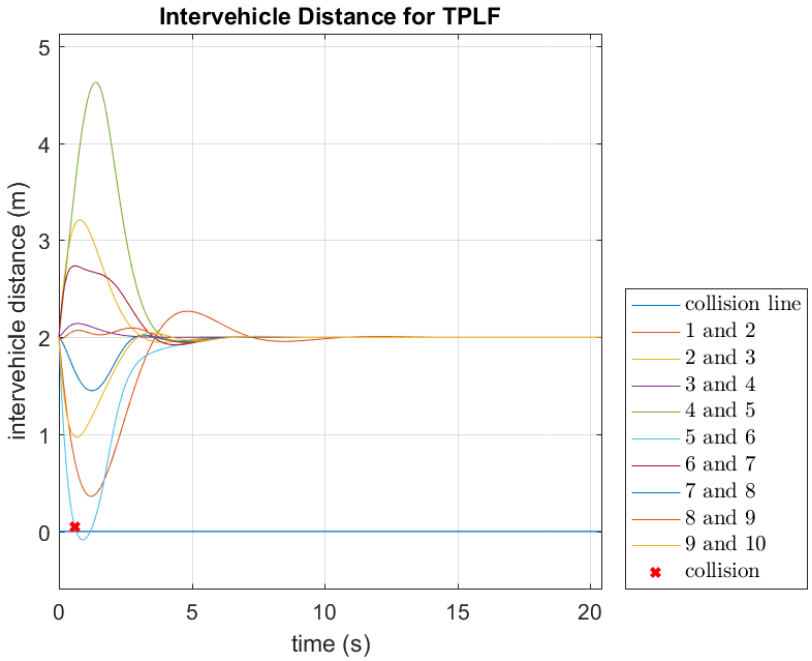

Figure 89 – TPLF Intervehicle distance with unity gains.

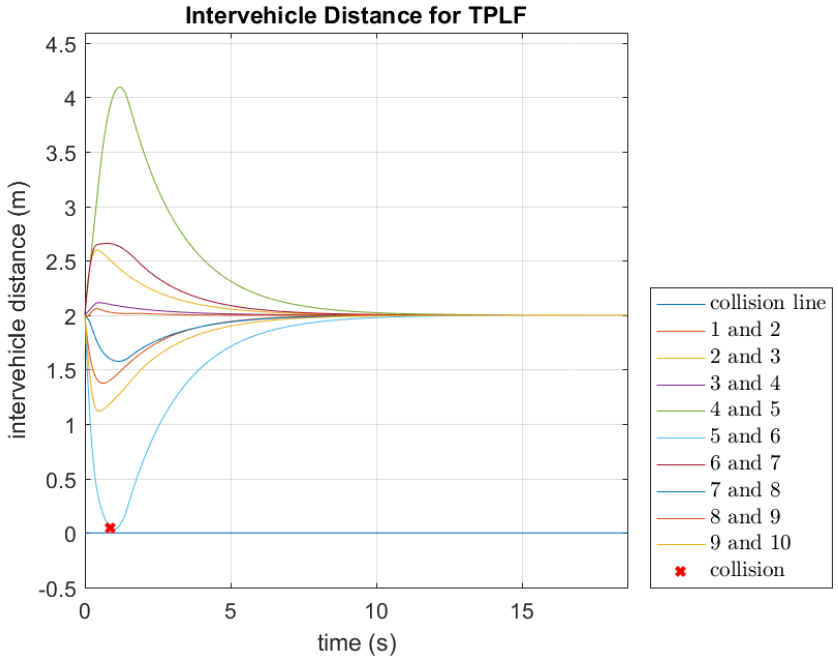

Figure 90 – TPLF Intervehicle distance with $c = 2, \gamma = 2$.

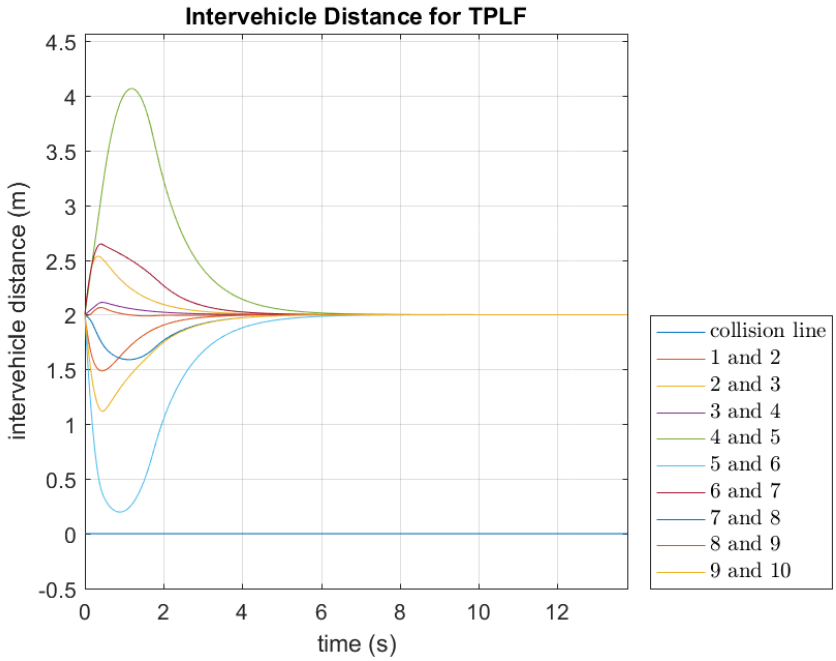

Figure 91 - TPLF Intervehicle distance with $c = 5, \gamma = 1$.

In this chapter we have seen that there is a connection between the topology, the initial conditions, the chosen controller gains, and collision occurrence or avoidance. The systems we have analyzed in this thesis have all been 20th order systems and therefore it is well beyond the scope of this thesis to suggest an explicit formula which relates the topology and initial conditions in a way that the controller gains can be chosen specifically to achieve collision avoidance. However, this chapter does suggest a method which can be used to find the controller gains to avoid collisions, albeit tedious and no doubt cumbersome. This method is to identify and define all possible initial condition scenarios and then simulate each scenario, finding the smallest possible gains which will avoid collision. Once all scenarios have been run, the controller gains should be the highest of those gains. This should be done for one topology only (i.e., each topology should be treated entirely separately).

Chapter 10:

Conclusion

Chapter 1 provided a literature review of platooning technology and platooning analysis techniques and formed the backdrop for this study of distributed control systems. Chapter 2 provided notations, preliminary information for information flowing in a platoon, and a brief overview of communication graph theory. Chapter 3 defined a 1LT graph, established an explicit method for identifying a 1LT graph, identified an error in [29] regarding the consensus value for 1LT graphs and proposed a formula for consensus values which relates to counting the number of directed trees in a graph. Chapter 4 provided thorough evidence to support Chapter 3. Chapter 5 provided a global form of the distributed position/velocity feedback with offset protocol and Chapters 6, 7, and 8 provided evidentiary support for Chapter 5. Chapter 9 discussed the notion of string instability for the various topologies and suggested with evidence a method for tuning the gains of the controllers such that collision can be avoided.

Reference List

[1] B. Van Arem, C. Tampere and K. Malone, "Modelling traffic flows with intelligent cars and intelligent roads," *Intelligent Vehicles Symposium, 2003. Proceedings. IEEE,* pp. 456-461, 2003.

[2] L. Y. Wang, A. Syed, G. G. Yin, A. Pandya and H. Zhang, "Control of vehicle platoons for highway safety and efficient utility: Consensus with communications and vehicle dynamics," *Journal of Systems Science and Complexity,* vol. 27, no. 4, p. 605–631, August 2014.

[3] R. Horowitz and P. Varaiya, "Control design of an automated highway system," *Proceedings of the IEEE,* vol. 88, no. 7, pp. 913-925, July 2000.

[4] G. Naus, R. Vugts, J. Ploeg and M. J. G. Van de Molengraft, "Towards on-the-road implementation of cooperative adaptive cruise control," in *Proc. 16th ITS World Congr.*, 2009.

[5] G. J. L. Naus, R. P. A. Vugts, J. Ploeg, M. J. G. van de Molengraft and M. Steinbuch, "String-Stable CACC Design and Experimental Validation: A Frequency-Domain Approach," *IEEE Transactions on Vehicular Technology,* vol. 59, no. 9, pp. 4268-4279, November 2010.

[6] J. Ploeg, E. Semsar-Kazerooni, G. Lijster, N. van de Wouw and H. Nijmeijer, "Graceful degradation of CACC performance subject to unreliable wireless communication," in *16th International IEEE Conference on Intelligent Transportation Systems (ITSC 2013)*, The Hague, 2013.

[7] P. Barooah, P. Mehta and J. P. Hespanha, "Mistuning-Based Control Design to Improve Closed-Loop Stability Margin of Vehicular Platoons," *IEEE Transactions on Automatic Control,* vol. 54, no. 9, pp. 2100-2113, September 2009.

[8] C.-C. Chien, Y. Zhang and P. Ioannou, "Traffic Density Control for Automated Highway Systems," *Automatica,* vol. 33, no. 7, pp. 1273-1285, Jul 1997.

[9] S. E. Shladover, "Automated highway systems: Petros A. Ioannou, Plenum Press, New York, 1997, ISBN: 0-306-45469-6," *Automatica,* vol. 36, no. 12, pp. 1929-1930, December 2000.

[10] Q. Xu, R. Sengupta, K. Hedrick and J. VanderWerf, "Effects of vehicle-vehicle/roadside-vehicle communication on adaptive cruise controlled highway systems," in *Vehicular Technology Conference, 2002. Proceedings. VTC 2002-Fall. 2002 IEEE 56th*, 2002.

[11] J. Ploeg, B. T. M. Scheepers, E. van Nunen, N. van de Wouw and H. Nijmeijer, "Design and experimental evaluation of cooperative adaptive cruise control," in *2011 14th International IEEE Conference on Intelligent Transportation Systems (ITSC)*, Washington, DC, 2011.

[12] M. E. Khatir and E. J. Davison, "Decentralized control of a large platoon of vehicles using non-identical controllers," in *American Control Conference, 2004. Proceedings of the 2004*, Boston, MA, 2004.

[13] J. Ploeg, "Connect & Drive: design and evaluation of cooperative adaptive cruise control for congestion reduction," *Journal of Modern Transportation,* vol. 19, pp. 207-213, 2011.

[14] A. A. Peters, R. H. Middleton and O. Mason, "Leader tracking in homogeneous vehicle platoons with broadcast delays," *Automatica,* vol. 50, no. 1, pp. 64-74, January 2014.

[15] P. Seiler, A. Pant and K. Hedrick, "Disturbance propagation in vehicle strings," *IEEE Transactions on Automatic Control,* vol. 49, no. 10, pp. 1835-1842, October 2004.

[16] E. Shaw and J. Hedrick, "String Stability Analysis for Heterogeneous Vehicle Strings," in *2007 American Control Conference*, New Yourk, NY, 2007.

[17] M. di Bernardo, A. Salvi and S. Santini, "Distributed Consensus Strategy for Platooning of Vehicles in the Presence of Time-Varying Heterogeneous Communication Delays," *IEEE Transactions on Intelligent Transportation Systems,* vol. 16, no. 1, pp. 102-112, February 2015.

[18] Y. Zheng, S. E. Li, J. Wang, L. Y. Wang and K. Li, "Influence of information flow topology on closed-loop stability of vehicle platoon with rigid formation," in *17th International IEEE Conference on Intelligent Transportation Systems (ITSC)*, Qingdao, 2014.

[19] J. Ploeg, N. van de Wouw and H. Nijmeijer, "Lp String Stability of Cascaded Systems: Application to Vehicle Platooning," *IEEE Transactions on Control Systems Technology,* vol. 22, no. 2, pp. 786-793, March 2014.

[20] A. Ghasemi, R. Kazemi and S. Azadi, "Stable Decentralized Control of a Platoon of Vehicles With Heterogeneous Information Feedback," *IEEE Transactions on Vehicular Technology,* vol. 62, no. 9, pp. 4299-4308, November 2013.

[21] K. Dey, L. Yan, X. Wang, Y. Wang, H. Shen, M. Chowdhury, L. Yu, C. Qiu and V. Soundararaj, "A Review of Communication, Driver Characteristics, and Controls Aspects of Cooperative Adaptive Cruise Control (CACC)," *EEE Transactions on Intelligent Transportation Systems,* vol. 17, no. 2, pp. 491-509, Feb 2016.

[22] D. Swaroop and J. Hedrick, "String stability of interconnected systems," *IEEE Transactions on Automatic Control,* vol. 41, no. 3, pp. 349-357, March 1996.

[23] S. Kato, S. Tsugawa, K. Tokuda, T. Matsui and H. Fujii, "Vehicle control algorithms for cooperative driving with automated vehicles and intervehicle communications," *IEEE Transactions on Intelligent Transportation Systems,* vol. 3, no. 3, pp. 155-161, Septmeber 2002.

[24] S. Öncü, J. Ploeg, N. van de Wouw and H. Nijmeijer, "Cooperative Adaptive Cruise Control: Network-Aware Analysis of String Stability," *IEEE Transactions on Intelligent Transportation Systems,* vol. 15, no. 4, pp. 1527-1537, August 2014.

[25] Y. Zheng, S. E. Li, J. Wang, D. Cao and K. Li, "Stability and Scalability of Homogeneous Vehiclular Platoon: Study on the Influence of Information Flow Topologies," *IEEE Transactions on Intelligent Transportation Systems,* vol. 17, no. 1, January 2016.

[26] H. Hao, P. Barooah and J. J. P. Veerman, "Effect of network structure on the stability margin of large vehicle formation with distributed control," in *49th IEEE Conference on Decision and Control (CDC)*, Atlanta, GA, 2010.

[27] I. Herman, D. Martinec, Z. Hurák and M. Šebek, "Nonzero Bound on Fiedler Eigenvalue Causes Exponential Growth of H-Infinity Norm of Vehicular Platoon," *IEEE Transactions on Automatic Control,* vol. 60, no. 8, pp. 2248-2253, August 2015.

[28] F. L. Lewis, H. Zhang, K. Hengster-Movric and A. Das, "Communication Graphs and Implementing Reynolds' Rules," in *Cooperative Control of Multi-Agent Systems: Optimal and Adaptive Design Approaches*, London, Springer-Verlag, 2014, p. Chapter 1.1.2.

[29] F. L. Lewis, H. Zhang, K. Hengster-Movric and A. Das, "Algebraic Graph Theory and Cooperative Control Consensus," in *Cooperative Control of Multi-Agent Systems*, London, Springer-Verlag, 2014, pp. Chapter 2.1-2.7.

[30] L.-H. Hsu and C.-K. Lin, "Counting Trees," in *Graph Theory and Interconnection Networks*, Boca Raton, CRC Press, 2009, pp. 68-71.

[31] P. Avery and R. Garcia, "Distributed Control in Multi-vehicle Systems," in *3rd International Multi-conference on Complexity, Informatics, and Cybernetics*, Orlando, FL, 2012.

[32] S.-B. Choi and J. Hedrick, "Vehicle longitudinal control using an adaptive observer for automated highway systems," in *American Control Conference, Proceedings of the 1995*, Seattle, 1995.

[33] G. Guo and W. Yue, "Sampled-Data Cooperative Adaptive Cruise Control of Vehicles With Sensor Failures," *IEEE Transactions on Intelligent Transportation Systems,* vol. 15, no. 6, pp. 2404-2418, December 2014.

[34] H. Hao and P. Barooah, "Control of large 1D networks of double integrator agents: Role of heterogeneity and asymmetry on stability margin," in *49th IEEE Conference on Decision and Control (CDC)*, Atlanta, GA, 2010.

[35] H. Hao, P. Barooah and P. G. Mehta, "Stability Margin Scaling Laws for Distributed Formation Control as a Function of Network Structure," *IEEE Transactions on Automatic Control,* vol. 56, no. 4, pp. 923-929, April 2011.

[36] W. B. Qin, M. M. Gomez and G. Orosz, "Stability analysis of connected cruise control with stochastic delays," in *2014 American Control Conference*, Portland, 2014.

[37] H. Hao and P. Barooah, "On Achieving Size-Independent Stability Margin of Vehicular Lattice Formations With Distributed Control," vol. 57, no. 10, pp. 2688-2694, October 2012.

[38] X.-Y. Lu, J. K. Hedrick and M. Drew, "ACC/CACC-control design, stability and robust performance," in *Proceedings of the 2002 American Control Conference*, Anchorage, AK, 2002.

Appendix

Simulation Script

```
% Choose simulation parameters
topo=1; %1=PF, 2=PLF, 3=BD, 4=BDL, 5=TPF, 6=TPLF
h_value=2; %constant distance spacing between cars (m)
c=1;  gamma=1; %choose protocol gain values
ICX=2; %which set of initial conditions to use (see line 113)
ExcludeNocap= 1; %0 to run sim without capped dynamics,
                 %1 to run sim with capped dynamics:
                    % acceleration limited to +0.3 g's, -1.0g's,
                    % velocity 0 to 44.7 m/s (100mph)
                 %(see line 138)
simtype=1; %0=local protocol, 1=global protocol (see line 152)
tfu=0.0010; %used in determining time to convergence (see line 189)
mindiff=0.05; %used in determining time to collision (see line 207)


% Define graph for chosen topology
switch topo
    case 1
        % PF
        top='PF';
        A=[0 0 0 0 0 0 0 0 0 0; %1 gets input from nothing
            1 0 0 0 0 0 0 0 0 0; %2 gets input from 1
            0 1 0 0 0 0 0 0 0 0; %3 gets input form 1
            0 0 1 0 0 0 0 0 0 0; %4 gets input from 3
            0 0 0 1 0 0 0 0 0 0; %5 gets input from 4
            0 0 0 0 1 0 0 0 0 0; %6 gets input from 5
            0 0 0 0 0 1 0 0 0 0; %7 gets input from 6
            0 0 0 0 0 0 1 0 0 0; %8 gets input from 7
            0 0 0 0 0 0 0 1 0 0; %9 gets input from 7
            0 0 0 0 0 0 0 0 1 0]; %10 gets input from 9
    case 2
        % PLF
        top='PLF';
        A=[0 0 0 0 0 0 0 0 0 0; %1 gets input from nothing
            1 0 0 0 0 0 0 0 0 0; %2 gets input from 1
            1 1 0 0 0 0 0 0 0 0; %3 gets input form 2 and 1
            1 0 1 0 0 0 0 0 0 0; %4 gets input from 3 and 1
            1 0 0 1 0 0 0 0 0 0; %5 gets input from 4 and 1
            1 0 0 0 1 0 0 0 0 0; %6 gets input from 5 and 1
            1 0 0 0 0 1 0 0 0 0; %7 gets input from 6 and 1
            1 0 0 0 0 0 1 0 0 0; %8 gets input from 7 and 1
            1 0 0 0 0 0 0 1 0 0; %9 gets input from 8 and 1
            1 0 0 0 0 0 0 0 1 0]; %10 gets input from 9 and 1
```

```
    case 3
        % BD
        top='BD';
        A=[0 0 0 0 0 0 0 0 0 0; %1 gets input from nothing
            1 0 1 0 0 0 0 0 0 0; %2 gets input from 1 and 3
            0 1 0 1 0 0 0 0 0 0; %3 gets input form 2 and 4
            0 0 1 0 1 0 0 0 0 0; %4 gets input from 3 and 5
            0 0 0 1 0 1 0 0 0 0; %5 gets input from 4 and 6
            0 0 0 0 1 0 1 0 0 0; %6 gets input from 5 and 7
            0 0 0 0 0 1 0 1 0 0; %7 gets input from 6 and 8
            0 0 0 0 0 0 1 0 1 0; %8 gets input from 7 and 9
            0 0 0 0 0 0 0 1 0 1; %9 gets input from 8 and 10
            0 0 0 0 0 0 0 0 1 0]; %10 gets input from 9
    case 4
        % BDL
        top='BDL';
        A=[0 0 0 0 0 0 0 0 0 0; %1 gets input from nothing
            1 0 1 0 0 0 0 0 0 0; %2 gets input from 1 and 3
            1 1 0 1 0 0 0 0 0 0; %3 gets input form 2 and 4 and 1
            1 0 1 0 1 0 0 0 0 0; %4 gets input from 3 and 5 and 1
            1 0 0 1 0 1 0 0 0 0; %5 gets input from 4 and 6 and 1
            1 0 0 0 1 0 1 0 0 0; %6 gets input from 5 and 7 and 1
            1 0 0 0 0 1 0 1 0 0; %7 gets input from 6 and 8 and 1
            1 0 0 0 0 0 1 0 1 0; %8 gets input from 7 and 9 and 1
            1 0 0 0 0 0 0 1 0 1; %9 gets input from 8 and 10 and 1
            1 0 0 0 0 0 0 0 1 0]; %10 gets input from 9 and 1
    case 5
        % TPF
        top='TPF';
        A=[0 0 0 0 0 0 0 0 0 0; %1 gets input from nothing
            1 0 0 0 0 0 0 0 0 0; %2 gets input from 1
            1 1 0 0 0 0 0 0 0 0; %3 gets input form 2 and 1
            0 1 1 0 0 0 0 0 0 0; %4 gets input from 3 and 2
            0 0 1 1 0 0 0 0 0 0; %5 gets input from 4 and 3
            0 0 0 1 1 0 0 0 0 0; %6 gets input from 5 and 4
            0 0 0 0 1 1 0 0 0 0; %7 gets input from 6 and 5
            0 0 0 0 0 1 1 0 0 0; %8 gets input from 7 and 6
            0 0 0 0 0 0 1 1 0 0; %9 gets input from 8 and 7
            0 0 0 0 0 0 0 1 1 0]; %10 gets input from 9 and 8
    case 6
        % TPLF
        top='TPLF';
        A=[0 0 0 0 0 0 0 0 0 0; %1 gets input from nothing
            1 0 0 0 0 0 0 0 0 0; %2 gets input from 1
            1 1 0 0 0 0 0 0 0 0; %3 gets input form 2 and 1
            1 1 1 0 0 0 0 0 0 0; %4 gets input from 2 and 3 and 1
            1 0 1 1 0 0 0 0 0 0; %5 gets input from 3 and 4 and 1
            1 0 0 1 1 0 0 0 0 0; %6 gets input from 4 and 5 and 1
```

```
            1 0 0 0 1 1 0 0 0 0; %7 gets input from 5 and 6 and 1
            1 0 0 0 0 1 1 0 0 0; %8 gets input from 6 and 7 and 1
            1 0 0 0 0 0 1 1 0 0; %9 gets input from 7 and 8 and 1
            1 0 0 0 0 0 0 1 1 0]; %10 gets input from 8 and 9 and 1
end

N=length(A); %number of nodes
D=diag(sum(A')); %sum A gives column sum, sum A' gives row sum%
L=D-A; %graph laplacian


% Define H based on chosen h_value; define G.
q=0;
for i=1:length(A)
    H(i)=q*h_value;
    q=q+1;
end
G=[0 0 0 0 0 0 0 0 0 0];


% Define Initial Conditions.
switch ICX
    case 1
        tf=500;
        IC=[10 9 8 7 6 5 4 3 2 1];
        v0=[1 .9 .8 .7 .6 .5 .4 .3 .2 .1];
        disturbance=0;%turn off added disturbance into leader acceleration.
    case 2
        tf=500;
        IC=[10 9 8 7 6 5 4 3 2 1];
        v0=[29 28 27 26 25 24 23 22 21 20];
        disturbance=0;%turn off added disturbance into leader acceleration.
    case 3
        tf=1000;
        IC=[20 18 16 14 12 10 8 6 4 2] ;
        v0=[29 32 28.4 28.1 25 32 28.4 28.7 29 33];
        disturbance=0;%turn off added disturbance into leader acceleration.
    case 4
        tf=500;
        IC=[20 18 16 14 12 10 8 6 4 2] ;
        v0=[29 29 29 29 29 29 29 29 29 29];
        disturbance=1;%turn ON added disturbance into leader acceleration.
end


% Define dynamics limitations
switch ExcludeNocap
    case 0 %run simulation WITHOUT dynamics limitations
```

```
        umax=inf; %m/s^2
        umin=-inf;%m/s^2
        vmax=inf;%m/s^2
        vmin=-inf;%m/s^2
    case 1 %run simulation WITH dynamics limitations
        umax=0.3*9.81; %g's to acceleration %m/s^2
        umin=-1*9.81;  %g's to acceleration %m/s^2
        vmax=44.7; %m/s
        vmin=0; %m/s
end


% Define and Run simulation

%Choose simulation
switch simtype
    case 0
        simname='node_dynamics_4212017_2304';%name of simulink model to run
    case 1
        simname='global_dynamics_4212017_2304';

        %Calculate global variable terms
        K=[1 gamma];
        Ad=[0 1; 0 0]; B=[0;1]; %node dynamics for all nodes (homogeneous)
        Ac=kron(eye(N),Ad)+(kron(-c*L,B*K));
        Fc=kron(-c*L,B*K);

        F=zeros(2*N,1); q=0; %initialize variables in for-loop
        for i=1:2*N
            if mod(i,2)==1
                F(i,1)=q*h_value;
                q=q+1;
            else
                F(i,1)=0;
            end
        end
        Q=Fc*F;

        init=reshape([IC; v0],20,1);
        uplim=reshape([vmax*ones(1,N);umax*ones(1,N)],20,1);
        lolim=reshape([vmin*ones(1,N);umin*ones(1,N)],20,1);
end


% Run Simulation
sim(simname,tf);
```

```
% Determine Time to Convergence (ttc)
```

%% Note that "tf" in the code is not the same as t_f discussed in the text of this document. In code, t_f is called "ttc". In code, "tf" is the end time of the entire simulation, which is arbitrarily chosen.

```
k=0;
m=[0 0 0 0 0 0 0 0 0 0];
for j=1:length(tout)
    ttc=tout(j);
    for l=1:10
        if u(j,l)<tfu && u(j,l)>-tfu
            m(l)=1;
        else
            m(l)=0;
        end
    end
    if m==[1 1 1 1 1 1 1 1 1 1]
        k=k+1;
    end
    if k>500
        break
    end
end


% Determine Time to Collision (CT)
for n=1:length(tout)
    collision_time=tout(n);
    Q=abs(diff(x(n,1:end)));
    R=(Q<mindiff);
    I=find(R);
    S=sum(R);
    if S>0
        break
    end
end


% Calculate Convergence Values for position and velocity
vC=v0(1)-G(end,:);
xC=(IC(1)-H)+ttc*vC;


% Calculate e and r
x1=x(:,1); x2=x(:,2); x3=x(:,3);x4=x(:,4);x5=x(:,5);...
```

```
    x6=x(:,6);x7=x(:,7);x8=x(:,8);x9=x(:,9);x10=x(:,10);
r=[x1-x2 x2-x3 x3-x4 x4-x5 x5-x6 x6-x7 x7-x8 x8-x9 x9-x10];
e=h_value-r;


% Create Plots
figure(1);
plot(tout,x);
title (['Position for ',num2str(top), ' (IC', num2str(ICX),...
    ', c=',num2str(c),', \gamma=', num2str(gamma), ')']);
hold on; plot(ttc,xC,'bx','LineWidth',2);
xlabel 'time (s)'
ylabel 'position (m)'
h = legend ('1', '2', '3', '4', '5', '6', '7', '8', '9' ,'10',...
    '$$\overline{x}$$','Location','SouthEastOutside');
set(h,'Interpreter','latex','FontName','Times New Roman','fontsize',10) ;
xlim([0,ttc]);
grid on;

figure(2);
plot(tout,v);
hold on; plot(ttc,v(round(ttc*100),10),'bx','LineWidth',2)
title (['Velocity for ',num2str(top), ' (IC', num2str(ICX),...
    ', c=',num2str(c),', \gamma=', num2str(gamma), ')']);
xlabel 'time (s)'
ylabel 'velocity (m/s)'
h = legend ('1', '2', '3', '4', '5', '6', '7', '8', '9' ,'10',...
    'convergence','Location','SouthEastOutside');
set(h,'Interpreter','latex','FontName','Times New Roman','fontsize',10) ;
xlim([0,ttc]);
grid on;

figure(3);
plot(tout,u/9.81);
hold on; plot(ttc,u(round(ttc*100),10)/9.81,'bx','LineWidth',2)
title (['Acceleration Input for ',num2str(top),  ' (IC', num2str(ICX),...
    ', c=',num2str(c),', \gamma=', num2str(gamma), ')']);
xlabel 'time (s)'
ylabel 'acceleration input (g)'
h = legend ('1', '2', '3', '4', '5', '6', '7', '8', '9' ,'10',...
    'convergence','Location','SouthEastOutside');
set(h,'Interpreter','latex','FontName','Times New Roman','fontsize',10) ;
grid on;
xlim([0,ttc]);
ylim([(min(min(u))/9.81)-0.05, (max(max(u))/9.81)+0.05]);

figure(4);
plot(tout,x);
```

```
title (['Position for ',num2str(top), ' (IC', num2str(ICX), ', c=',...
    num2str(c),', \gamma=', num2str(gamma), ')']);
hold on; plot(ttc,xC,'bx','LineWidth',2);
xlabel 'time (s)'
ylabel 'position (m)'
h = legend ('1', '2', '3', '4', '5', '6', '7', '8', '9' ,'10',...
    '$$\overline{x}$$','Location','SouthEastOutside');
set(h,'Interpreter','latex','FontName','Times New Roman','fontsize',10) ;
xlim([ttc-1.5,ttc]);
ylim([min(x(round(100*(ttc-1.5)),:))-1, max(x(round(100*(ttc)),:))+3]);
grid on;

figure(5);
if isempty(I)
    disp('No Collision Occurs.')
else
    disp(['Car ' num2str(I) ' gets rear ended by car ' num2str(I+1),'.'])
    CT(i)=collision_time;
    plot(tout,x);
    hold on; plot(collision_time,x(round(1+collision_time*100),I+1),...
        'rx','LineWidth',2);
    title (['Position for ',num2str(top), ' (IC', num2str(ICX), ...
        ', c=',num2str(c),', \gamma=', num2str(gamma), ')']);
    xlabel 'time (s)'
    ylabel 'position (m)'
    h = legend ('1', '2', '3', '4', '5', '6', '7', '8', '9' ,'10',...
        'collision','Location','SouthEastOutside');
    set(h,'Interpreter','latex','FontName','Times New Roman',...
        'fontsize',10);
    xlim([collision_time-0.5,collision_time+0.5]);
    grid on;
end

figure(6);
plot(tout,e);
title (['Intervehicle Distance Error for ',num2str(top)]);
xlabel 'time (s)'
ylabel 'intervehicle distance error (m)'
h = legend ('1 and 2', '2 and 3', '3 and 4', '4 and 5', '5 and 6', ...
    '6 and 7', '7 and 8', '8 and 9' ,'9 and 10','convergence',...
    'collision','Location','SouthEastOutside');
set(h,'Interpreter','latex','FontName','Times New Roman','fontsize',10) ;
grid on;
xlim([0,ttc]);
filename=['e ',num2str(top), ' IC', num2str(ICX), ', c',num2str(c),...
    ', gamma', num2str(gamma)];
saveas(gcf, filename, 'png');
```

```
figure(7)
plot(tout,zeros(1,length(tout)));
hold on; plot(tout,r);
if isempty(I)
else
    hold on; plot(collision_time,r(round(1+collision_time*100),I),...
        'rx','LineWidth',2);
end
title (['Intervehicle Distance for ',num2str(top)]);
xlabel 'time (s)'
ylabel 'intervehicle distance (m)'
h = legend ('collision line','1 and 2', '2 and 3', '3 and 4', '4 and 5',...
    '5 and 6', '6 and 7', '7 and 8', '8 and 9' ,'9 and 10','collision',...
    'collision','Location','SouthEastOutside');
set(h,'Interpreter','latex','FontName','Times New Roman','fontsize',10) ;
grid on;
xlim([0,ttc]);
lowy=min(min(min(r))-0.5,-0.5);
ylim([lowy, max(max(r))+0.5]);
filename=['r ',num2str(top), ' IC', num2str(ICX), ', c',num2str(c),...
    ', gamma', num2str(gamma)];
saveas(gcf, filename, 'png');
```

Simulink Models

Node Dynamics

'node_dynamics_4212017_2304'

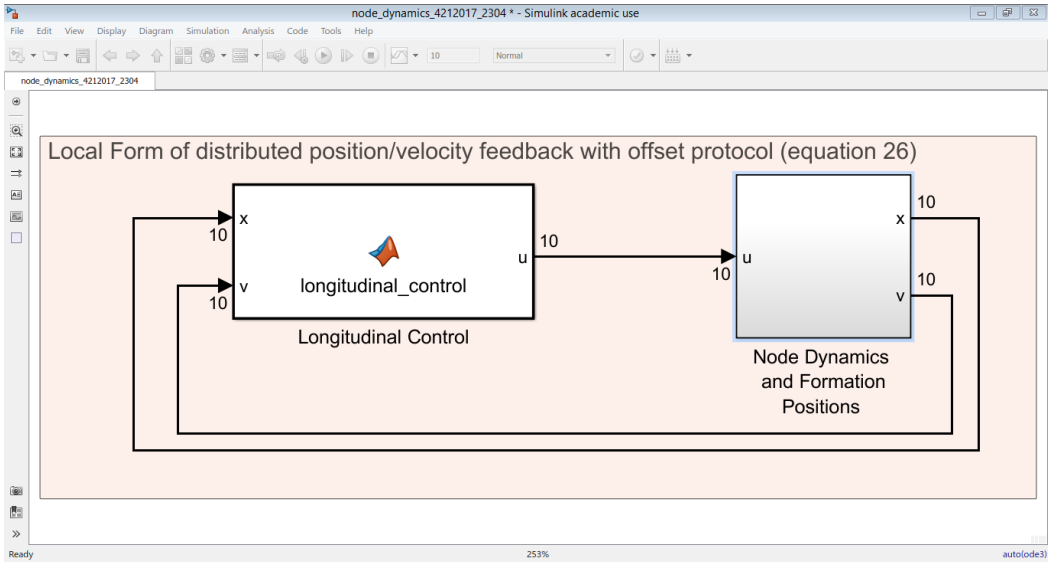

```
function u  = longitudinal_control(x, v, H, A, c, gamma)
% Initialize vectors
numagents=length(A); %determine the number of agents in the graph
numinputs=length(H); %determine the number of control inputs needed
u=zeros(numinputs,1); ux=zeros(numinputs,1);uv=zeros(numinputs,1);
x_error=zeros(numagents,1); v_error=zeros(numagents,1);

% Calculate u(i)
for i=1:numagents %begin calculating u
    sum_x=0; sum_h=0; sum_v=0;
    for j=1:numagents
        xdiff  = x(j)-x(i);
        hdiff  = H(j)-H(i);
        veldiff= v(j)-v(i);

        sum_xj= A(i,j)*xdiff;
        sum_hj= A(i,j)*hdiff;
        sum_vj= A(i,j)*veldiff;

        sum_x= sum_x+sum_xj;
        sum_h= sum_h+sum_hj;
        sum_v= sum_v+sum_vj;
    end

    x_error(i)=sum_x+sum_h;
    v_error(i)=sum_v;

    ux(i)=c*x_error(i);
    uv(i)=c*gamma*v_error(i);
    u(i)=ux(i)+uv(i);
end
```

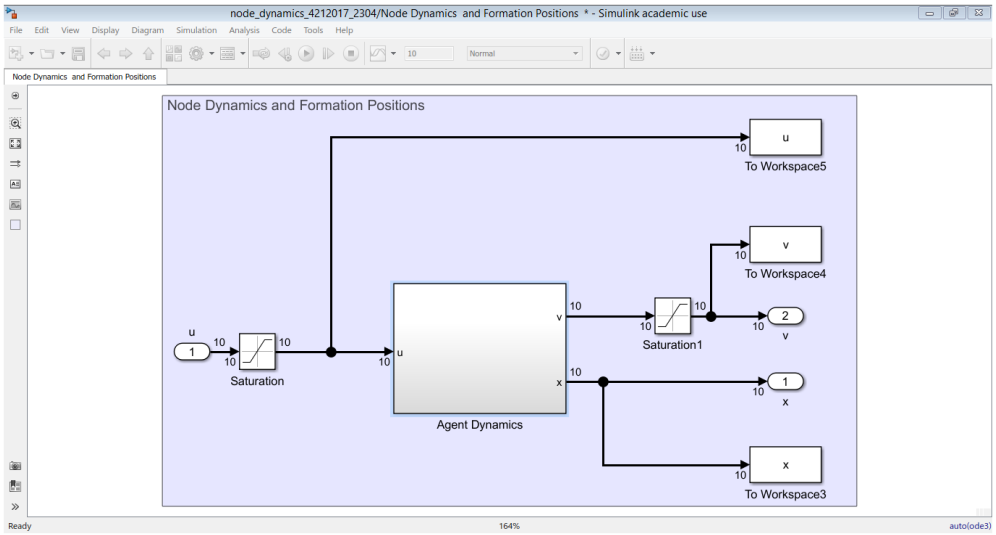

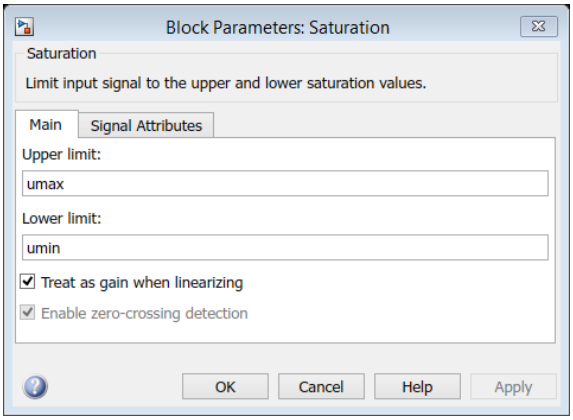
Block Parameters: Saturation
Saturation
Limit input signal to the upper and lower saturation values.
Main
Signal Attributes
Upper limit:
umax
Lower limit:
umin
Treat as gain when linearizing
Enable zero-crossing detection
OK
Cancel
Help
Apply

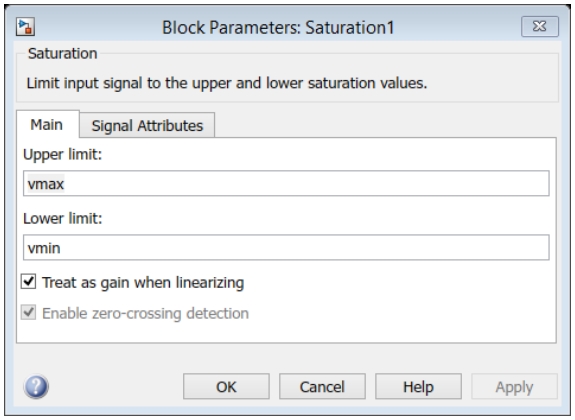
Block Parameters: Saturation1
Saturation
Limit input signal to the upper and lower saturation values.
Main
Signal Attributes
Upper limit:
vmax
Lower limit:
vmin
Treat as gain when linearizing
Enable zero-crossing detection
OK
Cancel
Help
Apply

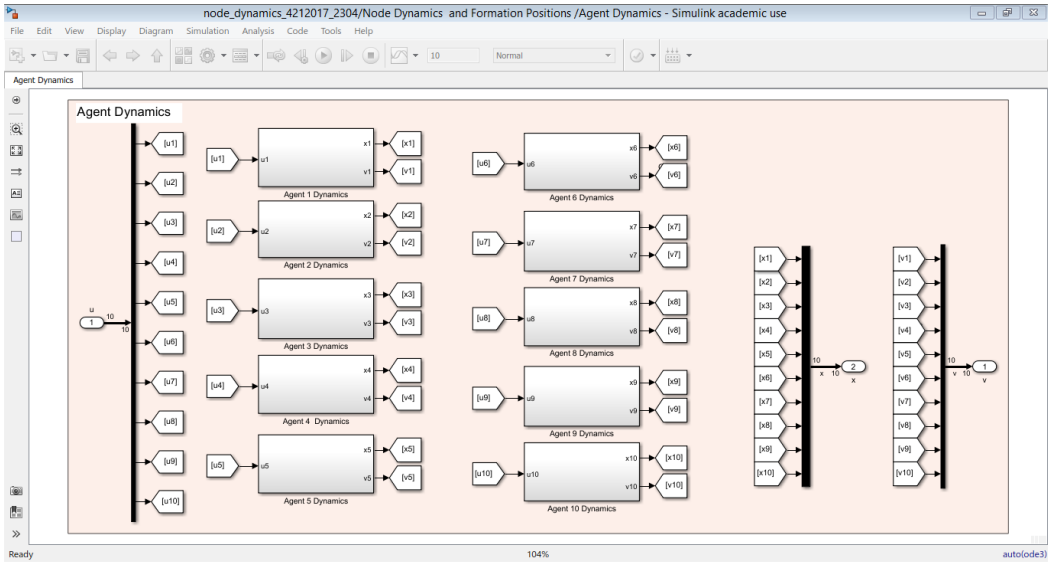
node_dynamics_4212017_2304/Node Dynamics and Formation Positions /Agent Dynamics - Simulink academic use
File Edit View Display Diagram Simulation Analysis Code Tools Help
Agent Dynamics
Agent Dynamics
Agent 1 Dynamics
Agent 2 Dynamics
Agent 3 Dynamics
Agent 4 Dynamics
Agent 5 Dynamics
Agent 6 Dynamics
Agent 7 Dynamics
Agent 8 Dynamics
Agent 9 Dynamics
Agent 10 Dynamics
Ready
104%
auto(ode3)

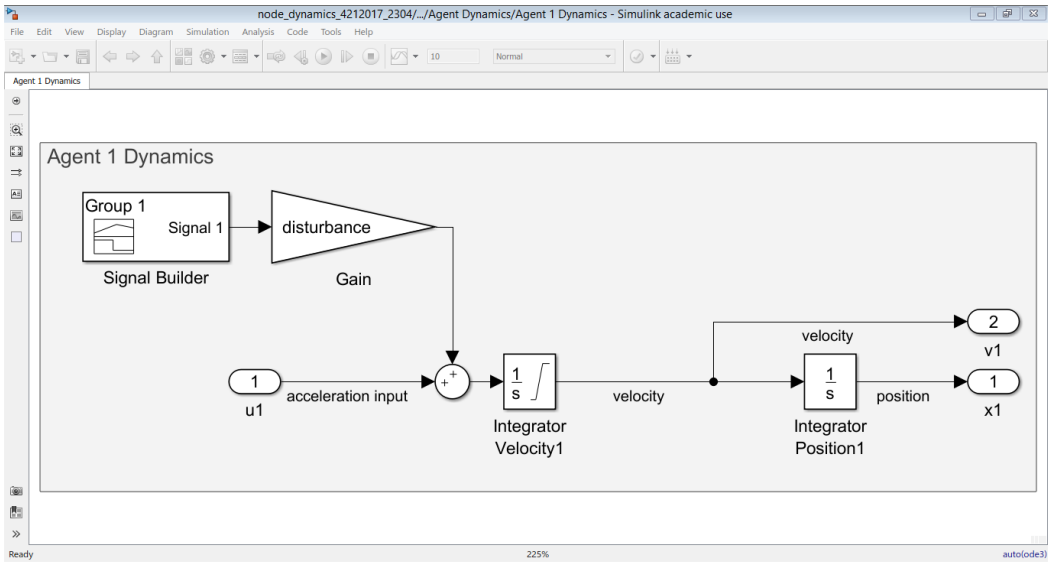
node_dynamics_4212017_2304/.../Agent Dynamics/Agent 1 Dynamics - Simulink academic use
File Edit View Display Diagram Simulation Analysis Code Tools Help
Agent 1 Dynamics
Agent 1 Dynamics
Group 1
Signal 1
Signal Builder
disturbance
Gain
1
u1
acceleration input
1
s
Integrator
Velocity1
velocity
1
s
Integrator
Position1
position
2
v1
1
x1
Ready
225%
auto(ode3)

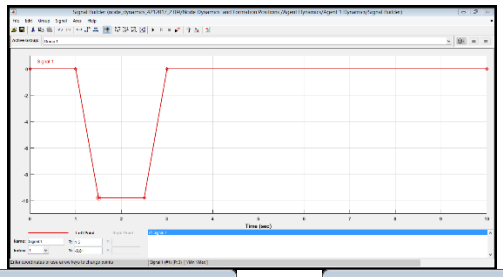

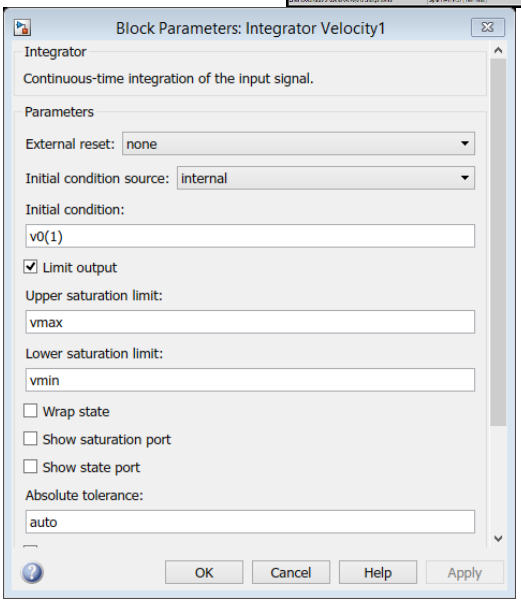
Block Parameters: Integrator Velocity1
Integrator
Continuous-time integration of the input signal.
Parameters
External reset: none
Initial condition source: internal
Initial condition:
v0(1)
Limit output
Upper saturation limit:
vmax
Lower saturation limit:
vmin
Wrap state
Show saturation port
Show state port
Absolute tolerance:
auto
OK
Cancel
Help
Apply

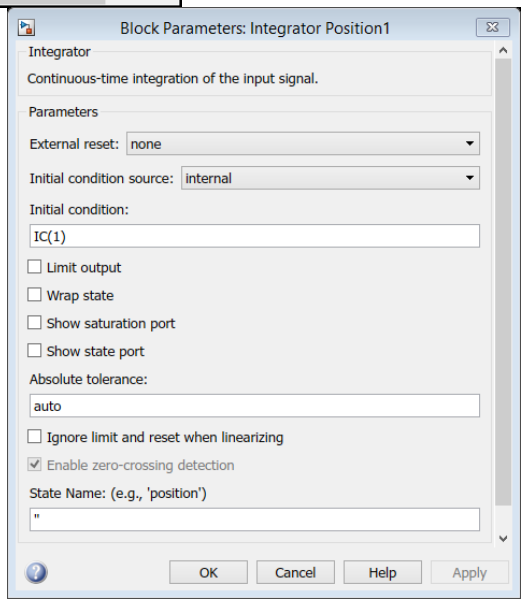
Block Parameters: Integrator Position1
Integrator
Continuous-time integration of the input signal.
Parameters
External reset: none
Initial condition source: internal
Initial condition:
IC(1)
Limit output
Wrap state
Show saturation port
Show state port
Absolute tolerance:
auto
Ignore limit and reset when linearizing
Enable zero-crossing detection
State Name: (e.g., 'position')
''
OK
Cancel
Help
Apply

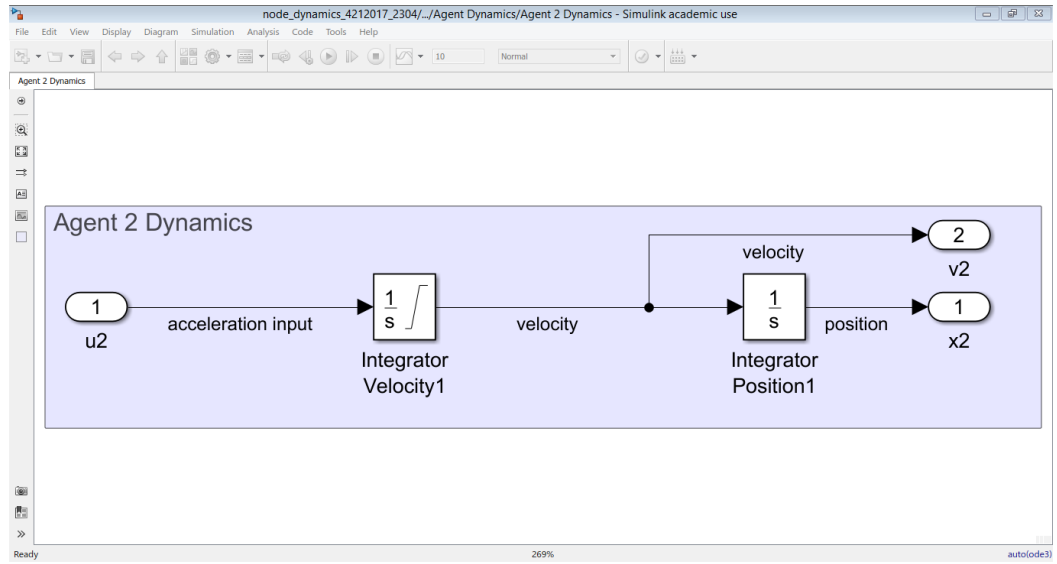

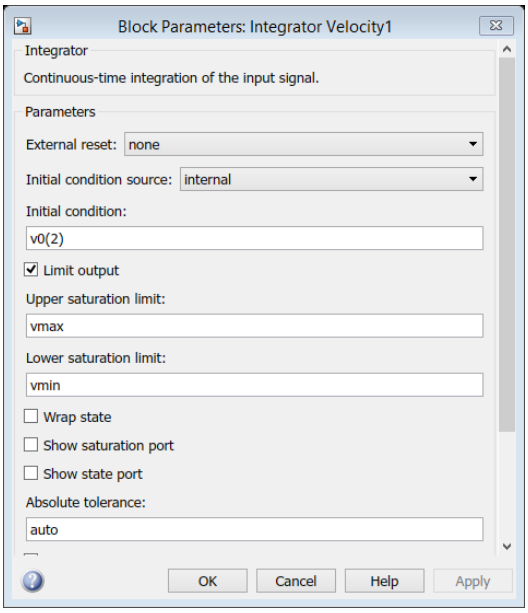

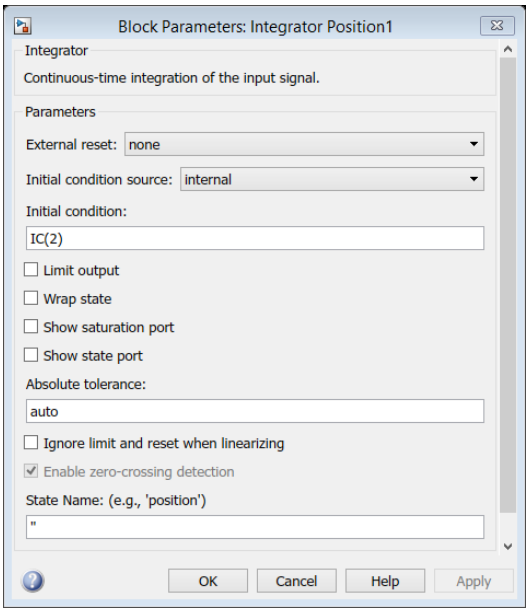

Note Agent 3 through Agent 10 are identical to Agent 2 except for the initial condition parameter. For example, Agent X has v0(X) and IC(X) as its initial inputs for the integrator blocks.

'global_dynamics_4212017_2304'

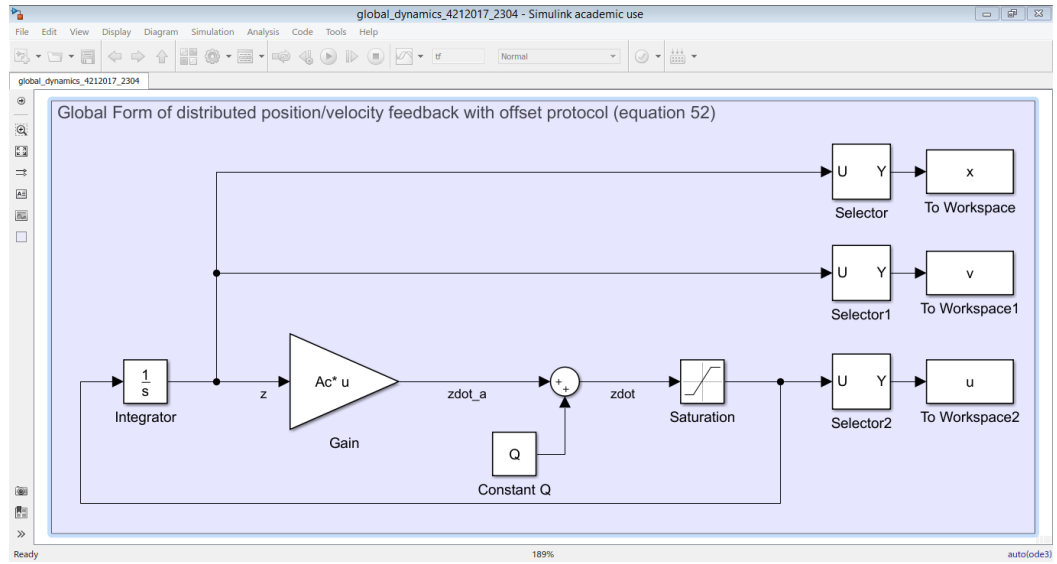

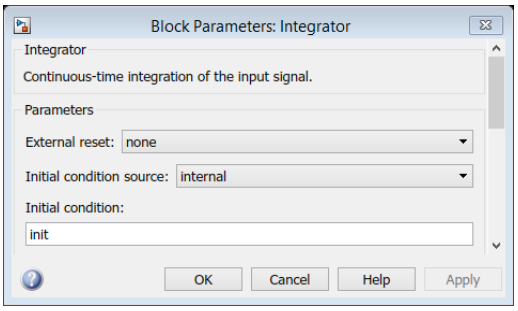

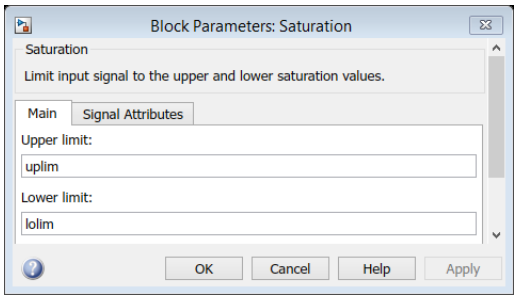

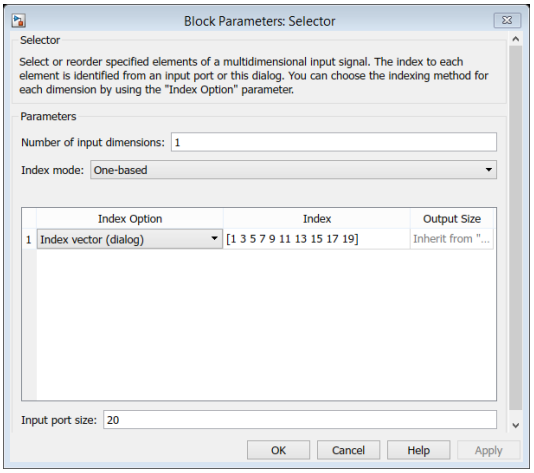

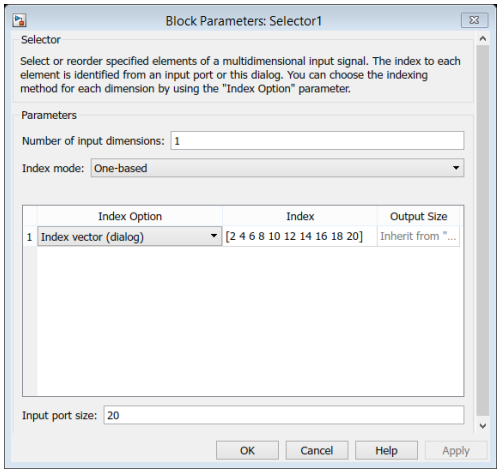

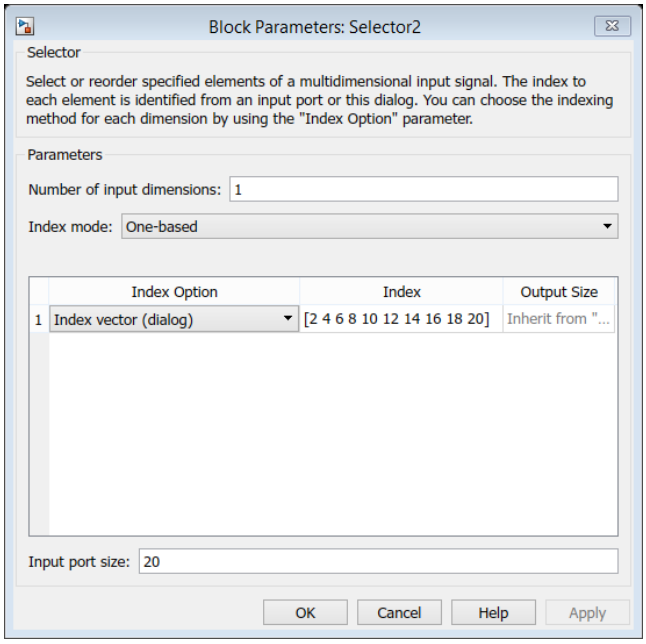
Block Parameters: Selector2
Selector
Select or reorder specified elements of a multidimensional input signal. The index to each element is identified from an input port or this dialog. You can choose the indexing method for each dimension by using the "Index Option" parameter.
Parameters
Number of input dimensions: 1
Index mode: One-based
Index Option
Index
Output Size
1
Index vector (dialog)
[2 4 6 8 10 12 14 16 18 20]
Inherit from "...
Input port size: 20
OK
Cancel
Help
Apply